LAYERED DOUBLE HYDROXIDES MATERIALS FOR PHOSPHATE RECOVERY AND PHOTOELECTRODE APPLICATIONS

AKIHIRO SHIMAMURA

A thesis submitted in fulfilment of the requirements for the degree of

Doctor of Philosophy in Chemistry

The University of Auckland, 2014

Abstract

Layered double hydroxide (LDH) materials have been applied in many applications. Use as an environmental adsorbent is one of the most common applications of LDHs because of their anion exchange function and recyclability. However a lot of these studies have focussed on the adsorption process rather than the equally important desorption process. Desorption is critical to improve the recyclability of the LDH material.

This thesis examines a new phosphate recovery system from phosphate intercalated Mg/Al-LDH, based on the use of surfactant anions. The surfactant anion is used to exchange the interlayer phosphate of the Mg/Al-LDH material. This new method is shown to remove interlayer phosphate with a higher desorption ratio than conventional methods using concentrated sodium carbonate solution or mixed solutions of sodium chloride and sodium hydroxide. The mechanism for the improved ratio for phosphate desorption with surfactant anions is demonstrated by several case studies in this thesis.

In addition to the new phosphate recovery system, the thesis reports development of a new photo electrode based on decomposition of Zn/Al-LDH. Photocatalysis from films on zinc substrates is observed following calcination of Zn/Al-LDH. The thermal behaviour of powdered Zn/Al-LDH is also examined to understand thermal transformation of the Zn/Al-LDH and the photocatalytic properties of the calcined Zn/Al-LDH. The Zn/Al-LDH is fabricated on a zinc metal substrate by hydrothermal treatment and then converted to an active photocatalyst by thermal treatment.

Acknowledgements

I would like to express my most sincere gratitude to my supervisor Professor James B. Metson and Professor Mark I. Jones. Their guidance helped me in all the time in research and writing of the thesis.

Besides my advisors, I would like to thank all the staff in the University of Auckland who have taken care of my experiments. Especially, Dr. Geoff Waterhouse has supported my experiments from the beginning of my PhD. I also have appreciated the help of Dr. Bruce Cowie, Dr. Anton Tadish and Dr. Justin Kimpton from the Australian Synchrotron.

I am grateful to Professor Kanezaki, Professor Moriga, Professor Murai, Professor Yabutani, Dr. Kurashina and rest of people from the University of Tokushima for their support to my Ph.D study.

A great thank to all the friends of the PhD students and Doctoral researchers in both the University of Auckland and the University of Tokushima.

Publications

"Complete desorption of interlayer hydrogen phosphate in Mg/Al-layered double hydroxides by means of anion exchange with 1-octanesulfonate", Akihiro Shimamura、Mark I. Jones、Eiji Kanezaki, James B. Metson、Journal of Material Science, vol47, pp1142-1147, 2012.2

"Intercalation of hydrogen phosphate into Mg/Al-layered double hydroxides with dodecyl benzene sulfonate", Akihiro Shimamura、Mark I. Jones、 James B. Metson, Modern Physics Letters B, vol.26, pp125011:1-6, 2012.7

"Anionic surfactant enhanced phosphate desorption from Mg/Al-layered double hydroxides by micelle formation", Akihiro Shimamura、Mark I. Jones、James B. Metson, Journal of Colloid and Interface Science, vol.411, pp1-7, 2013.12

Table of Contents

Abstract ...**i**

Acknowledgements ...**ii**

Publications ...**iii**

Chapter 1: Introduction

1-1 Layered double hydroxides (LDH) ...2

1-2 Application of the LDH ...4

1-3 Phosphate recovery systems from wastewater ...7

1-4 Catalyst application of calcined LDH material ...13

1-5 Objectives of this study ...14

Chapter 2: Experimental procedure and characterization

2-1 Formation of LDH material ...18

2-1-1 Synthesis of carbonate intercalated Mg/Al-LDH ...18

2-1-2 Anion exchange interlayer carbonate for chloride ...19

2-1-3 Anion exchange interlayer chloride for phosphate ...20

2-2 Phosphate desorption methods ...21

2-3 Synthesis of carbonate intercalated Zn/Al-LDH ...21

2-4 Zn/Al-LDH fabrication on Zinc substrate by hydrothermal treatment ...22

2-5 Characterization ...23

Chapter 3: Complete desorption of interlayer hydrogen phosphate in Mg/Al-layered double hydroxides (Mg/Al-LDH) by means of anion exchange with 1-octanesulfonate

3-1 Previous studies of phosphate adsorption with LDH materials ...29

3-2 Complete desorption of interlayer phosphate from Mg/Al-LDH ...31

3-3 Intercalation of 1-octanesulfonate into Mg/Al-LDH by anion exchange with interlayer phosphate ...34

3-4 Summary ...40

Chapter 4: Anionic surfactant enhanced phosphate desorption from Mg/Al-layered double hydroxides

4-1 Surfactant absorption behavior on Mg/Al-LDH material before and after micelle formation ...43

4-2 Kinetic study of phosphate desorption with surfactant micelle ...45

4-3 Phosphate desorption from Mg/Al-LDH by anion exchanged with surfactant micelles ...48

4-4 Phosphate re-absorption on to Mg/Al-LDH material with surfactant micelles ...59

4-5 Summary ...62

Chapter 5: XANES characterization of Zinc/Aluminium mixed oxides derived from Zn/Al-layered double hydroxides (Zn/Al-LDH).

5-1 General study of calcined Zn/Al-LDH ...65

5-2 Synthesis and characterization of calcined Zn/Al-LDH by XRD and TG-DTA ...67

5-3 Characterization of calcined Zn/Al-LDH by XANES spectra ...71

5-4 Optical properties of calcinated Zn/Al-LDH ...80

5-5 Summary ...84

Chapter 6: Fabrication and characterization of zinc/aluminum mixed oxide films on metal substrate via formation of Zn/Al-layered double hydroxides

6-1 Study of LDH fabrication on metal substrate ...87

6-2 Zn/Al-LDH fabrication on Zinc substrate by hydrothermal treatment ...90

6-2-1 Role of hydrothermal temperature and reaction time ...90

6-2-2 Surface analysis of Zn/Al-LDH on Zn substrate by XPS ...95

6-2-3 Mechanism of Zn/Al-LDH formation on Zn substrate by hydrothermal treatment ...97

6-3 Thermal transformation to amorphous phase Zinc/Aluminium mixed metal oxides (ZAO) and investigation of photocatalytic properties of the amorphous phase ...98

6-3-1 Thermal transformation of Zn/Al-LDH to the amorphous phase ...99

6-3-2 Photocurrent property of ZAO depending on hydrothermal conditions ...104

6-4 Summary ...108

Chapter 7: Conclusions and Outlook ...109

References ...115

Chapter1:

Introduction and literature review

1-1 Layered double hydroxides (LDH)

Layered double hydroxides (LDH) material has a similar structure to the brucite [$Mg(OH)_2$] structure. Figure 1-1 provides an illustration of a common form of this LDH structure. The Mg^{2+} ion in the layer is octahedrally surrounded by six OH^- ions and the octahedrons share edges to build up layers with high aspect ratio. Some of the Mg^{2+} ions in $Mg(OH)_2$ are isomorphously replaced by Al^{3+} and the charge imbalance is compensated by interlayer anions. The stacking sequence of LDH can be represented as AC CB BA AC ..., where the upper case symbols A, B, and C represent the hydroxyl ion positions. The hydrotalcite polytype is known as a 3R1 (Rhombohedral) structure. The lattice parameter c_0 is as same size as 3 times the basal spacing, which is the sum of the interlayer distance and the layer thickness (0.48 nm). The basal spacing is typically calculated from the (*00l*) reflection the diffraction pattern calculated from the Bragg equation(equation I-I).

$$2d\sin\theta = n\lambda \quad \text{Bragg equation} \ldots\text{(I-I)}$$

(d= spacing between the planes in the atomic lattice, θ= diffraction angle, λ=wavelength, n=integer)

The general composition of the most common LDH material is described as $Mg_{1-x}Al_x(OH)_2A_{x/n} \cdot mH_2O$, where A is an interlayer anion with negative charge n. The charge-balancing interlayer anions can be exchanged with other anions, which leads to much of the utility of these materials, for example in phosphate recovery as described below.

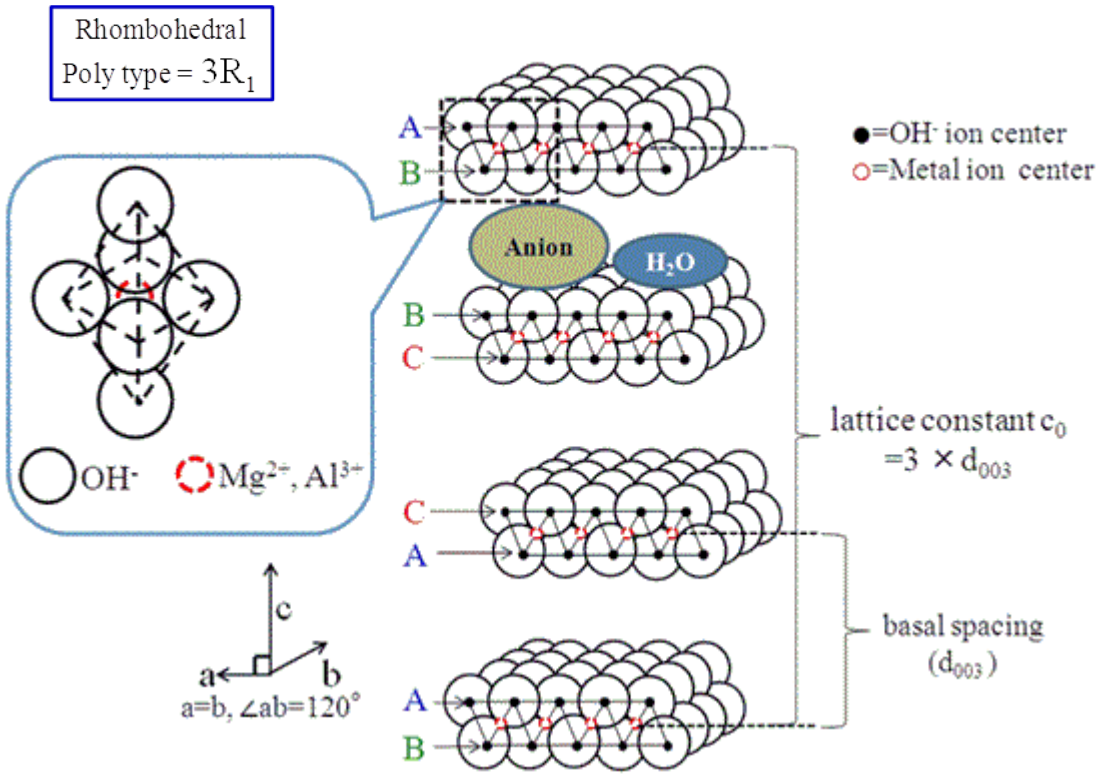

Figure 1-1. Illustration of the layered double hydroxides structure.

Anion intercalation of the LDH can be classified as anionic exchange, or by reconstruction of the layered structure (reaction1-1).

- *Anion exchange:*

The most common reaction for anion intercalation into the LDH material:

$Mg_{0.7}Al_{0.3}(OH)_2(Cl^-)_{0.3}xH_2O + A^{n-} \rightarrow Mg_{0.7}Al_{0.3}(OH)_2(A^{n-})_{0.3/n}xH_2O + 0.3Cl^-$…1-1

- *Reconstruction:*

The reconstruction process is known as the "memory affect" method. In the

reconstruction method, the LDH material is calcined between 400 ˚C and 500 ˚C. (reaction1-2)[1] The calcined LDH (water molecules, anions and hydroxyl groups are removed) is able to regenerate the layered structure when it is exposed to water and anions. (reaction1-3)

$$Mg_{0.7}Al_{0.3}(OH)_2(CO_3^{2-})_{0.15}\,xH_2O \rightarrow$$

$$\text{amorphous Mg/Al mixed oxide} + (2+x)H_2O\uparrow + CO_2\uparrow \ldots 1\text{-}2$$

$$\text{Mg/Al mixed oxide} + A^{n-} + (2+x)H_2O \rightarrow Mg_{0.7}Al_{0.3}(OH)_2(A^{n-})_{0.3/n}\,xH_2O \ldots 1\text{-}3$$

1-2 Application of the LDH

The LDH, both as directly prepared, or after thermal treatment, has been widely applied in many fields, such as water treatment, catalysis, lubricants, drug delivery systems, polymer additives and other areas.[2] The variety of applications is due to their high versatility, easily tailored properties and low cost, which make it possible to produce material designed to fulfill specific requirements.

There has been considerable interest in the use of the LDH to remove negatively charged species by both of surface adsorption and anion exchange reactions. There has also been considerable interest in using LDHs to remove environmental contaminants from water systems since environmental pollution has emerged as an important issue in recent decades. Significant progress has been achieved in the research and development of LDHs'

application in environmental protection, such as their use as an environmental adsorbent in removing organic and inorganic wastes. The anion exchange capacity of the LDH is affected by the nature of the interlayer anions initially present. The LDH material has greater affinities for multivalent anions compared with monovalent anions.[3]

So far, inorganic anions adsorbed by the LDH material include oxo-anions (arsenite (H_3AsO_3 or $H_2AsO_3^-$), arsenate ($HAsO_4^{2-}$ or AsO_4^{3-}), chromate (CrO_4^{2-} or $Cr_2O_7^{2-}$), phosphate (PO_4^{3-} or HPO_4^{2-}), selenite ($HSeO^{3-}$ or SeO_3^{2-}), selenate ($HSeO^{4-}$ or SeO_4^{2-}), nitrate (NO_3^-),) and monoatomic anions (e.g. F^-, Cl^-, Br^-, I^-).[4] The reported adsorption capacities of LDHs for oxo-anions can be generally grouped into the following ranges: 0.1–87.5mg/g LDHs for arsenite (As(III)); 5–615 mg/g LDHs for arsenate (As(V)); 9–160 mg/g LDHs for chromate (Cr(VI));7.3–81.6mg/g LDHs for phosphate (as P); 29–270mg/g LDHs for selenite (Se(IV)); 14–20 mg/g LDHs for borate (as B); and 2.3–4.6 mg/g LDHs for nitrate (as N).

Oxo-anion adsorption by LDHs is influenced by several factors. For example, the pH during the adsorption reaction effects on the capacity for oxo-anion adsorption. In general, the adsorption of oxo-anions such as arsenate, chromate, phosphate, and selenite by LDHs tends to decrease with increasing pH. As(V) adsorption on LDHs has been reported as sensitive to changes in pH between 4-7,[5] whereas As(V) and Se(IV) adsorption on the LDHs is sensitive to changes in a wider pH range of 2-11.[6] For Cr(VI) adsorption on LDHs, Manju et al. and Terry et. al. have reported that high adsorption occurred at about pH 2.[7]

However, another study has reported that high Cr(VI) adsorption by the LDHs was favored at pH 6.[8] Das et. al. have reported that phosphate removal by LDHs reached a maximum at pH 5.[9] Chitrakar et al have reported pH of the maximum adsorption is pH 7.9.[10] Phosphate removal by LDHs was also studied from the viewpoint of the pH buffering effect by Seida and Nakano.[11] They revealed that the pH buffering effect of LDH worked effectively to enhance the phosphate removal through dissolution-coagulation and/or dissolution-precipitation processes.

The effect of competitive anions is also one of the influential factors. The effect of competing anions on As(III) adsorption by LDHs was found to reduce in the order HPO_4^{2-} >SO_4^{2-}> CO_3^{2-}>F->Cl^->Br^->NO_3^-,[12] while the interfering effects of competing anions on As(V) adsorption by LDHs were reported to follow the order HCO_3 >HPO_4^{2-}>SO_4^{2-}>Cl-,[13] and HPO_4^{2-}>(HCO_3^- and CO_3^{2-})> SO_4^{2-}>NO_3^- .[6] The adsorption behavior of Cr(VI) with various competing anions has also been studied.[14] For example, the amount of Cr(VI) released from LDHs by different competing anions followed the order CO_3^{2-}>Cl^->water.[14a] In phosphate adsorption by LDH, divalent anions were observed to have a profound interfering effect compared to the monovalent anions.[9] In general, it could be concluded that the anions of higher valence have a more significant interfering effect than the monovalent anions in the oxo-anion adsorption by LDHs. Among the divalent anions, HPO_4^{2-} appears to be the most competitive anion that retards the adsorption of other oxo-anions by the LDH. This may be due to stronger affinity of phosphate to the LDH material rather than other divalent anions.

1-3 Phosphate recovery systems from wastewater

Environmental pollution has become a major problem in the development of modern society. New technologies for improving and maintaining water quality are one of the highest priority issues due to increasing water and soil pollution and the consequent risks to both human health and the environment. The pollution due to the chemicals requiring remediation ranges from inorganic, (heavy metals, arseniate, chromate, cyanide, fluoride, etc.) to organic (petroleum by-products, pesticides, among others). In particular, inorganic anions have high solubilities in aqueous systems and constitute a widespread problem.

Inorganic anions are also less susceptible to sorption since most natural materials have negative surface charges. Oxyanions have a negative charge and some, such as arsenate, selenate, etc. are toxic to both humans and wildlife at either μg/L~mg/L levels.[15] However some oxyanions such as phosphate, nitrate, sulfate, chromate, molybdate, vanadate are useful resources for human life. They frequently have to be removed from an environment, but also can be recovered from water systems as a resource.

Phosphate is one of the most useful oxyanions and is an exhaustible and valuable resource since the phosphate is a mineral resource used as a fertilizer, in medicines, washing powders, etc. On the other hand, when a lot of phosphate goes into closed water systems such as lakes, bays and rivers, the phosphate becomes one of the causative agents for eutrophication of waterways. Phosphate is known to form several species depending on pH in solution. Figure 1-2 is a phosphate speciation diagram as a function of pH. In typical

environments, mildly acidic or mildly alkaline conditions are realistic for phosphate species. Therefore, the dominant phosphate species in the environment could be either $H_2PO_4^-$ or HPO_4^{2-}.

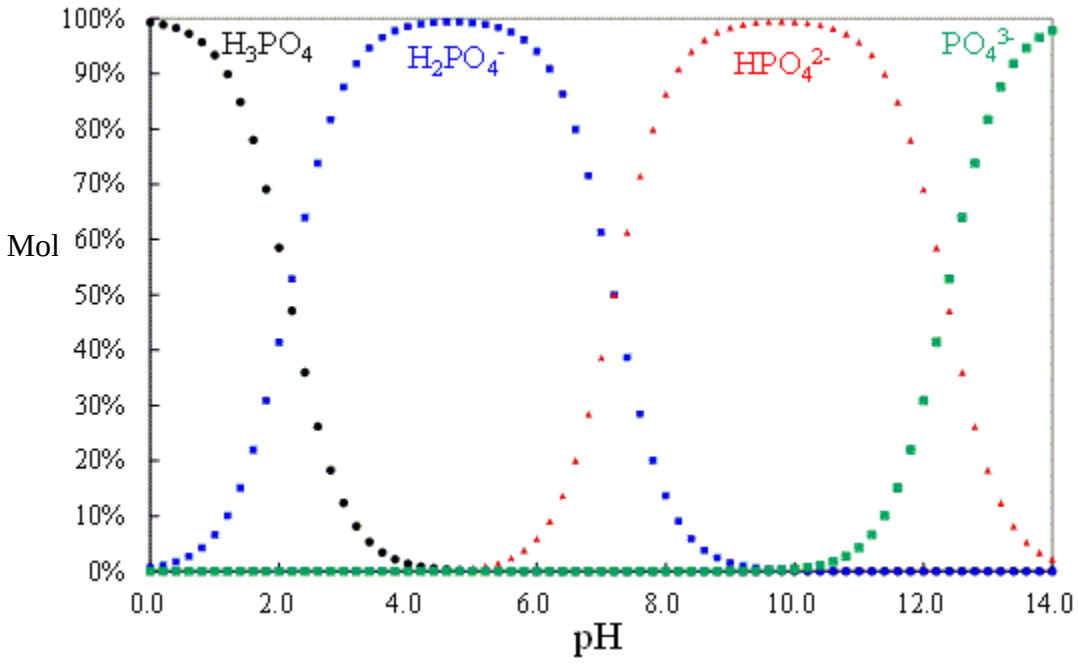

Figure1-2. The molar fraction of phosphate species as function of pH using dissociation constants; pK_1=2.15, pK_2=7.09, pK_3=12.32

Apart from the phosphates that are leached from natural mineral deposits, phosphates enter groundwater and wastewaters from agriculture and sewage disposal. However, the phosphates arising as potential pollutants from agricultural sources are in many parts of the world relatively small and isolated compared to the phosphate loadings contained in liquid urban wastes.[16] Sewage and urban wastewaters issues arise in large conurbations and in greater quantity and the potential for adverse environmental impact from the phosphates they contain are usually more serious.

Figure 1-3 is scheme of a typical water treatment system for recovery of phosphates from sewage. The treatment of sewage merely consist of the primary sedimentation of the solids, but nowadays the treatment also involves secondary treatment (aeration), so that the biological oxygen demand is reduced sufficiently for wastewaters to be discharged into natural bodies of water. Typical wastewaters from such treatments can contain 10-25 ppm.[17] Phosphates in solution can be precipitated by the addition of mild alkaline metal salts, such as those of calcium, magnesium and aluminum. The Hydroxyapatite(HAP: reaction1-4) and Monoammonium phosphate(MAP: reaction1-5) methods are traditional as the primary treatment for phosphate recovery.

HAP Method

$10Ca^{2+} + 2OH^{-} + 6PO_4^{3-} \leftrightarrow Ca_{10}(OH)_2(PO_4)_6$ …(1-4)

MAP Method

$Mg^{2+} + NH_4^{+} + PO_4^{3-} \leftrightarrow Mg(NH_4)(PO_4)$ …(1-5)

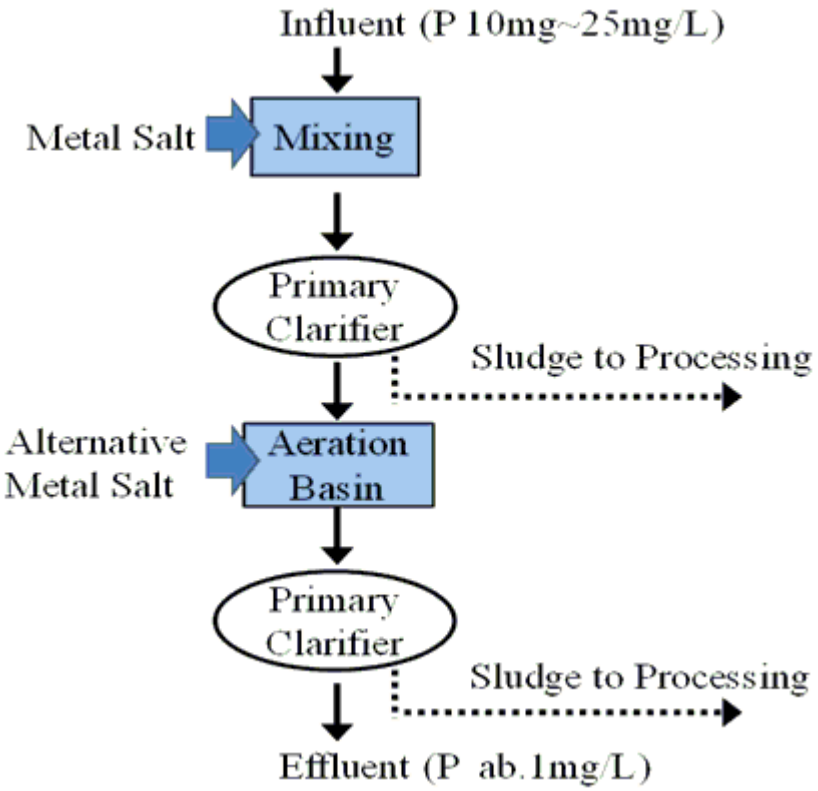

Figure 1-3. Scheme of typical water treatment system for recovery of phosphate from sewage

Phosphate content after the secondary clarifier goes down to around 1ppm. The pH of the solution after the primary treatment is likely to be mildly alkaline because of the mild alkaline metal salt used for phosphate recovery. The phosphate species after the primary treatment is mainly HPO_4^{2-}. The 1ppm of HPO_4^{2-} is lower than the concentration which the precipitation can be produced without using large amounts of the metal salt. Therefore, several adsorbents have been applied to remove phosphates from dilute solutions such as active carbon, ion exchange resins and anion clays.[4] In particular, LDH has been attracting attention as an adsorbent of phosphate from such dilute solutions. The LDH material has

succeeded in removing 99% phosphate from dilute concentrations (1ppm~0.2ppm).[4, 11, 18] Other interesting properties of LDHs assisting performance in this application include large surface area, high anion exchange capacity (2–3meq/g) comparable to those of anion exchange resins, recyclability and good thermal stability.[4] Some studies have reported that the reconstruction method leads to a higher adsorption capacity than the anion exchange method.[4] However, Shin et.al. reported the phosphate adsorption capacity of the LDH decreased following recycling by the reconstruction method and they pointed out that phosphate left in the interlayer may cause decreasing adsorption capacity.[19]

The general recycling process of phosphate recovery with the "reconstruction method" is described in Figure 1-4. After the reconstruction process, the intercalated phosphate is removed from the LDH material by anion exchange with carbonate since carbonate has the strongest affinity with the LDH material.[3b] However, all the phosphate cannot be removed by the anion exchange method. Some phosphate remains in the interlayer space. Previous research investigated the thermal behavior of phosphate intercalated Mg/Al-LDH and revealed that the interlayer phosphate is immobilized on the LDH layer by bonding to the metal cations of the LDH layer after thermal treatment above 150 ˚C.[20] This is the reason why the adsorption capacity of the LDH decreases when recycling by the reconstruction method. Therefore, these studies concluded that the anion exchange method is more appropriate for phosphate adsorption than the reconstruction method in term of recyclability, unless all the phosphate is removed before the calcination process. However, it is difficult to remove interlayer phosphate completely from LDH material by anion

exchange because phosphate (especially HPO_4^{2-} and PO_4^{3-}) has such a strong affinity to the LDH layer.

So far, the most efficient counter anions reported to remove phosphate from the LDH are probably carbonate or chloride, used with NaOH.[21] However, these reports have not achieved complete desorption of phosphate by anion exchange.

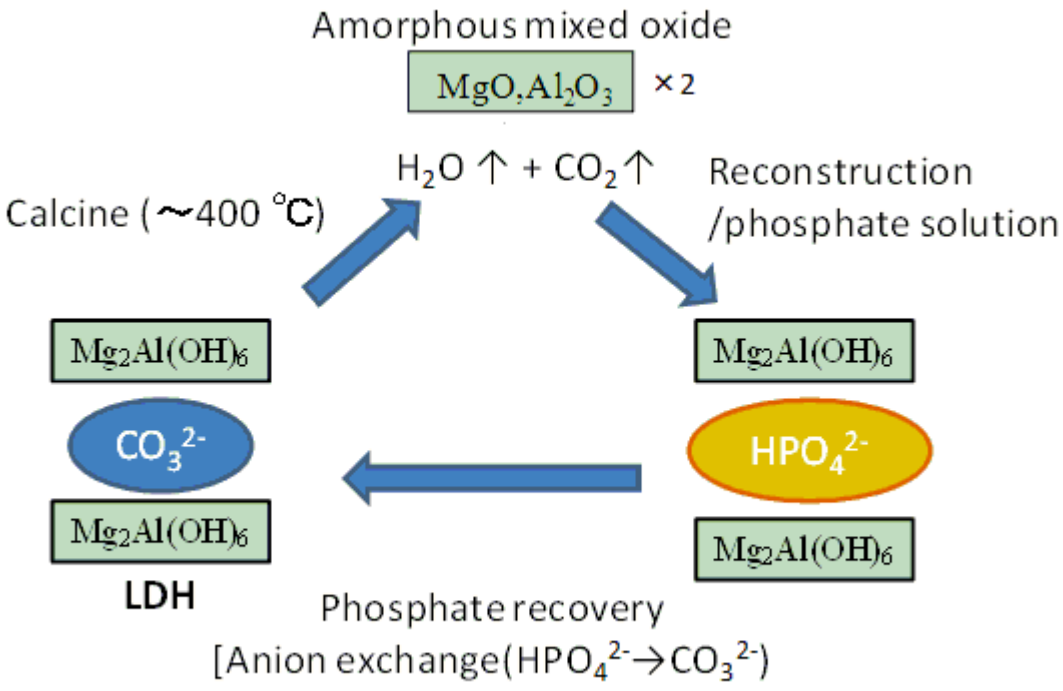

Figure 1-4. Schematic of phosphate recovery system by means of the reconstruction method of the LDH.

1-4 Catalyst application of calcined LDH material

Besides absorbent applications of the LDH material, LDH has been studied as a precursor of catalysts based on the metal oxides (Ni/Al, Co/Al, Cu/Zn and so on) since the two metal cations are well dispersed.[22] The LDH is transformed to the metal oxide by thermal treatment above 600 ˚C. These catalysts have been studied in the oxidation of phenol, decomposition of methanol, oxidation organic products such as acetic acid and acetone.[23] Recently, the photocatalysis properties of the metal oxides delivered from LDH materials such as in dye degradation, photodegradation of organic solvents in the gas-phase have attracted significant attention.[24]

The most popular LDH material as precursor of the photocatalysis material is the Zn/Al-layered double hydroxides (Zn/Al-LDH), also known as hydrotalcite-like materials. These are a kind of clay mineral with general composition $[Zn_{1-x}Alx(OH)_2]A^{n-}{}_x/n{\cdot}mH_2O$, where the value of the coefficient x is equal to the molecular ratio $Al^{3+}/(Zn^{2+}+Al^{3+})$, and A^{n-} is an anion with charge n. The metal oxide delivered from Zn/Al-LDH has similar photocatalytic properties to ZnO materials, widely used in gas sensors, photocatalysts, field-emission displays, and field-effect transistors because of it wide band gap energy and high exciton binding energy. The Zn/Al-LDH is usually calcined above 600 ˚C in order to transform the Zn/Al-LDH to crystalline metal oxide phase composed with ZnO and $ZnAl_2O_4$. On the other hand, the use of lower temperatures below 600 ˚C has rarely been studied for thermal treatments as a path to formation of the catalyst. This may be due to the amorphous structure of the calcined Zn/Al-LDH between 300 ˚C and 500 ˚C. Though this amorphous phase is thought of as a kind of metal oxide state, on the basis of thermal analysis results

showing dehydration reactions of the metal hydroxides occur around 300 ˚C,[25] the photocatalytic properties have rarely been studied.

The lower thermal treatment is important for the formation of LDH materials on metal substrates, especially if the substrate has a low melting point, such as zinc (melting point:416 ˚C). Since ZnO is a material considered for UV sensors or solar cell devices, the calcined Zn/Al-LDH on zinc substrates have potential applications in these new types of UV sensors or solar cell devices. This photoelectrode synthesis should be simplified because it does not require expensive equipment or large scale devices such as sputtering or chemical vapor deposition for fabrication. There appear to be no reports on the study of photoelectrodes from calcined Zn/Al-LDH on zinc substrates. This is because research has rarely been reported on the fabrication of Zn/Al-LDH on zinc substrates, despite the potential advantages in adhesion and film growth.

1-5 Objectives of this study

In this PhD research, two distinct applications of LDHs have been investigated. The first is in the development of an efficient phosphate recovery system using the LDH. Improved phosphate desorption from the LDH by an anion exchange method has been demonstrated. Surfactant anions are chosen as a counter anion to interlayer phosphate. Linear alkyl sulfonate or alkylbenzene sulfonate have been selected as surfactant anions in this study because the linear alkyl sulfonate or alkylbenzene sulfonate are known as low risk

chemicals for humans and the environment. These are low-cost materials and biodegradable since the linear alkyl sulfonate or alkylbenzene sulfonate are used as the main chemical components of dish detergent and laundry detergent.[26]

The effect of phosphate desorption as a function of surfactant anion species, anionic surfactant conditions such as concentration and reaction time, has been investigated to achieve complete phosphate desorption from the LDH material. To understand the mechanism of the surfactant effect for phosphate desorption, the LDH material after the phosphate desorption reaction has been characterized by X-ray diffraction, Fourier Transform Infrared Spectroscopy and Scanning Electron Microscopy. The recycle properties of this method have been compared with conventional methods using highly concentrated sodium carbonate solutions (1.0M)[27] and mixed solutions of sodium chloride and sodium hydroxide (1.0M and 0.1M).[21]

The second topic of this research is in developing new photoelectrodes derived from the Zn/Al-LDH materials deposited on zinc substrates by thermal treatment. The LDHs present an interesting templating system as precursors for highly doped thin films in this case for photoactive applications. Since the melting point of zinc substrate is 416 ˚C, the thermal treatment has to be below the melting point of zinc metal. Therefore, thermal behavior of the Zn/Al-LDH powder material has been investigated below the melting point of zinc metal. The single phase Zn/Al-LDH powder is synthesized by co-precipitation method using urea in order to simplify the thermal behavior. The calcined Zn/Al-LDH powder

sample is characterized by TG-DTA, XRD, XANES and a UV-diffuse reflection method.

The Zn/Al-LDH is fabricated on zinc substrates by hydrothermal treatment. The conditions of the Zn/Al-LDH fabrication are optimized to form a single phase of the Zn/Al-LDH without impurity materials by varying hydrothermal temperature and reaction time. The Zn/Al-LDH on the zinc substrate is then thermally treated. The synthesized Zn/Al-LDH and calcined material were characterized by XRD, SEM and XPS. The photocatalysis properties of the calcined Zn/Al-LDH were investigated under 365 nm light using a conventional potentiostat.

Chapter 2:

Experimental procedure and characterization methods

2-1 Formation of LDH material

2-1-1 Synthesis of carbonate intercalated Mg/Al-LDH

Intercalation of hydrogen phosphate into the interlayer of LDH is conducted in three steps. The first step is the synthesis of carbonate intercalated LDH which follows the reaction 2-1

$$0.66MgCl_2\cdot 6H_2O+0.34AlCl_3\cdot 6H_2O+3.5CO(NH_2)_2\rightarrow$$

$$Mg_{0.66}Al_{0.34}(OH)_2(CO_3)_{0.5}\cdot H_2O+7NH_4Cl+3CO_2+1.5H_2O\ldots(2\text{-}1)$$

Table 2-1 shows the experimental conditions for synthesis of carbonate intercalated Mg/Al-LDH and observed data of the carbonate intercalated Mg/Al-LDH. $MgCl_2\cdot 6H_2O$, $AlCl_3\cdot 6H_2O$ and urea were dissolved in de-ionized water to give the final concentrations of Table 2-1. After the mixed solution was refluxed under continuous stirring for 48 h (Figure 2-1), the resulting white solid was filtered, washed twice with deionized water and finally dried under a reduced pressure for 12 h.

Table2-1 Experimental conditions for the synthesis of carbonate intercalated Mg/Al-LDH

The quantity of starting materials for preparing					Observed data	
Mg / mM	Al / mM	Urea / mM	Mg/Al	urea/(Mg+Al)	*1pH	*2Mg/Al
6	2	160	3	20	9.5	1.97

*1 pH of resulting suspension.*2 Mg/Al is white powder after drying

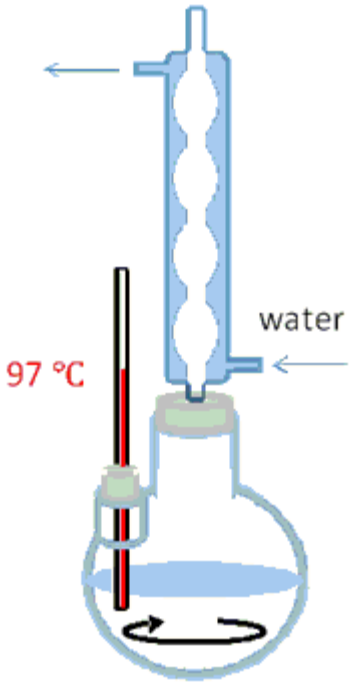

Figure 2-1. Schema of reflux conditions to prepare carbonate intercalated Mg/Al layered double hydroxides

2-1-2 Anion exchange interlayer carbonate for chloride

Interlayer carbonate is exchanged to chloride by the method reported by Iyi.[28] A portion of the product (0.1 g) was suspended in an aqueous solution (100 mL) containing NaCl (0.5 mol) and HCl (3.3 mM) to expel carbonate species. The suspension was stirred for 24 h at room temperature and filtered. (reaction 2-2).

$$Mg_{0.66}Al_{0.34}(OH)_2(CO_3)_{0.50}\text{-}H_2O+0.5NaCl+0.5HCl\rightarrow$$

$$Mg_{0.66}Al_{0.34}(OH)_2(Cl)_{0.34}\cdot H_2O+0.5NaHCO_3 \ldots (2\text{-}2)$$

The resulting white solid was filtered, washed twice with deionized water and finally dried under a reduced pressure for 12 h.

2-1-3 Anion exchange interlayer chloride for phosphate

HPO_4^{2-} was intercalated into LDH by an anion-exchange with interlayer Cl^- ions of the precursor LDH (abbr. as LDH-Cl). The precipitate was washed twice with deionized water to obtain a white slurry of LDH-Cl which was further dispersed in a 0.1 M KH_2PO_4 aqueous solution (200 mL) at pH 9.8 adjusted using NH_3. The speciation as HPO_4^{2-} in the solution is 99.5 % at this pH value calculated from the dissociation constants (reaction 2-3).

$$Mg_{0.66}Al_{0.34}(OH)_2(Cl)_{0.17}\cdot H_2O + 0.5KH_2PO_4 + 0.5NH_3 + 0.5H_2O \rightarrow$$
$$Mg_{0.66}Al_{0.34}(OH)_2(HPO_4)_{0.17}1.02H_2O + 0.5KCl + 0.5NH_4Cl + 0.498H_2O \quad \ldots(2\text{-}3)$$

The amount of excess KH_2PO_4 was more than 10 times that of the Al^{3+} ion in the LDH. The dispersion was stirred for 12 h at 35 ˚C followed by filtration. The precipitate was washed with deionized water, filtered again and dried at room temperature under N_2 to obtain a white product of LDH-HPO_4.

2-2 Phosphate desorption methods

LDH-HPO_4 (10 mg) was suspended in surfactant aqueous solutions (40 mL) and the suspension was stirred at 35 ºC for between 0.5 h to 96 h and then filtered. Surfactant anions used in this study are 1-Octanesulfonate (OS), dodecylbenzenesulfonate (DBS) and dodecylsulfate (DS). The concentrations of the surfactants were adjusted from 0.0001 M to 0.3 M. The resulting precipitate was washed with deionized/purified water (Milli-Q) and was dried in air before experimental measurements. The filtrate was collected to determine the amount of desorbed phosphate from the solid sample. The LDH precipitation was mixed with surfactant solutions. The desorption ratio (D) was calculated using the equation below(equation II-I), where $(P/Al)_{before}$ and $(P/Al)_{after}$ represent the atomic ratio of P/Al in the LDH before and after the anion-exchange with the counter anions, respectively.

$$D(\%) = \frac{(P/Al)_{before} - (P/Al)_{after}}{(P/Al)_{before}} \times 100 \qquad \text{...(II-I)}$$

2-3 Synthesis of carbonate intercalated Zn/Al-LDH

Synthesis of highly crystalline Zn/Al-LDH was conducted using the method described by Sasaki's group.[29] $ZnCl_2$, $AlCl_3$ and urea were dissolved in Mill-Q water to give final concentrations of 5mM, 2.5mM and 20mM, respectively. The mixed solution was stirred at 95 ˚C for 24 hours under reflux conditions. The chemical reaction in the solution under reflux condition was as below(reaction 2-4),

$0.66ZnCl_2+0.34AlCl_3{\cdot}6H_2O +3.5CO(NH_2)_2\rightarrow$

$$Zn_{0.66}Al_{0.34}(OH)_2(CO_3)_{0.17}xH_2O+7NH_4Cl + 3.3CO_2 + (1.2-x)H_2O \quad \ldots(2\text{-}4)$$

The resulting white solid was filtered, washed twice with de-ionized water and finally dried at 80 ˚C for 12h. The chemical formula of synthetic Zn/Al-LDH was determined by ICP-AES and TG-DTA analysis as $Zn_{0.65}Al_{0.35}(OH)_2(CO_3)_{0.17}0.95H_2O$.

2-4 Zn/Al-LDH fabrication on Zinc substrate by hydrothermal treatment

The Zn/Al-LDH was fabricated on Zinc metal substrate by hydrothermal treatment. The zinc substrates were cleaned with HCl solution (0.1M) in order to remove the oxide material on the surface. The zinc substrate was then soaked in a mixed solution of $AlCl_3 \cdot 6H_2O$ and urea, at concentrations of 5mM and 10mM, respectively and placed in a 100mL autoclave constructed of stainless steel with a Teflon^R(Polytetrafluoroethylene) interior (Figure 2-2). The autoclave was then subjected to different combinations of temperature and reaction time. After the reaction, the zinc substrate was washed with milli-Q water under sonication for a few seconds and was dried under atmosphere overnight. Characterization was carried out using XRD and SEM.

Figure 2-2. Picture of the autoclave vessel which was made of stainless steel (outside vessel), with the inside lined with a Teflon resin.

2-5 Characterization

- X-ray diffraction (XRD)

Most spectra were recorded on a Rigaku MiniFlex diffractometer using Ni-filtered CuKα radiation (λ=0.1541 nm) with a graphite monochromator, operating at 30 kV and 15 mA. Data were collected over a 2θ range of 5-65˚ with a step size angle of 0.02˚ and a scanning speed of 2˚min^{-1}.

Indexing was conducted by using equation II-II,[30] where *h,k,l* represent index number, the *d* is constant parameter, a and c are lattice parameter *a* and *c*.

$$\frac{1}{d^2} = \frac{4}{3} \times \frac{h^2+hk+k^2}{a^2} + \frac{l^2}{c^2} \quad \ldots(\text{II-II})$$

Calculated constant parameter (d_{cal}) was calculated by using equation II-II with adjusting index number. The d_{cal} was compared with observed constant parameter (d_{obs}) in order to obtain correct index number. The lattice parameter *a* and *c* are estimated with the equation II-II and reported lattice constant of surfactant intercalated LDH, for example, $3 \times d_{003}=c$, and $2 \times d_{110}$=a, respectively.[31]

- Thermogravimetry-Differential thermal analysis(TG-DTA)

DTA/TG was carried out using a ShimadzuDTA-50 instrument under N_2 flow with a heating rate of 1 K min^{-1} from room temperature to 1000 C and with $\alpha-Al_2O_3$ as a reference material.

- Fourier Transform Infrared Spectroscopy (FT-IR)

FT-IR spectra were obtained using a Perkin Elmer Spectrum100 FT-IR spectrometer over the range of 500–4000cm^{-1}.

- Inductively Coupled Plasma-Atomic Emission Spectroscopy (ICP-AES)

Atomic ratio (Mg/Al, P/Al and Zn/Al) of samples were determined by ICP-AES (SPS 3500, Hitachi-High-Tech Science Corporation).

- Scanning Electron Microscopy(SEM)

SEM images were obtained using a Hitachi S-4700 scanning electron microscope with an accelerating voltage of 10 kV. Samples were attached to a metal mount and lightly coated with platinum to reduce surface charging.

- X-ray photoemission spectroscopy (XPS)

XPS spectra were recorded using a Sigma Probe, Thermo Scientific. XPS measurements were carried out using Al-K X-rays at 1489.6 eV, with a source width 0.85 eV. The position of the C1s peak of adventitious hydrocarbon was taken as a standard with a binding energy of 285.0 eV.

- X-ray absorption near-edge structure (XANES)

XANES measurements were conducted at the Australian Synchrotron on the soft X-ray beamline, using an elliptically polarized undulator and a grating monochromator capable of providing photons in the energy range between 100 and 2500 eV. The Zn L-edge (1020-1060eV), and Al K-edge (1555-1595 eV) regions were examined. Photoemission spectra were measured with a SPECS Phoibos, 150 mm mean radius electron energy analyser. The Au 4f7/2 core level was used to calibrate the photon energy. The XANES measurements were carried out in fluorescence yield mode (FLY).

- Photo current measurement

Photocurrent of samples were measured using a three electrode potentiostat (working electrode, counter electrode and reference electrode) in methanol. Figure 2-3 shows a schematic of the system. The working electrode was a sample of the zinc substrate, whilst the counter electrode was platinum, and the reference electrode was composed of silver metal wire and a silver chloride electrolyte. Methanol was used to scavenge the holes from the sample.[32] High pressure mercury, which has a maximum peak at 365 nm was used as light source for the photocatalysis experiment. Figure 2-4 shows UV light spectrum of the high pressure mercury lamp.

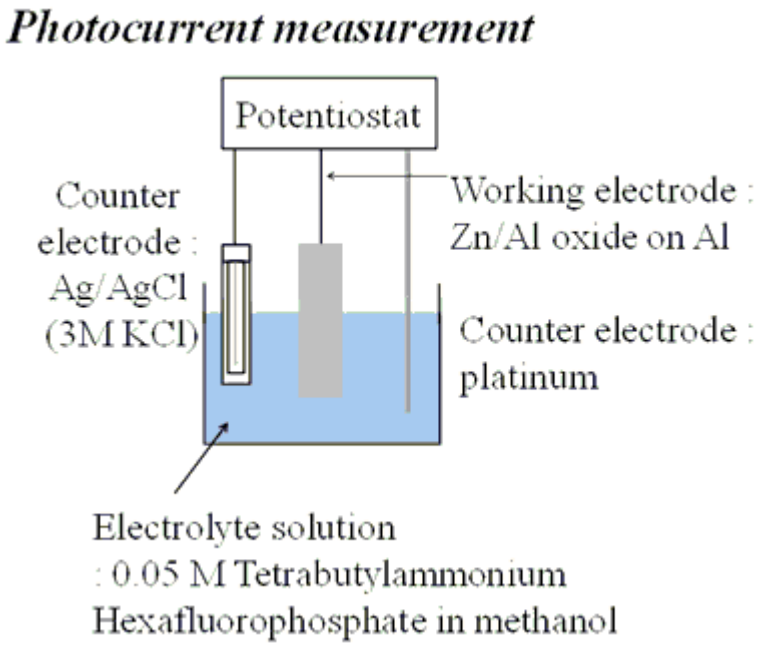

Figure 2-3. Configuration for Photocurrent measurements of the surface films with a potentiostat

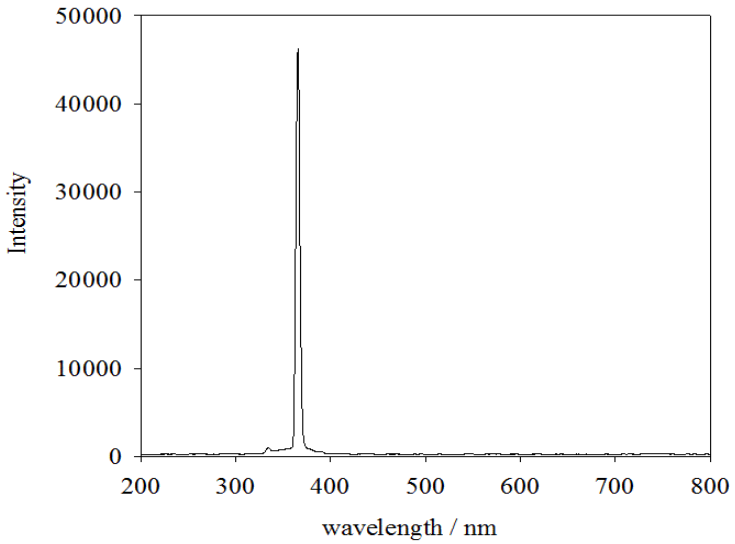

Figure 2-4. UV spectrum of the high pressure mercury lamp

- UV-vis diffuse reflection (UV-vis DR)

The band gap energy of the sample was examined by UV-VIS DR

The UV-VIS DR spectra were converted by the Kubelka-Munk equation II-III.

$F(R_\infty) = (1-R_\infty)^2/2R_\infty$ - Kubelka-Munk equation …(II-III)

Where $F(R_\infty)$ is called the remission or Kubelka-Munk function, and the diffuse reflection of the examined sample is $(R_\infty) = R_{sample}/R_{standard}$.

Chapter 3:

Complete desorption of interlayer hydrogen phosphate in Mg/Al-layered double hydroxides (Mg/Al-LDH) by means of anion exchange with 1-octanesulfonate

3-1 Previous studies of phosphate adsorption with LDH materials.

Many kinds of inorganic adsorbents, including paddy field soil, have been tested for the removal of phosphates in groundwaters.[33] Since the LDH structure possesses anion exchange capacity, these materials have been used as an anion exchanger, replacing the interlayer anion with phosphate, and it has been reported that some types of LDH adsorb phosphate in water by making insoluble metal phosphate salts; for example Ca/Al-LDH adsorbs phosphate and forms an insoluble hydroxyl apatite or $Ca_3(PO_4)_2$.[34]

Radha *et al*. have also reported that $MgHPO_4 \cdot 3H_2O$ and $(NH_4)MgPO_4 \cdot H_2O$ are formed at low pH and $NH_4MgPO_4 \cdot H_2O$ is formed under neutral conditions, although intercalation of phosphate occurred under basic conditions when Mg^{2+} was used as the divalent metal cation.[35] When ZrO_2 is incorporated in the interlayer region of LDH, phosphate is adsorbed on the surface of nano-size ZrO_2 particles.[36] High phosphate loading, up to 300 mgP/gLDH, has been reported when calcined Mg/Al-LDH was used with some of the Al^{3+} replaced by Fe^{3+}.[37] The unexpectedly high loading of phosphate probably includes adsorption onto the LDH particles. Early studies by Badreddine *et al*., Khaldi *et al*. and Ookubo *et al*. have reported that hydrogen phosphate is intercalated by means of anion exchange with interlayer chloride of the pristine Zn/Al/Cl-LDH and Mg/Al/Cl-LDH[38], respectively. Nomura et. al. reported that in Mg/Al/Cl-LDH, phosphate is intercalated by anion exchange with interlayer chloride.[18] As part of this work, it has been reported that the crystal morphology of the pristine LDH is maintained after the intercalation of hydrogen phosphate, and $Mg_3(PO_4)_2$ has been observed in XRD patterns after heating the resulting Mg/Al/HPO_4-

LDH at 1273K.[39] High selectivity for phosphate has also been reported when calcined Zn/Al-LDH was used.[34c]

Since the phosphate is a natural resource steadily being exhausted and uncontrolled release into the environment is undesirable, effective methods of capture and recovery of phosphate are required.[9] For this purpose, adsorbed phosphate should be released by desorption into water. LDH is a candidate material as an anion exchanger for adsorption/desorption of inorganic phosphate in water. Das *et al*. have reported that a maximum desorption of 63% was achieved when an aqueous solution containing 0.1M NaOH and 4M NaCl was used in anion exchange of the interlayer phosphate.[9] It has been noted that care should be taken not to overestimate the amount of desorbed phosphate in spectrophotometric measurements since fine LDH particles pass through the membrane filter used in the separation of sample solutions containing desorbed phosphate from the particles, and are dissolved in the solution when the solution is acidified.[35]

On the other hand, intercalation of anionic surfactants as interlayer anions of LDH has been reviewed and a linear dependency of the basal spacing on the alkyl chain length of the surfactants has been reported.[40] Among the anionic surfactants trialed, 1-octanesulfonate ($C_8H_{17}O_3S$; OS) has rarely been used in the intercalation of LDH probably because the basal spacing of the intercalated LDH is smaller than that of the other aliphatic surfactants such as Dodecyl Sulfate (=$C_{12}H_{25}SO_4^-$:DS) and Dodecyl benzene Sulfonate (=$C_{12}H_{25}C_6H_4SO_3^-$:DBS).[41]

In this chapter, the interlayer hydrogen phosphate of synthetic Mg/Al/HPO_4-LDH was eliminated by anion exchange with chloride, carbonate and OS. Among the three types of exchanging surfactant anions trialed in this study, OS was the most effective and the interlayer phosphate was completely eliminated following two treatment steps with an aqueous solution of OS.

3-2 Complete desorption of interlayer phosphate from LDH

The phosphate intercalated Mg/Al-LDH(LDH-HPO_4) was synthesized by the co-precipitation method using carbonate intercalated Mg/Al-LDH(section:2-1) and anion exchange to phosphate (section:2-2 and 2-3). The chemical formula of the synthesized LDH-HPO_4 was $Mg_{0.66}Al_{0.34}(OH)_2HPO_{0.17}1.07H_2O$ with a loading of 57.3 mgP/gLDH.

Interlayer phosphate was removed from the LDH by exchange and the reaction reached equilibrium after a certain reaction time (see figure 3-1). Desorption of the interlayer HPO_4^{2-} from LDH-HPO_4 was carried out by treating the LDH with aqueous solutions of sodium 1-octanesulfonate (OS; 0.3 M).

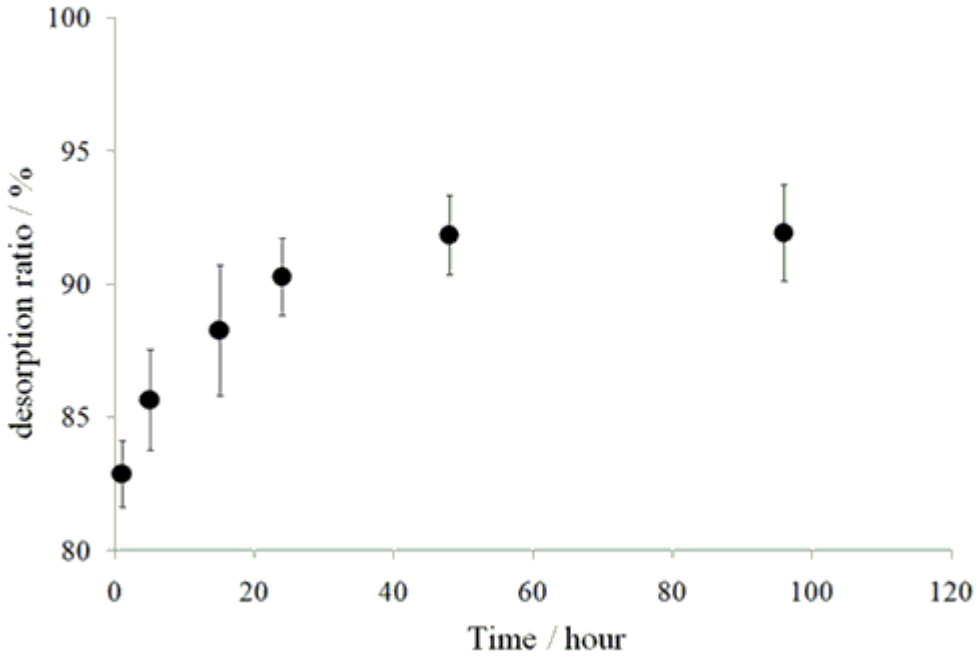

*Figure 3-1. Time dependence of HPO_4^{2-} desorption from LDH-HPO_4 with OS. The data points represent the mean of three repeat experiments with the spread in data given by the error bars. *pH after reaction for 48 hours*

Figure 3-1 shows the HPO_4^{2-} desorption ratio vs. reaction time with an aqueous solution of OS (0.3 M). The ratio increased rapidly until around 15 hours and then increased more gradually up to 48 hours. Since the desorption ratio did not change for reaction times longer than 48h, the HPO_4 desorption was considered to have reached equilibrium at this time, with an equilibrium desorption ratio of 92.0 ± 1.8 %, and all further experiments were carried out for this length of time. When the HPO_4^{2-} desorption with OS was conducted a second time, the desorption ratio went to 100 % and no phosphate was detected in the

analysis of the anion-exchanged solid. The effective elution of the interlayer hydrogen phosphate has been reported when an aqueous solution of Na_2CO_3 (1.0 M) was used.[42] An NaCl-NaOH mixed solution has also been reported as another effective anion-exchanging solution to remove HPO_4 from LDH.[21]

In this study, these two aqueous solutions were tested for comparison and the results are listed in Table 3-1, together with the result of anion-exchange when using OS solution. Aqueous solutions of Na_2CO_3 (0.1M) and NaCl (0.9M) +NaOH (0.8M) were used for the elution. The Mg, Al, phosphate and OS amounts were measured by ICP-AES and the chemical speciation of phosphate was predicted based on the pH of the solution. The amount of water was calculated from the mass remaining after subtraction of the species measured above. The desorption ratio D, when using OS was much higher than for the other two solutions, which removed only around 59 and 46% of the phosphate respectively. The low D values observed for the LDH(Na_2CO_3) and LDH(NaCl+NaOH) did not increase when the reaction time was increased to 96 h.

Table3-1. Desorption ratio of hydrogen phosphate from LDH-HPO_4^{2-} using different solutions

Name	D / %	pH*	Chemical formula
LDH(OS-1)	93.3	9.2	$Mg_{0.65}Al_{0.35}(OH)_{2.01}(HPO_4)_{0.01}(CH_3(CH_2)_7SO_3^-)_{0.31}0.35H_2O$
LDH(OS-2)	100	9.2	$Mg_{0.65}Al_{0.35}(OH)_{2.02}(CH_3(CH_2)_7SO_3^-)_{0.33}0.29H_2O$
LDH(Na_2CO_3)	58.8	11.6	$Mg_{0.67}Al_{0.33}(OH)_{2.0}(HPO_4)_{0.04}(PO_4)_{0.03}(CO_3)_{0.12}0.68H_2O$
LDH(NaCl-NaOH)	46.4	13.4	–

3-3 Intercalation of 1-octanesulfonate into LDH by anion exchange with interlayer phosphate

Figure 3-2 shows XRD patterns of LDH-HPO_4, LDH (Na_2CO_3), LDH (NaCl-NaOH), LDH (OS-2), and LDH(OS-2) following heating to 1000 °C. The XRD pattern of LDH-HPO_4 was similar to that which has been previously reported.[39] In the XRD patterns of LDH(Na_2CO_3) and LDH(NaCl-NaOH), in addition to the LDH-HPO_4 phase, other peaks assigned to Mg/Al/CO^3-LDH were also observed.[43] Therefore, it is concluded that both LDH(Na_2CO_3) and LDH(NaCl-NaOH) are mixtures of the pristine LDH and Mg/Al/CO_3-LDH. This is not due to insufficient reaction time, since increasing the time to 96 h in the desorption experiments did not increase the D value. On the other hand, the XRD pattern of LDH(OS-2) is the same as that reported previously for Cu/Al-LDH with interlayer 1-octanesulfonate.[40] All peaks in the XRD pattern of LDH(OS-2) are indexed as a single phase having a hexagonal unit cell with the R3m structure of hydrotalcite and following the

–h+k+l≠3n rule. The parameters for this phase were determined as c_0=6.19 nm and a_0=0.31 nm. Table3-2 shows the indexing of both LDH-HPO_4 and LDH (OS-2). The basal spacing calculated from the (003) diffraction peak of LDH (OS-2) was 2.05 nm, whereas that of LDH-HPO_4 was 1.06 nm. Thus the interlayer spacing is increased by the intercalation of the larger OS anion. Metal phosphates were not detected in the XRD pattern of LDH(OS-2) heated at 1000 $^{\circ}$C indicating clearly that the phosphate was completely removed from the interlayer space of LDH(OS-2) due to the anion exchange of HPO_4^{2-} with 1-octanesulfonate.

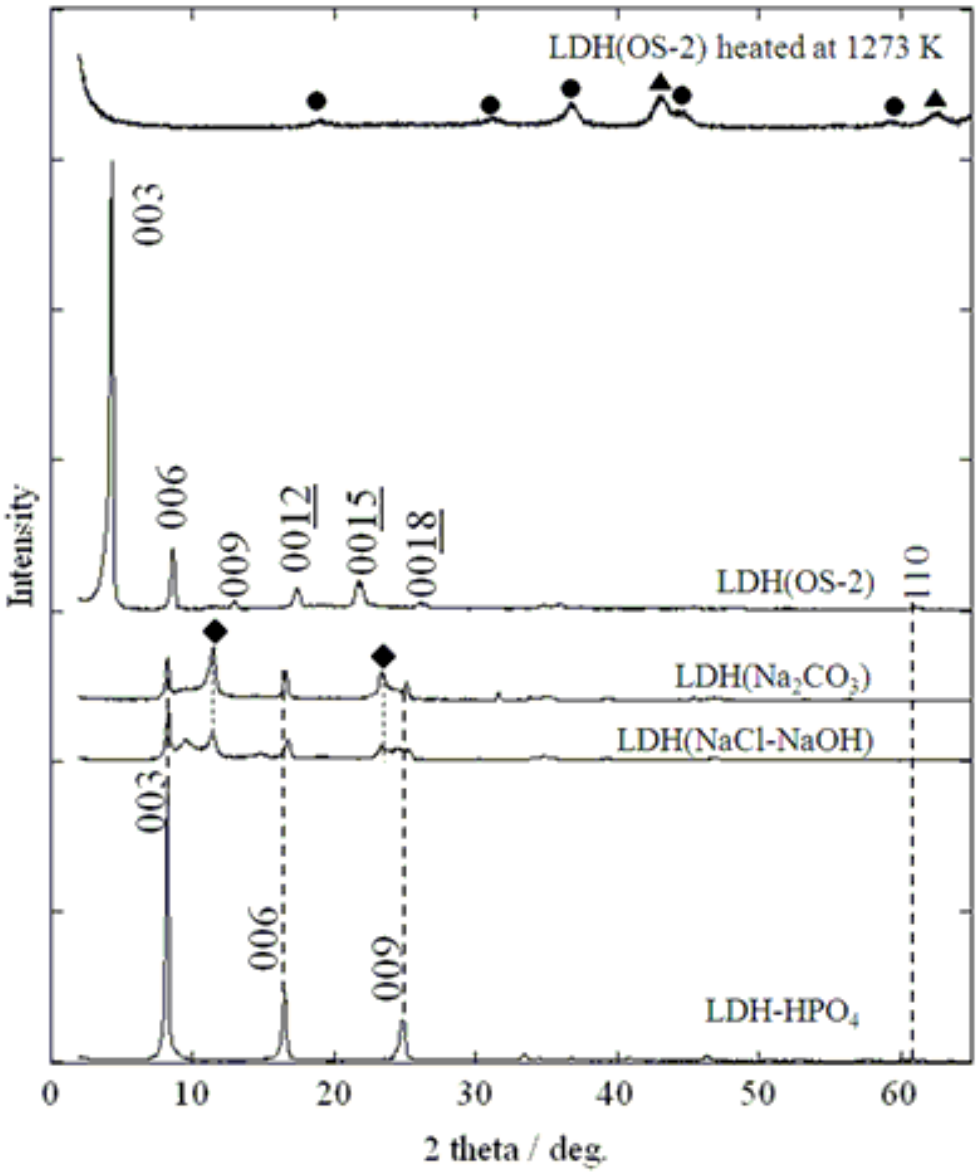

Figure 3-2. XRD patterns of LDH-HPO_4, LDH (NaCl-NaOH),, LDH (Na_2CO_3), LDH (OS-2), and LDH(OS-2) heated at 1273 K. ●: $MgAl_2O_4$, ▲:MgO and ♦ :carbonate intercalated Mg/Al-LDH

Table 3-2. Indexing of the XRD patterns with lattice constants of LDH-HPO_4 and LDH (OS-2)

LDH-HPO_4			LDH(OS-2)		
Obs.	Calc.		Obs.	Calc.	
d/ nm	*hkl*	d/ nm	d/ nm	*hkl*	d/ nm
1.06	0 0 3	-	2.05	0 0 3	-
0.530	0 0 6	0.527	1.03	0 0 6	1.03
0.356	0 0 9	0.352	0.697	0 0 9	0.69
0.266	0 0 12	0.265	0.515	0 0 12	0.52
0.259	0 1 2	0.260	0.411	0 0 15	0.413
0.244	0 1 5	0.244	0.343	0 0 18	0.344
0.221	0 1 8	0.219	0.260	0 1 2	0.262
0.195	0 1 11	0.194	0.153	1 1 0	-
0.180	1 0 13	0.170	a_0/nm	0.31	
0.173	0 1 14	0.172	c_0/nm	6.19	
0.160	0 1 16	0.158			
0.152	1 1 0	-			
0.151	1 1 3	0.151			
0.147	1 1 6	0.146			
a_0/nm	0.31				
c_0/nm	3.18				

Figure 3-3 shows FT-IR spectra of sodium 1-octanesulfonate (NaOS), LDH(OS-2) and LDH-HPO_4. The spectrum of NaOS shows strong absorption bands at 2957, 2920, 2873 and 2852 cm^{-1} all of which are assigned to the C-H stretching vibrations of the alkyl chains in OS.[44] The strong absorptions at 1179cm^{-1} and 1052 cm^{-1} are also assigned to the S-O stretching vibration band in the $–SO_3$ group of OS.[45] These absorption bands are also detected in the spectrum of LDH (OS-2), together with some characteristic bands due to LDH around 3340 cm^{-1} for an O-H stretching vibration and around 1650 cm^{-1} for an H-O-H bending vibration of the interlayer water molecule. In the spectrum of LDH-HPO_4, absorption bands due to the LDH are observed together with both symmetrical and asymmetric absorption bands assigned as ν_{as}(P-O), ν_s(P-O), ν_{as}(P-OH) and ν_{as}(O-P-O) at 1093, 960, 844 and 563 cm^{-1} respectively, all due to the interlayer hydrogen phosphate.[46] The spectrum indicates that the phosphate is in a similar environment to HPO_4^{2} in solution.[47]

These bands of interlayer HPO_4^{2-} were not observed in the spectrum of LDH(OS-2), indicating again that the interlayer hydrogen phosphate was fully exchanged with OS. All of the absorption bands observed in the FT-IR spectra are indexed in Table3-3.
It has been pointed out that anion exchange proceeds more readily when an anion with large anionic charge is used.[3b] From this point of view, divalent anions such as carbonate, phosphate and sulfonate are preferable as the exchanging anion in solution.

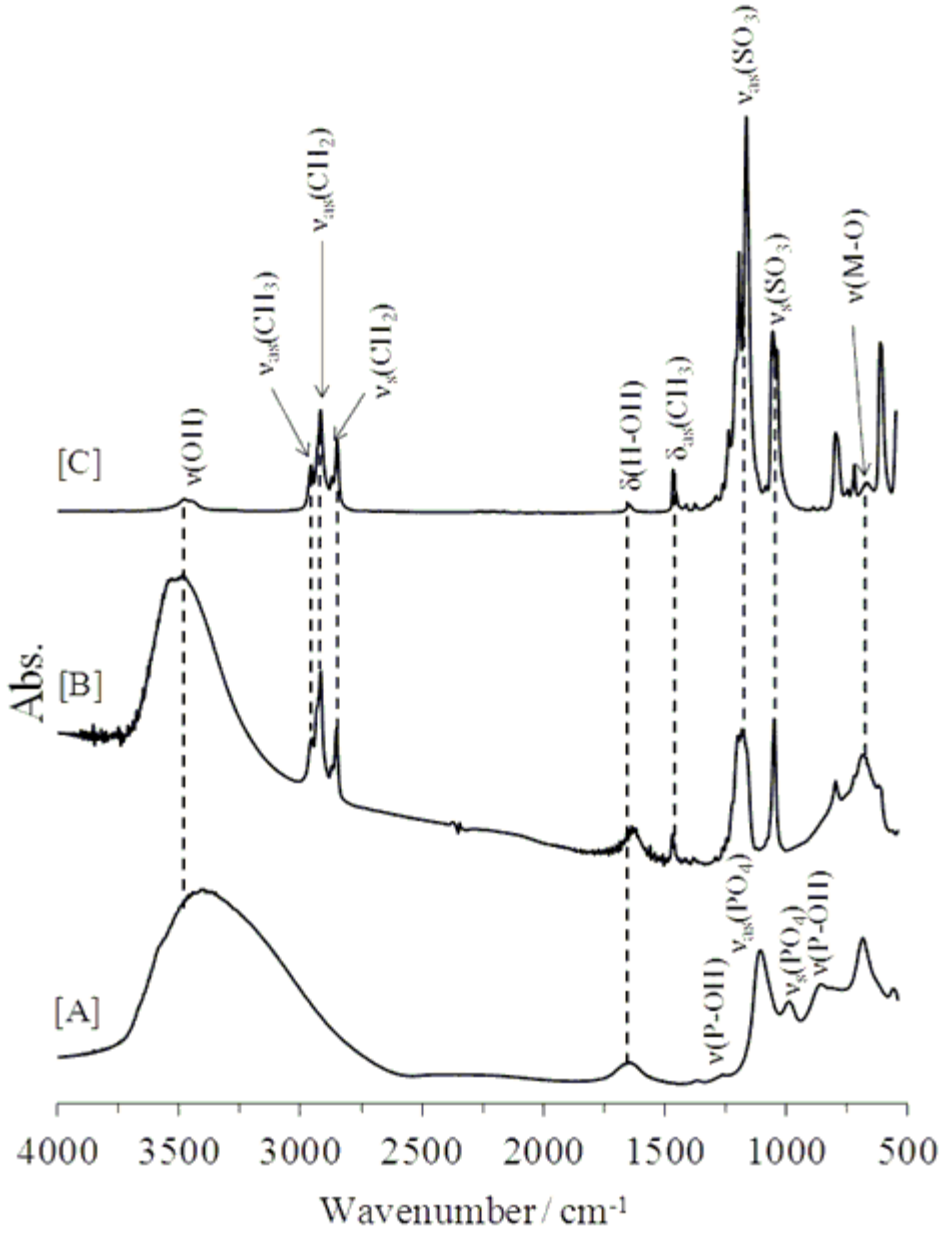

Figure 3-3. FT-IR spectra of LDH-HPO_4[A], LDH(OS-2)[B] and Sodium 1-Octanesulfonate[C]

Table 3-3. Indexing of IR absorption bands[j] , in $cm^{-1,}$ for LDH(OS-2), LDH-HPO_4 and Sodium 1-octanesulfonate(Na-OS).

Na-OS	LDH-OS 2nd	LDH-HPO_4	Assigment
3483	3484	3400	ν(OH)
2957	2954		$\nu_{as}(CH_3)$
2920	2917		$\nu_{as}(CH_2)$
2873	2872		$\nu_{s}(CH_3)$
2852	2852		$\nu_{s}(CH_2)$
1654	1650	1650	δ(H-OH)
1470	1467		$\delta_{as}(CH_3)$
1179	1180		$\nu_{as}(SO_3)$
		1097	$\nu_{as}(PO_4)$
1052	1048		$\nu_{s}(SO_3)$
		975	$\nu_{s}(PO_4)$
		840	$\nu_{as}(OPO)$
	685	680	ν(M-O)

This was not the case in the present study, however, since the interlayer anion used in the desorption experiment is divalent HPO_4^{2-} and the exchanging 1-octanesulfonate is a monovalent anion. The high desorption ratio when using OS may be due to the large concentration (0.3 M) of the exchanging OS in the solution. However the basal spacing of the LDH-OS was also significantly larger than that of LDH-HPO_4, whereas carbonate intercalated Mg/Al-LDH had a smaller basal spacing than that of the LDH-HPO_4. It is thought that increasing the interlayer spacing decreases the interaction between the interlayer phosphate and the LDH layers and enhances phosphate desorption. Thus the ease of desorption is not necessarily dictated by the type of anion species used for the exchange,

but rather the strength of the bonding between the original intercalated species and the LDH layer.

The high desorption efficiency observed in this work when using OS is thought then to be related to the two factors; the OS concentration and the resultant interlayer spacing when intercalating the species into the interlayer gallery. The former factor is advantageous for increasing the concentration difference of 1-octanesulfonate between the interlayer space and the aqueous solution surrounding the LDH crystalline particles, and thus increasing the driving force to intercalate OS into the interlayer space of LDH. The latter assists in propping open the interlayer spacing and thus is favorable for the exchanged hydrogen phosphate to move within the interlayer space and be eliminated from the LDH crystallite into the surrounding solution.

3-4 Summary

Interlayer HPO_4 has been completely removed from the interlayer space of LDH- HPO_4 by repeated anion exchange with OS in aqueous solution at room temperature. This appears to be the first time that complete removal of interlayer HPO_4 from LDH by simple anion exchange has been observed. The anion exchange with 1-octanesulfonate is a much more efficient method to remove the interlayer hydrogen phosphate when the results are compared with existing methods such as using Na_2CO_3 or NaOH-NaCl solutions.

It is thought that the high removal of interlayer phosphate is due to the relatively high concentration of OS and to the fact that the interlayer spacing after intercalating with OS anions is large. This provides a driving force for the intercalation of OS and allows the hydrogen phosphate in the interlayer space to more easily move through the interlayer and be eliminated. In next chapter, the mechanism of anion exchange in LDH solids using anionic surfactants is reported.

Chapter4:

Anionic surfactant enhanced Phosphate desorption from Mg/Al-Layered Double Hydroxides

4-1 Surfactant absorption behavior on Mg/Al-LDH material before and after micelle formation

The previous chapter explained that anion exchange with 1-Octanesulfonate (OS), succeeded in completely removing the interlayer hydrogen phosphate in Mg/Al-LDH. In contrast, a 1.0 M Na_2CO_3 solution and NaOH(0.5 M) –NaCl (1.0 M) solution removed just 46.4 % and 58.8 % of the interlayer hydrogen phosphate from hydrogen phosphate intercalated LDH even though both concentration were higher than OS concentration. As concluded in previous chapter, the high removal of interlayer phosphate was due to the relatively high concentration of OS and increasing the interlayer spacing after intercalating with OS anions allows the hydrogen phosphate in the interlayer space to more easily move through the interlayer and be eliminated. However this still required a relatively high concentration of OS solution (0.1 M). From the point of view of environmental burden and economics, it would be advantageous to use lower concentrations.

However, we have to consider one further phenomenon when the concentration of OS anion was decreasing below 0.1 M. The surfactant is known to undergo aggregation above a certain concentration. This aggregate is referred to as a "Micelle". The concentration when a surfactant forms micelles is called the critical micelle concentration (CMC). The CMC is different depending on the surfactant species. It has been reported that the CMC of DBS and DS are independent of pH in solution between pH 7- pH 9[12].

Many surfactant anions are known to intercalate into the interlayer region of LDH materials and the intercalation results in an expansion of the interlayer spacing[9]. The most

widely studied surfactant anions for intercalation in to LDH are Dodecylbenzenesulfonate (DBS) and dodecylsulfate (DS).[10] The interlayer spacing after intercalation of the surfactant increases to almost the same size as the surfactant chain length. One possible arrangement of the surfactant anion within the LDH interlayer region is the formation of a monolayer where the long chain axes lie perpendicular to the layers of the LDHs[11].

Pavan et al. reported surfactant adsorption on the surface of carbonate intercalated LDH and showed that the absorption behavior is divided into three or four different stages due to the multicomponent nature of the surfactant adsorptive system.[13] The first stage was characterized by non-aggregative adsorption, in other words, only unimer (i.e. surfactant monomer) ions are present at this stage. The second stage was characterized by the beginning of aggregate formation of unimers at concentrations close to the CMC. The transition between the first and second stages occurs when the surfactant aggregates are formed more quickly. Therefore, second stage is characterized by a rapid increase in adsorption with concentration. The third stage was characterized by a surfactant bilayer with a consequent saturation of the surface of LDH at concentrations close to the CMC. Thus, it is expected that the aggregation of surfactant monomers results in a strong interaction between the surface of the LDH material and the surfactant anion. However, the intercalation behavior of surfactant anion desorption depending on surfactant concentration has not been reported. In particular, DBS has a lower CMC than that of DS and OS, and so it may be that DBS has a stronger interaction with LDH at lower concentrations. Furthermore, DBS is a Linear Alkylbenzene Sulfonate (LAS) recognized for its low

toxicity risk, low cost and biodegradability. Since the LDH is a potentially recyclable absorbent, methods which enhance this can improve the performance of LDH as an absorbent for water treatment applications.

In this chapter, the de-intercalation behavior of interlayer hydrogen phosphate with surfactants below and above the CMC was investigated. Three types of surfactant solution were used as the counter anion to displace the interlayer hydrogen phosphate. Concentration of surfactant were adjusted from 0.0001 M to 0.3 M. The reported CMCs of dodecylbenzenesulfonate (DBS), dodecylsulfate (DS), sodium octylsulfate (OS) are 0.003 M, 0.009 M and 0.1 M, respectively.[14] Surfactant intercalation was studied by Powder X-ray diffraction (XRD), Fourier transform infrared spectroscopy (FT-IR), and scanning electron microscopy (SEM).

4-2 Kinetic study of phosphate desorption with surfactant micelle

Figure 4-1 shows the time dependence of HPO_4 desorption from LDH-HPO_4 with the different surfactant solutions. The HPO_4 concentration in the eluted solution increased rapidly after mixing with the surfactant solution and plateaued after around 36 h. The desorption behavior of LDH materials has been described as pseudo second-order.[16]

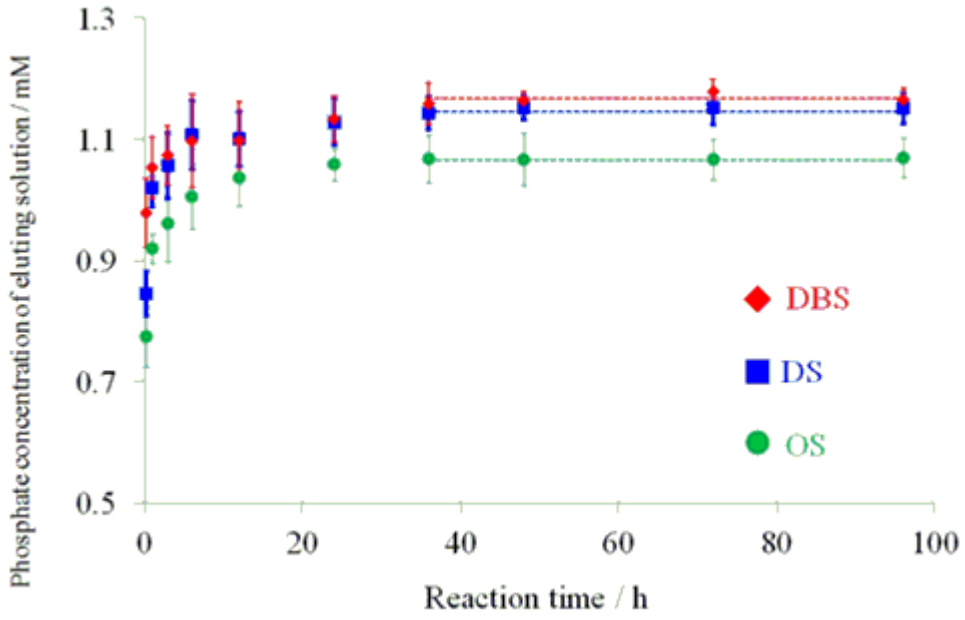

Figure 4-1. Time dependence of HPO_4^{2-} desorption from LDH-HPO_4 with OS. The data points represent the mean of three repeat experiments with the spread in data given by the error bars.

Kurashina et. al. also reported that the desorption kinetics of absorbed phosphate on LDH by anion exchange with sodium carbonate and sodium sulfonate solutions followed pseudo second-order rather than pseudo first-order kinetics.[17]

The pseudo second-order kinetic rate equation is expressed as (equationIV-I):

$$\frac{dq_t}{dt} = k_2(q_e - q_t)^2 \qquad \ldots(\text{IV-I})$$

where q_t and q_e are respectively the concentration of phosphate in the eluted solution at time t and at equilibrium($mmol \cdot L^{-1}$), and k_2 is the pseudo second-order rate constant ($mmol^{-1} \cdot L \cdot h^{-1}$).

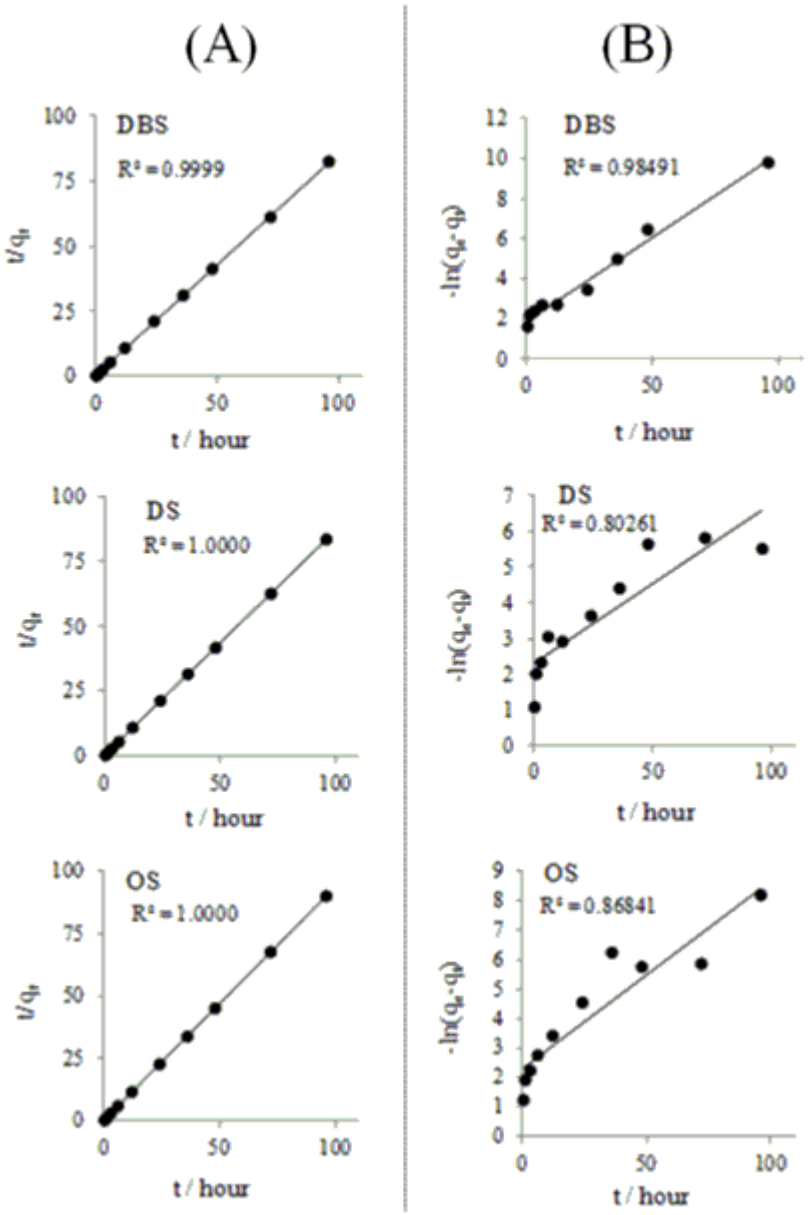

Figure 4-2. Linear regression curves of phosphate desorption data by surfactants (DBS,DS and OS) fitting with pseudo-second-order kinetic model (A) or pseudo-first-order kinetic model (B)

Table 4-1. Rate constant by fitting the desorption data to pseudo-second-order kinetics model

Surfactant	q_e ($\mu mol \cdot L^{-1}$)	k_2 ($\mu mol^{-1} \cdot L \cdot h^{-1}$)	R^2
DBS	1.163	0.8575	0.9998
DS	1.147	0.8700	0.9999
OS	1.116	0.9370	1.0000

Since the phosphate concentration was constant beyond 36h, a time of 48h was taken as being at equilibrium. In the present work, a pseudo second–order equation also provides a better description of the desorption kinetics behaviour of HPO_4 from LDH.(Figure 4-2) The k_2 and correlation coefficient (R^2) value obtained from the kinetic fits are listed in Table 4-1.

4-3 Phosphate desorption from Mg/Al-LDH by anion exchange with surfactant micelles

Figure 4-3 shows HPO_4 desorption isotherms for the different surfactants anions at 35 °C and a pH of 9.0 ±0.2 after 48 h reaction time, as a function of surfactant concentration. The isotherm plots of desorption ratios for OS, DS and DBS were started from 0.0006M, 0.0002M and 0.0001 M, respectively because of the detection limit of the surfactant concentration. For the OS, the lowest desorption was around 20% at a concentration of 0.0006 M and showed almost no change until the concentration was increased to 0.008 M.

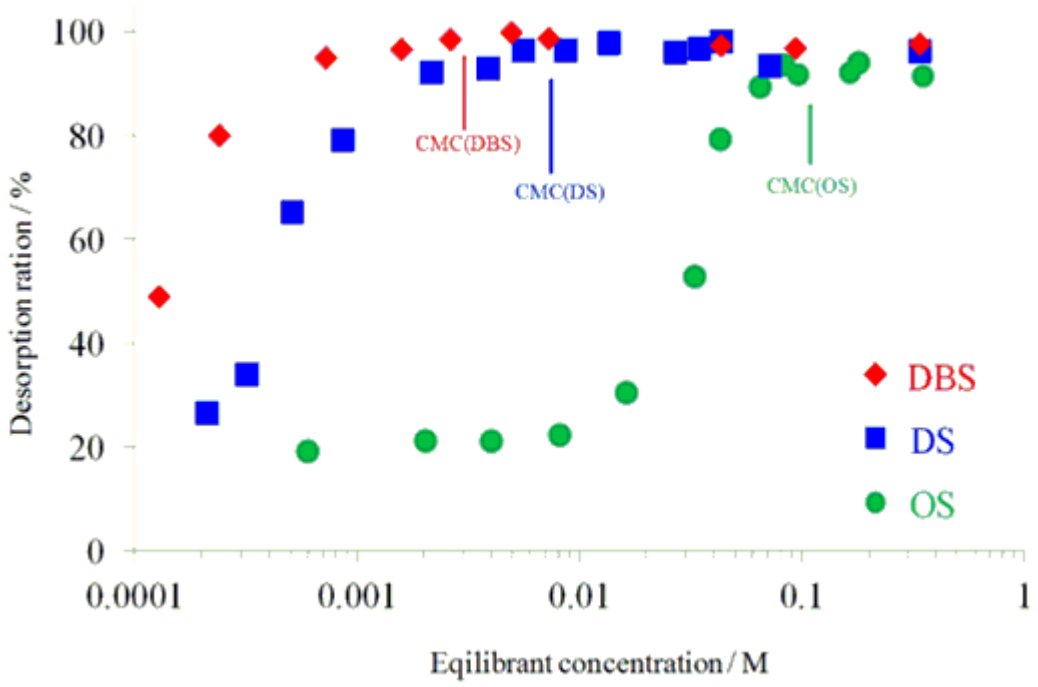

Figure4-3. Surfactant adsorption isotherms on an LDH: DBS, DS and OS. Reaction time for 48 h at 298 K and pH 9.

Above a concentration of 0.008 M, desorption increased rapidly reaching around 93 % at 0.1 M and then plateaued. The concentration at which maximum desorption was achieved is very close to the reported CMC of OS(0.1 M). The hydrogen phosphate isotherm plots for DBS and DS showed that the desorption was around 25% for DS at the lowest concentration of 0.0002M and around 50% for DBS at a lowest concentration of approximately 0.0001M. The fact that the desorption using these two solutions increased continuously from the beginning of the experiment, as opposed to the relatively flat behavior of OS, is perhaps a reflection of their much lower CMC when compared with OS. However, as with the OS solution, desorption using DS and DBS increased with

concentration and also reached a maximum at, and plateaued beyond, their respective CMCs. Thus, the desorption of HPO_4 from LDH was enhanced at concentrations near the CMC for each surfactant and did not increase further beyond the CMC.

In general, it has been assumed that there is a distribution of monomers and pre-micelles when the concentration is below the CMC. Cui et.al reported the mechanism of anionic surfactant micelle formation by 1H NMR and NMR self-diffusion experiments and showed that there are three stages in anionic surfactant behavior at different concentrations[18]. Firstly, at concentrations lower than the CMC the surfactant exists as monomers and then these monomers form small aggregates called pre-micelles at concentrations near the CMC. The size of these pre-micelles grows as the concentration increases. In the final stage, micelles are formed at the CMC.

The desorption results in Figure 4-3 can be explained by the changing state of the surfactant anion from monomer to micelle. The affinity between interlayer anions and LDH depends on their charge number and density with Miyata and Sato reporting that divalent anions have higher ion selectivity for LDH materials than monovalent anions.[19] Below the CMC of OS, the OS surfactant existed as monomers which have one negative charge. Since hydrogen phosphate has a charge of two, the OS intercalation did not occur to any great extent until higher concentrations are reached (0.01 M). The small amount of desorption observed at low concentrations may be due to surface absorbed hydrogen phosphate on the LDH.

However, as the monomer surfactant starts to aggregate at concentrations near the CMC, the hydrophilic parts (SO_3^- or SO_4^-) of the surfactant come closer to each other and the local charge density of the surfactant will increase. The size of the pre-micelle increases with increasing concentration of surfactant, and since the LDH layer has a positive charge, the interaction between surfactant anion and the LDH layer also increases. This increasing concentration of surfactant solution increases the size of the pre-micelle and allows exchange with the interlayer hydrogen phosphate. The formation of micelles is crucial for the desorption as can be seen by comparing desorption using different solutions at the same concentration.

At 0.01M the OS solution was below its CMC and desorption was still low at around 20%. The DBS and DS solutions at this concentration were above the CMC and the desorption was almost 100%, despite the fact that aggregation means the micelle concentration in these two solutions would be lower than the monomer concentration in the OS. The high desorption when using the DBS solution (94%) was achieved at a much lower concentration (0.003 M) than that reported for conventional desorption methods, such as using a high concentration solution of $NaCO_3$ and NaCl(>0.1 M). Therefore, the desorption isotherm results demonstrate that desorption of interlayer HPO_4 is enhanced by micelle formation and that this is more effective in interlayer hydrogen phosphate desorption than simply increasing the concentration of the anion. Table 4-2 shows the chemical formulae of DBS, DS and OS intercalated LDH, and the calculated desorption ratios, determined by

EDS data, which agree well with the measured desorption shown in Figure 4-3. The desorption ratio was calculated from the atomic ratio between phosphorus and aluminium (P/Al) as reported previously.[8]

Surfactant intercalation into the LDH material before and after the CMC was confirmed by XRD and FT-IR results. Figure 4-4 shows XRD patterns from 2θ = 2˚ to 30 ˚ showing the peak shift of the 00l diffraction peaks that describes the basal spacing of the LDH structure.[1] For the XRD pattern of LDH-HPO_4 with 0.0006 M OS solution, the three intense diffraction peaks are indexed as the 003, 006, and 009 planes of pristine LDH-HPO_4[15] and show that OS was not intercalated into LDH, even though about 20 % of phosphate was desorbed at this concentration. This small desorption was probably due to desorption only from surface absorbed hydrogen phosphate on LDH. At a concentration of 0.02 M the position of these peaks moves to smaller angles consistent with the 00l diffractions of OS intercalated LDH.[8]

Table 4-2. Chemical composition of phosphate desorbed LDH after surfactant intercalation

Surfactant	E.C.	Chemical formula	desorption
DBS	0.003	$Mg_{0.67}Al_{0.33}(OH)_2(DBS)_{0.28}(HPO_4)_{0.02}0.62H_2O$	91%
DS	0.01	$Mg_{0.64}Al_{0.36}(OH)_2(DS)_{0.31}(HPO_4)_{0.02}0.72H_2O$	90%
OS	0.2	$Mg_{0.65}Al_{0.35}(OH)_2(OS)_{0.26}(HPO_4)_{0.03}1.02H_2O$	87%

E.C.=equilibrium concentration of surfactant in Fig. 2

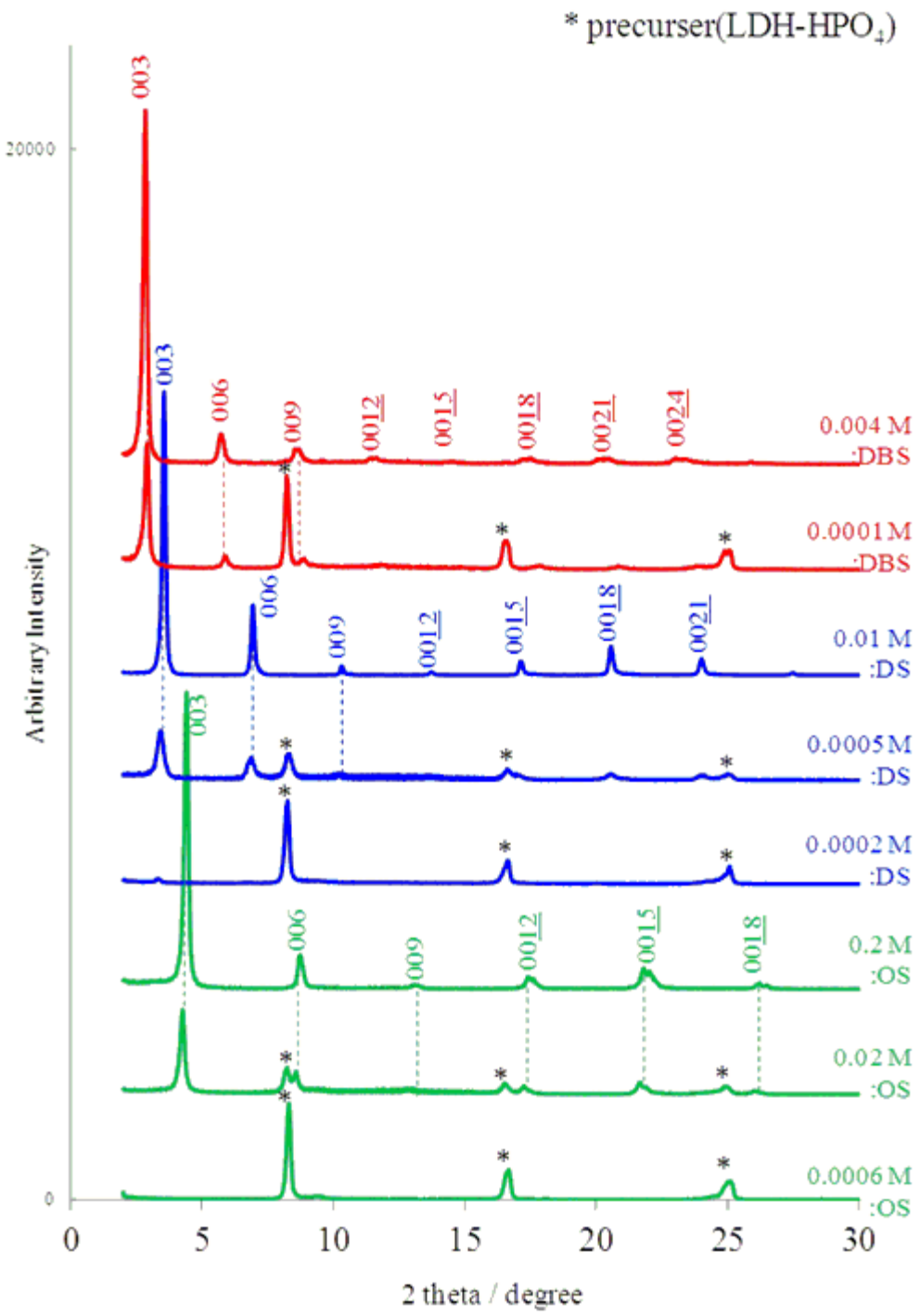

Figure 4-4. XRD patterns of LDH samples before and after surfactant intercalation

There are still small peaks in the original position which would imply that not all of the LDH has been intercalated at this concentration. However at concentrations beyond the CMC, the original 00l diffractions of LDH-HPO_4 pattern had completely disappeared and only those peaks associated with *00l* diffraction from the OS intercalated LDH were observed.

The same trends were seen for intercalation with the DS and DBS solutions. For the DS solution at the lowest concentration (0.0002M) the primary peaks observed were those associated with the pristine LDH, although there was a small diffraction peak at a 2θ value of 3.5˚ which corresponds to the 003 diffraction of DS intercalated LDH, and indicates that even at these low concentrations a small amount of the surfactant was intercalated (The desorption at this concentration was also slightly higher than for the 0.0006M OS solution where no intercalation had occurred). At higher concentrations, peaks from both pristine LDH and the DS intercalated LDH were observed[20] and above the CMC only the surfactant intercalated structure peaks were observed. For the DBS solution, peaks from both the pristine and intercalated LDH were observed at a concentration of 0.0001 M but again only the intercalated peaks were observed beyond the CMC (0.003M).

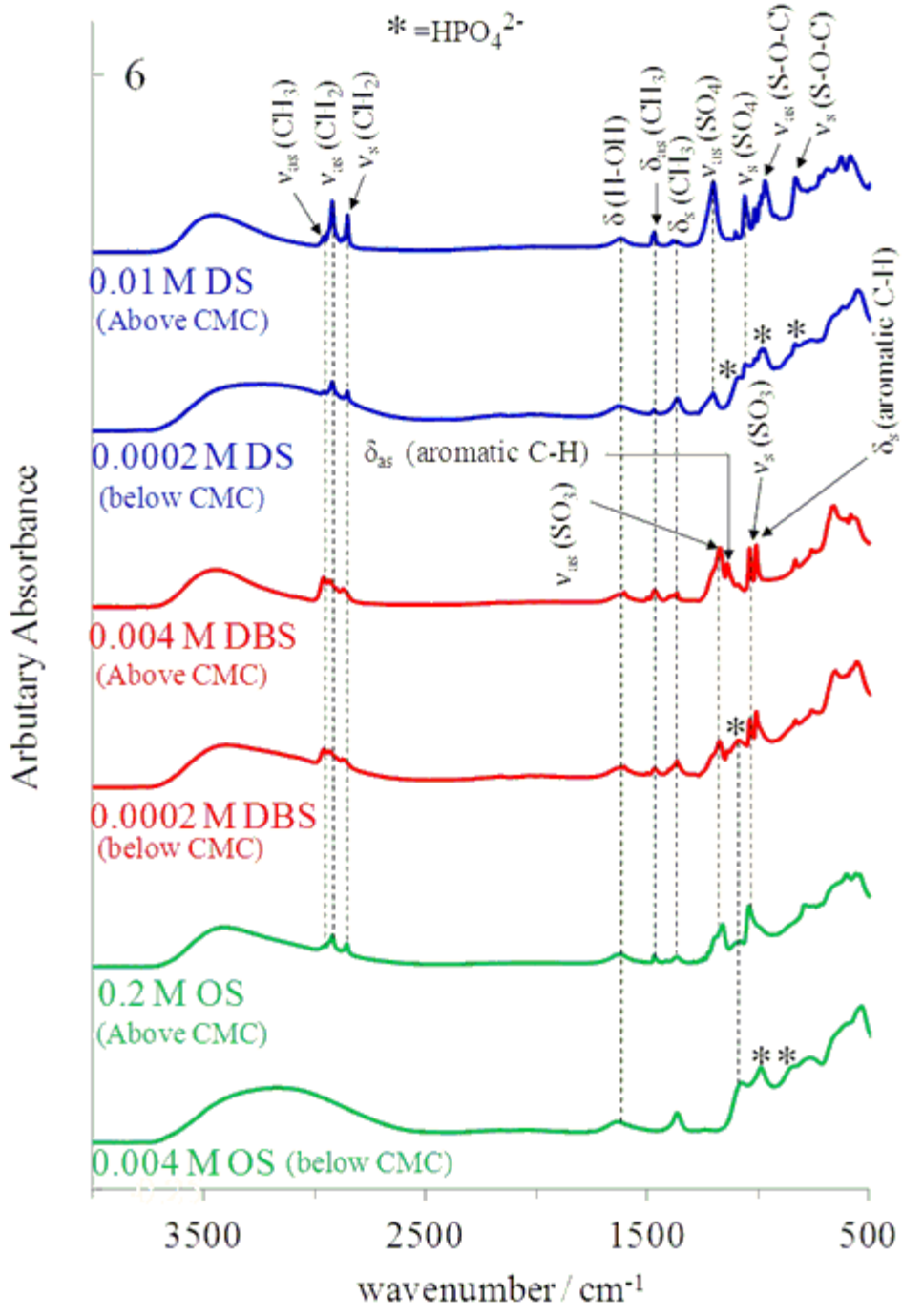

Figure 4-5. FT-IR spectra of LDH samples before and after surfactants intercalation

FT-IR spectra of the LDH samples with the three different surfactant solutions both below and above the CMC are shown in Figure 4-5. When the surfactant concentrations are below the CMC, hydrogen phosphate assigned absorptions were observed in each spectrum. Furthermore, the samples with DBS and DS showed several absorption bands from the surfactant. The DBS sample showed typical DBS IR absorptions, which are the C-H bending absorption from the aromatic ring and the stretching vibration from absorption of SO_3. The DS sample showed the stretching vibration absorption of SO_4 and stretching vibration absorption of S-O-C typical of DS absorptions.[21]

Beyond the CMC, all of the spectra showed the dominant peaks of the surfactant and no absorption peaks for hydrogen phosphate, due to the small amount of hydrogen phosphate remaining in the samples. The results from XRD and FT-IR analyses confirmed the intercalation of surfactant with de-intercalation of interlayer hydrogen phosphate at concentrations above the CMC. Therefore, for each solution, micelle formation of the surfactant enhanced its intercalation by anion exchange with the interlayer hydrogen phosphate.

Figure 4-6 shows SEM images of the pristine LDH material and following surfactant intercalation. The original hydrogen phosphate intercalated LDH has a plate like morphology with a particle diameter of around 5 μm and a thickness of approximately 220 nm. This large aspect ratio is typical of the LDH single crystal.[22]

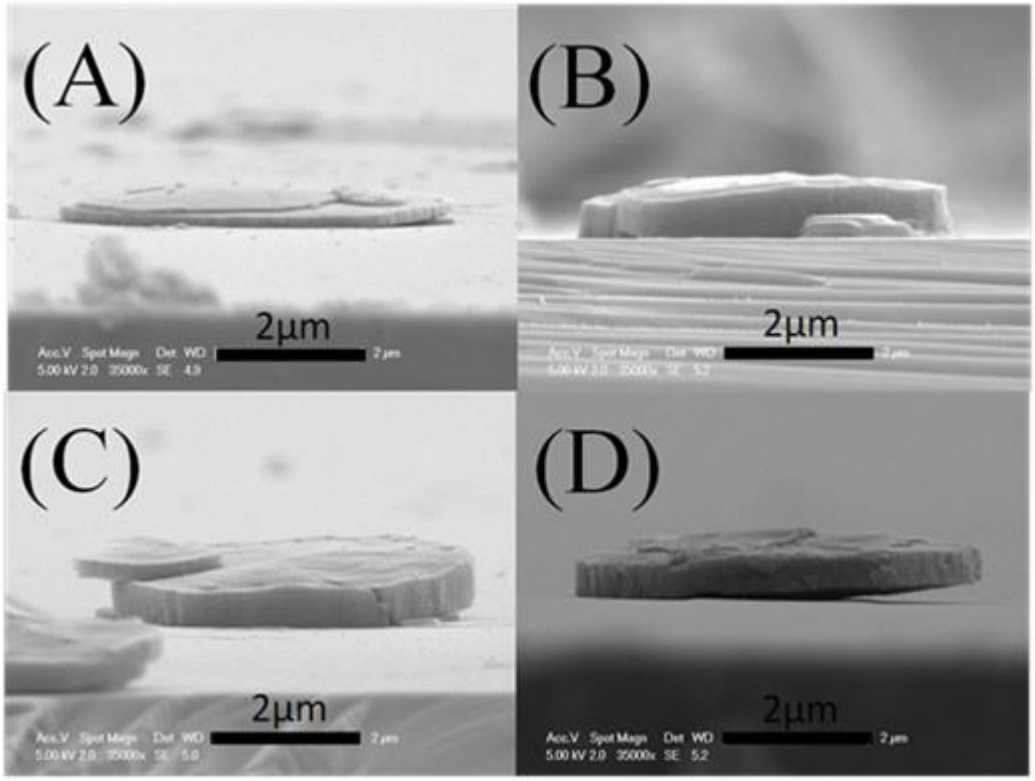

Figure 4-6. SEM image of LDH single crystal before and after surfactants intercalation. (A) is HPO_4 intercalated LDH. (B), (C), (D) were DBS at 0.004 M, DS at 0.01 M and OS at 0.2 M intercalated LDH, respectively.

After surfactant intercalation into LDH, the diameter (layer dimensions) of the material was similar to the original LDH-HPO_4, however the thickness was apparently increased due to the surfactant intercalation. Table 4-3 shows the thickness of the LDH measured from the SEM image before and after intercalation and the basal plane spacing data calculated from XRD peak positions. The thickness of the LDH crystals following intercalation with DBS, DS and OS increased from around 220 nm to around 680, 610 and 540 nm respectively. The basal spacing, as determined from the XRD data, also showed an increase, and the ratio

of the basal spacing following intercalation to that of the pristine material was in good agreement with the increase in thickness of the crystals measured from SEM images.

Table 4-3 Compared SEM data and XRD data of phosphate intercalated LDH before and after surfactant intercalation

Name	LDH-HPO_4	DBS intercalation	DS intercalation	OS intercalation
SEM(ratio*)/ nm	203±24	675±66(3.3)	609±50(3.0)	477±31(2.3)
Basal spacing(ratio**) / nm	1.1	3.1(2.9)	2.6(2.5)	2.0(1.9)

ratio** = basal spacing of surfactant intercalated LDH/basal spacing of LDH-HPO_4. The error were calculated from three sample.

ratio* = thickness of surfactant intercalated LDH/thickness of LDH-HPO_4.

The summary of de-intercalation mechanism of interlayer phosphate with surfactant anions is shown in Figure 4-7. The surfactant monomers become aggregated with increasing surfactant concentration. The de-intercalation behavior of the interlayer phosphate with surfactant anions can be divided into three regions. The first region is where the surfactant anion exists as monomer anions. In this region, the surfactant anion cannot intercalate into the LDH due to the interlayer phosphate having a higher charge density than the monomer surfactant anion. The second region is defined where the monomers start to aggregate. The phosphate desorption increased with increasing number of these pre-micelles, presumably due to SO_3^- or SO_4^- aggregation and increased local charge density. Most of the interlayer phosphate was desorbed by the end of the second region which is just

below the CMC. The desorption ratio reaches a maximum at the CMC in the third region and then plateaus as there is no further surfactant aggregation.

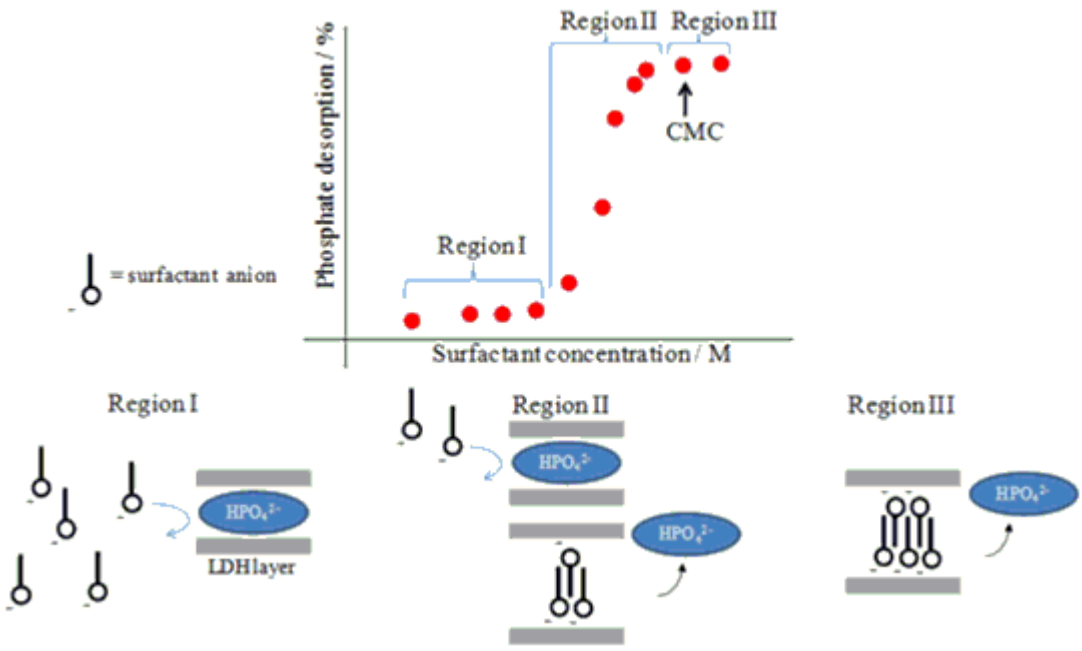

Figure 4-7. Summary of phosphate desorption from LDH by surfactant anion intercalation.

4-4 Phosphate re-absorption on to Mg/Al-LDH material with surfactant micelles

Figure 4-8 shows the results of the re-absorption of phosphates on to the LDH material following desorption with the elute solutions. When the interlayer phosphate was desorbed with 0.003 M DBS solution, which is above the CMC of DBS, the LDH could re-absorb about 90% of phosphate compared with the initial LDH-HPO_4. This high absorption was maintained for the subsequent second and third repeats, with a slight decrease of around 7%

absorption on each cycle, although this may be explained by losses of LDH due to handling.

On the other hand, the phosphate re-absorption following desorption with the NaCl-NaOH and Na_2CO_3 solutions were only about 35 % and 23 %, respectively. Figure 4-9 shows XRD and FT-IR patterns of the LDH following the re-absorbtion of phosphate. For the samples that had been desorbed with the DBS solution, the XRD pattern showed intense *00l* diffraction peaks of LDH-HPO_4 with no diffraction attributable to DBS intercalated LDH. The FT-IR spectrum also showed typical HPO_4^{2-} absorption peaks, and these results indicate that the phosphate was re-intercalated into the LDH following phosphate desorption with DBS. However, when the phosphate was desorbed with either NaCl-NaOH or Na_2CO_3 solutions, the XRD pattern showed un-identified diffraction peaks which can be identified to LDH. The FT-IR spectra for these samples also showed relatively low intensity of HPO_4 absorptions, implying that the intercalation of phosphate in to the LDH was interfered with by the NaCl-NaOH or Na_2CO_3 solutions. Using DBS solution for phosphate desorption not only achieved high desorption but also achieved higher phosphate absorption in recycle tests with smaller concentrations than those using conventional methods (Na_2CO_3, NaCl-NaOH).

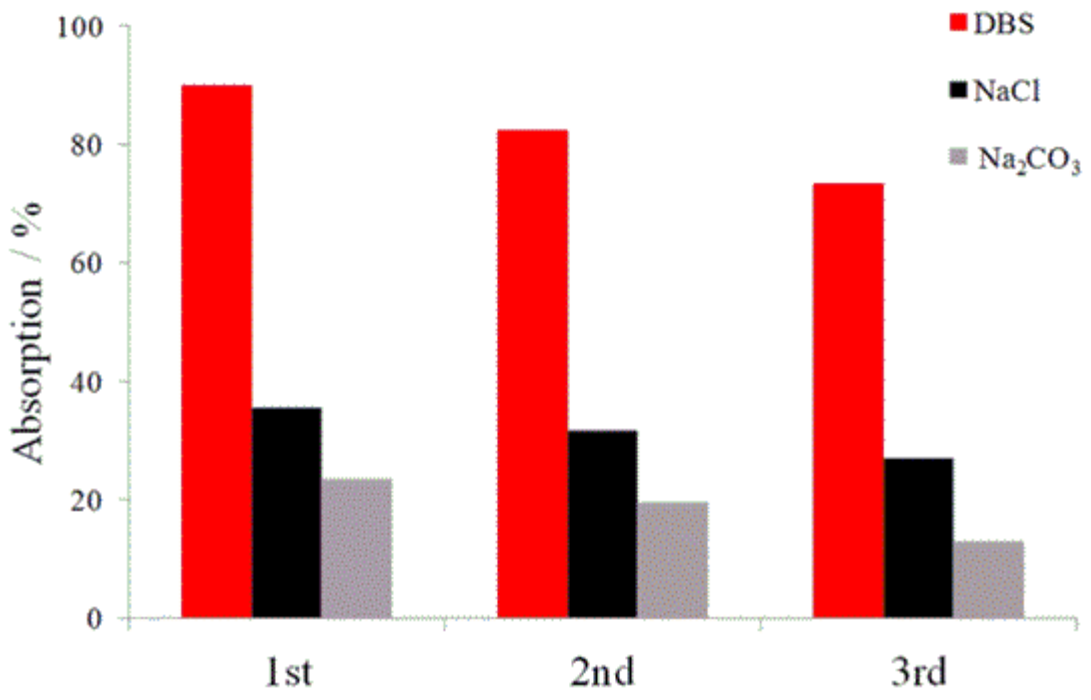

Figure 4-8. Phosphate re-absorption of LDH using DBS, NaCl-NaOH and Na_2CO_3 solution as the eluting solution over three cycles.

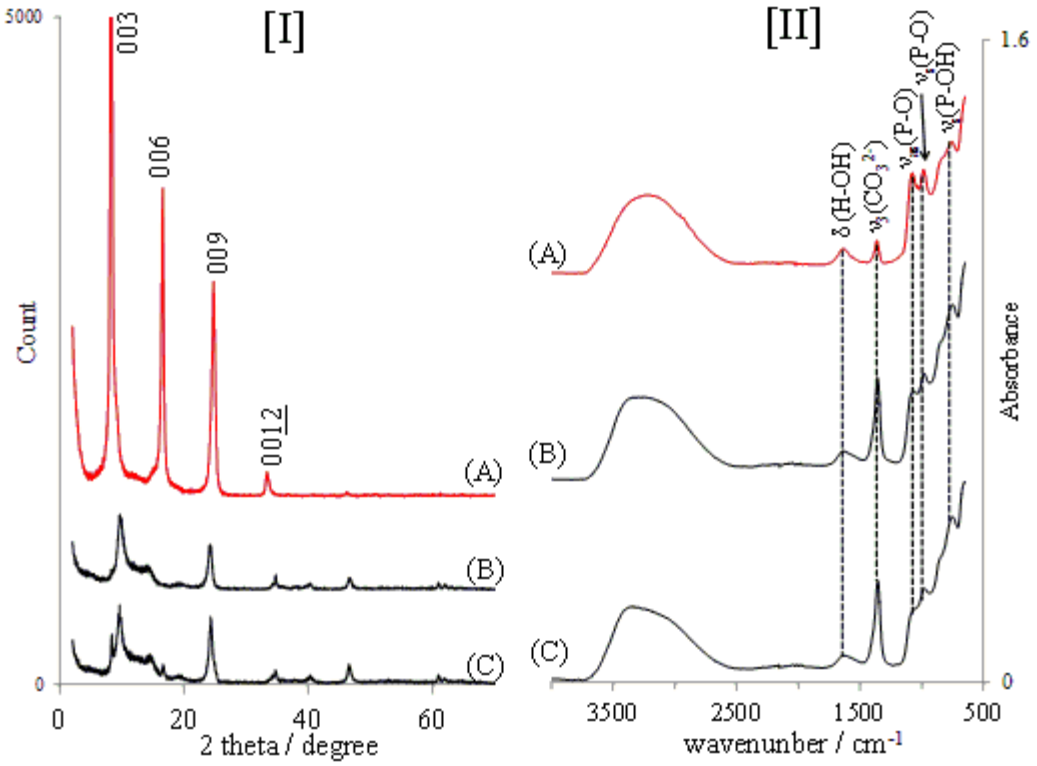

Figure 4-9. XRD patterns[I] and FT-IR spectra[II] of phosphate re-absorbed LDH after desorbed phosphate with DBS(A), NaCl-NaOH(B) and Na_2CO_3(C) solution.

4-5 Summary

The desorption behavior of hydrogen phosphate from LDH using different surfactant anions has been studied as a function of surfactant concentration. This section has revealed that for all solutions the removal of interlayer hydrogen phosphate by anion exchange with the surfactant is enhanced at concentrations where the surfactants form micelles (CMC). Micelle formation results in an increase in charge density of the aggregated surfactant

compared with single surfactant anions and results in a stronger interaction with the LDH, removing the interlayer hydrogen phosphate. Furthermore, this method allowed the removal of more than 90 % of the interlayer hydrogen phosphate at much lower concentration of surfactant solution than the conventional methods such as using Na_2CO_3 solution or NaCl-NaOH as the eluting solution. For the DS and DBS solutions, almost complete removal of the hydrogen phosphate was achieved at concentrations of only 0.003 and 0.008M respectively. Furthermore, using DBS solution (0.003 M) for phosphate desorption allowed subsequent higher phosphate absorption during recyclability tests, with smaller concentrations than using Na_2CO_3 or NaCl-NaOH solution.

Chapter 5:

XANES characterization of Zinc/Aluminum mixed oxides derived from Zn/Al-layered double hydroxides (Zn/Al-LDH)

5-1 General study of calcined Zn/Al-LDH

During the thermal transformation of the Zn/Al-LDH it has been reported that the Zn/Al-LDH crystalline phase becomes amorphous by 500 ˚C and then is re-crystallized forming a spinel structure after 600 ˚C.[48] Molecular Dynamics Simulation and in-situ XRD results explained that the layer structure becomes disordered around 180 ˚C because Zn/Al-LDH cannot maintain the typical LDH structure when interlayer water is completely lost.[49] High temperature Raman spectra reported the metal hydroxyl layer of LDH was stable until 200 ˚C.[50] With thermal treatment above 200 ˚C, dehydroxylation of the LDH layer is observed and an amorphous phase was formed around 300 ˚C.[51] Zhao et. al. observed an interplanar distance of 0.25 nm, which is the same as the (1011) plane of ZnO measured in the amorphous phase of the calcined Zn/Al-LDH at 300 ˚C by high resolution transmission electron microscopy (HRTEM). They concluded that amorphous ZnO nucleation gradually occurred with progressive transition into the amorphous phase of the Zn/Al-LDH.[51]

The amorphous phase then gradually crystallized to wurtzite-ZnO and $ZnAl_2O_4$ (spinel) starting between 500 and 700 ˚C.[24d, 48b, 52] Refinement of the XRD data indicated that poorly crystalline diffraction at 600 ˚C was caused by the 33 % of Al incorporated into the ZnO structure.[48c, 53] Thus, the Zn/Al-LDH was transformed to the amorphous phase between 300 ˚C and 400 ˚C and changed to a crystalline phase above 600 ˚C. Despite many reports about the thermal behavior of Zn/Al-LDH, characterization studies of the amorphous phase between 300 ˚C to 400 ˚C have rarely been discussed. This is probably due to the difficulty in characterizing the amorphous material by XRD.

One of the useful methods to characterize amorphous material is X-ray absorption near-edge structure (XANES) (or Near edge X-ray absorption fine structure (NEXAFS)) which have been also known as an non-intrusive technique.[54] The XANES spectra show the detail of chemical environment of the target element because the XANES spectrum is usually characterized by intense resonance features arising from excitations of core-level electrons to unoccupied orbital and continuum levels and from multiple scattering of the emitted photoelectrons. These scattering effects are sensitive to the geometrical arrangement of neighbouring atoms around the target atom.[55]

Many synchrotron-based Zn XANES studies have been carried out on the K-edge (~9690 eV) where the Zn 1s →4p transition is probed. The Zn K-edge XANES has been widely utilized to determine the speciation of Zn based on coordination number and geometry, such as ZnO, $Zn(OH)_2$ and $ZnFe_2O_4$.[56] However, since the K-edge spectra basically reflect the chemical environment of the core levels, it is difficult to determine the Zn speciation or even impossible to observe differences between Zn species from the Zn K-edge because of the lack of distinguishable features in the selected reference compounds. For ZnO, the electronic state of the Zn corresponds to a $3d^{10}$ configuration. Thus, the strongest bonding effect in this 3d oxide is given by the overlap between the oxygen 2p band (filled) and the Zn 4s and 4p bands (empty). Thus, XANES at the $L_{2,3}$-edge is more promising because the $L_{2,3}$-edge spectra show more distinguishable features. However, only a small number of Zn

L-edge studies of ZnO have been reported. The Zn L-edge spectra have not been applied for thermal characterization of the Zn/Al-LDH so far.

This chapter studies the thermal transition of Zn/Al-LDH. Crystalline Zn/Al-LDH was synthesized by the homogeneous precipitation method with urea in order to synthesize single phase LDH and to distinguish thermal structure changes of the Zn/Al-LDH.[29] XRD, and TG-DTA measurement were used to determine the temperature range at which the amorphous phase was formed, The amorphous phase was characterized by XANES (Zn L-edge, Al K-edge and O K-edge) and UV-vis Diffuse Reflection (DR).

5-2 Synthesis and characterization of calcined Zn/Al-LDH by XRD and TG-DTA

Synthesis of highly crystalline Zn/Al-LDH was conducted using the method described by the Sasaki's group.[29] The Zn/Al-LDH was synthesized by the precipitation method with urea under reflux conditions at 90 $^{\circ}$C (Section 2-5).

Figure 5-1 shows a TG-DTA curve of the Zn/Al-LDH with two steps in weight loss, with endothermic peaks below and above 200 ˚C. The first weight loss with an endothermic

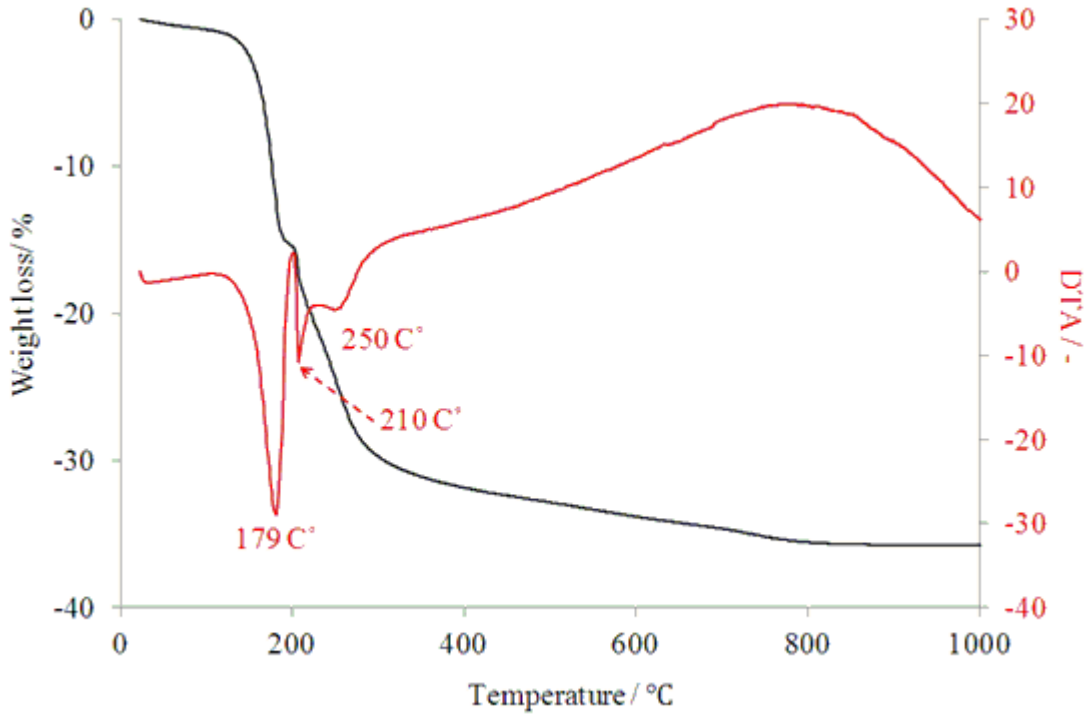

Figure 5-1. TG-DTA curve of ZnAl-LDH

peak at 179 ˚C is assigned as elimination of interlayer water.[6] The second weight loss below around 300 ˚C with two endothermic peaks at 210 ˚C and 250 ˚C corresponds to dehydroxylation of the hydroxide layer and elimination of carbonate, respectively.[53, 57] Thus, there were two strong endothermic reaction due to dehydration during thermal treatment of the Zn/Al-LDH.

The crystal structure change of the Zn/Al-LDH during thermal treatment was investigated by XRD. The synthesized Zn/Al-LDH powder was thermally treated in a furnace for 2 hours at temperatures up to 900 ˚C. After thermal treatment, the samples were cooled down to room temperature and then analysed. Figure 5-2 shows the XRD pattern of Zn/Al-LDH before and after thermal treatment, where it is confirmed that single phase crystalline Zn/Al-LDH was synthesized. The peak intensity of the Zn/Al-LDH before thermal treatment was some 10 times higher than that observed after treatment. All diffraction peaks of the Zn/Al-LDH where is at the bottom of Figure 5-2 are indexed as corresponding to a hexagonal unit cell, following the $-h+k+l \neq 3n$ rule in agreement with the R3m (rhombohedral) structure of hydrotalcite.[31b, 58] Lattice constants calculated from the diffraction pattern of unheated Zn/Al-LDH are a_0=0.3069 nm, c_0=2.268 nm. These lattice constants are almost the same as those reported for carbonate intercalated Zn/Al-LDH.[29] The relative intensity of the LDH diffraction decreased and in particular the *00l* diffraction peaks became broader by 200 ˚C. Lombardo et. al. reported that the disorder of *00l* diffraction is due to increasing heterogeneity of the material and a reduction of interlayer spacing by dehydration of interlayer water.[49] Thomas et al. also reported that the broadening of the *00l* peaks of Zn/Al-LDH is due to turbostratic disorder induced by elimination of interlayer water.[53] The *00l* diffractions completely disappeared at 300 ˚C and the diffraction pattern changed to reflect an amorphous phase until 400 ˚C. The amorphous phase gradually crystallized with increasing temperature with two diffraction peaks around 32˚ and 37˚ becoming relatively intense. At 900 ˚C, the diffraction pattern showed two diffraction patterns of crystalline ZnO and $ZnAl_2O_4$. Therefore, TG-DTA, XRD results

showed that the LDH transformed to an amorphous phase between 300 ˚C and 400 ˚C due to dehydroxylation and then this amorphous phase transformed in to ZnO and $ZnAl_2O_4$ by re-crystallization. The following section described the investigation of the amorphous phase by XANES and diffuse reflection spectra.

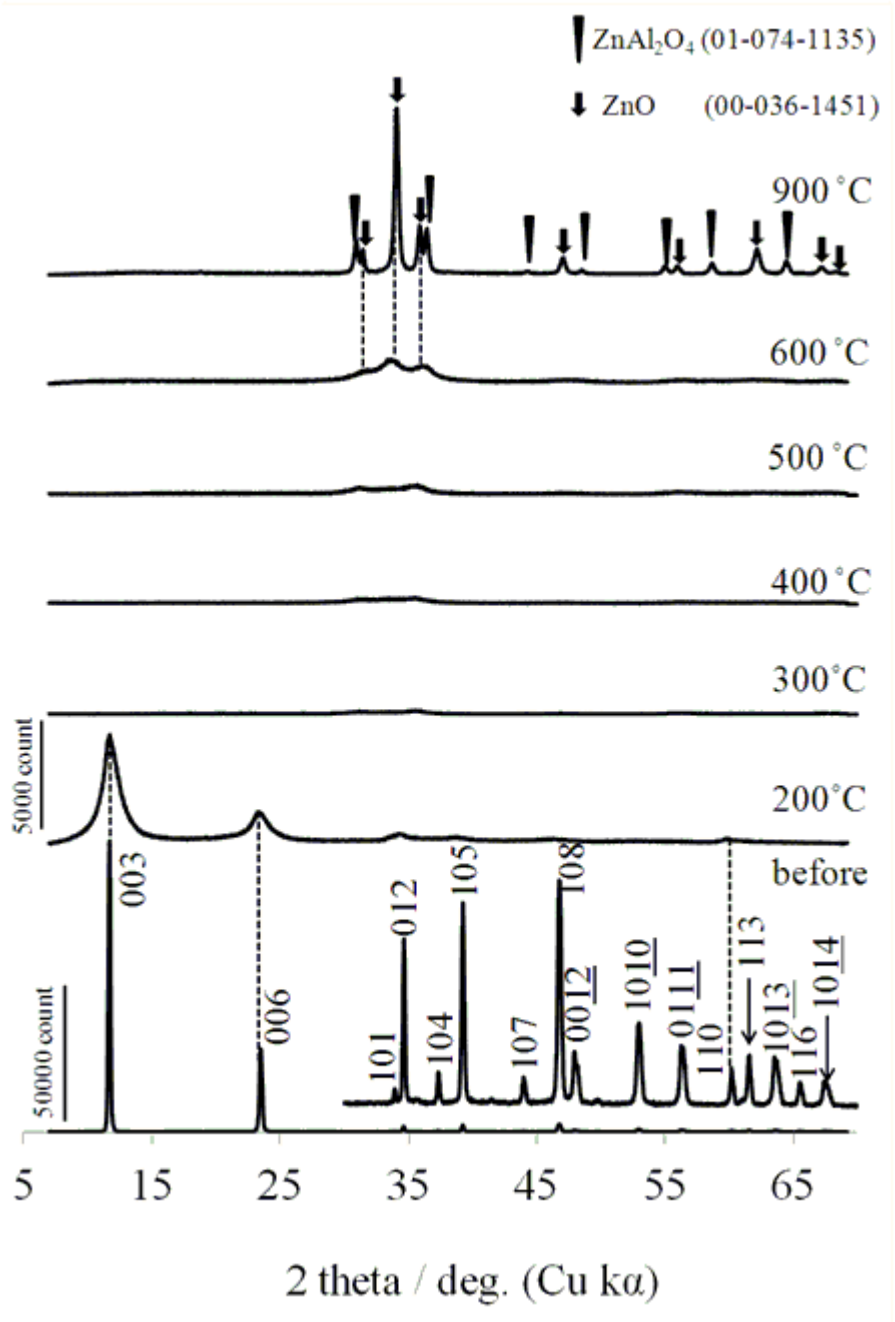

Figure 5-2. XRD patterns of ZnAl-LDH before and after thermal treatment up to 900 ˚C.

5-3 Characterization of calcined Zn/Al-LDH by XANES spectra

The Zn/Al-LDH powder samples before and after thermal treatment were characterized by XANES analysis. The thermal treatment method for Zn/Al-LDH was the same as described in the method in the section 5-2.

Figure 5-3 shows Zn L_3-edge spectra of Zn/Al-LDH before and after thermal treatment up to 600 ˚C and wurtzite-ZnO (w-ZnO) as reference material. The XANES spectra provided two insights into the thermal behaviour of Zn/Al-LDH. The first is the changing coordination number of Zn^{2+} in these samples. Both the Zn L-edge spectra of Zn/Al-LDH before and after heating at 200 ˚C showed three set of peaks which were named as A_o, E_o and T_o, respectively and are similar to rock salt structured ZnO where the Zn^{2+} posseses 6-fold coordination number with O^{2-}.[59] Since the Zn^{2+} in the LDH layer is surrounded by six oxygen ions with octahedral symmetry,[58] the spectra both the original material and following thermal treatment at 200 ˚C can be assigned as octahedral Zn^{2+} in the Zn/Al-LDH structure. However, the coordination number was changed by 400 ˚C. At 400 ˚C an additional broad peak around 1027 eV appeared at the Zn L-edge, which was also observed in the Zn L-edge spectrum of w-ZnO. It has been reported that Zn^{2+} in w-ZnO, or related oxides, usually has tetrahedral symmetry, except for the case of high-pressure ZnO having the rock-salt structure.[60] Therefore, this spectrum change can be assigned as a change in coordination number from six to four. These spectral changes can be explained as a changing of the primitive unit cell of Zn^{2+}. Figure 5-4 shows the lowest unoccupied orbital

for $Zn^{2+}$is the 4s, followed by 4p and 4d. In the octahedral point group, the 4s orbital is only allowed to contribute to the a_1 molecular orbital. The 4p becomes t_{1u} and the 4d becomes t_{2g} and e_g.

Theoretically, the L_3-edge XANES measures $2p_{3/2} \rightarrow$ s-like transition at lowest energy and then $2p_{3/2} \rightarrow$ d-like transition at higher energy, but $2p_{3/2} \rightarrow$ p-like transition are not allowed. Those features were attributed to electron transitions from Zn 2*p* to unoccupied Zn 4*s*(=A_o) and 4*d* (=T_o and E_o) states. Electron energy–loss near edge structure (ELNES) spectra reported for octahedral Zn^{2+} analogous to XANES, also showed three features which are assigned to transition from 2p to 4s(A_o) and 4d(E_o and T_o).[61] When the coordination number changes from six to four, the transition from 2p to p-like states is allowed due to 4p-4d hybridization in the symmetry change from Octahedral(Oh) to Tetrahedral(Td). It has been reported that the XANES Zn L-edge spectrum of w-ZnO has four sets of peaks (A_t, T_{t1}, E_t and T_{t2}) which can be assigned as transitions from 2p to 4s(a_1), 4p (t_1) and 4d(e and t_2).[62] Thus, when the Zn/Al-LDH was heated to 400 ˚C, the T_{t1} peak occurs around 1023 eV which can be assigned as transitions from Zn 2p to 4p (T_{t1}). The other three peaks were assigned as the A_t, E_t and T_{t2} of w-ZnO. This is due to changing coordination number of Zn from six to four, which means the metal oxide phase was formed above 400 ˚C. This XANES data is the first direct evidence of the coordination number of Zn^{2+} in the Zn/Al-LDH and amorphous phases of calcined the Zn/Al-LDH.

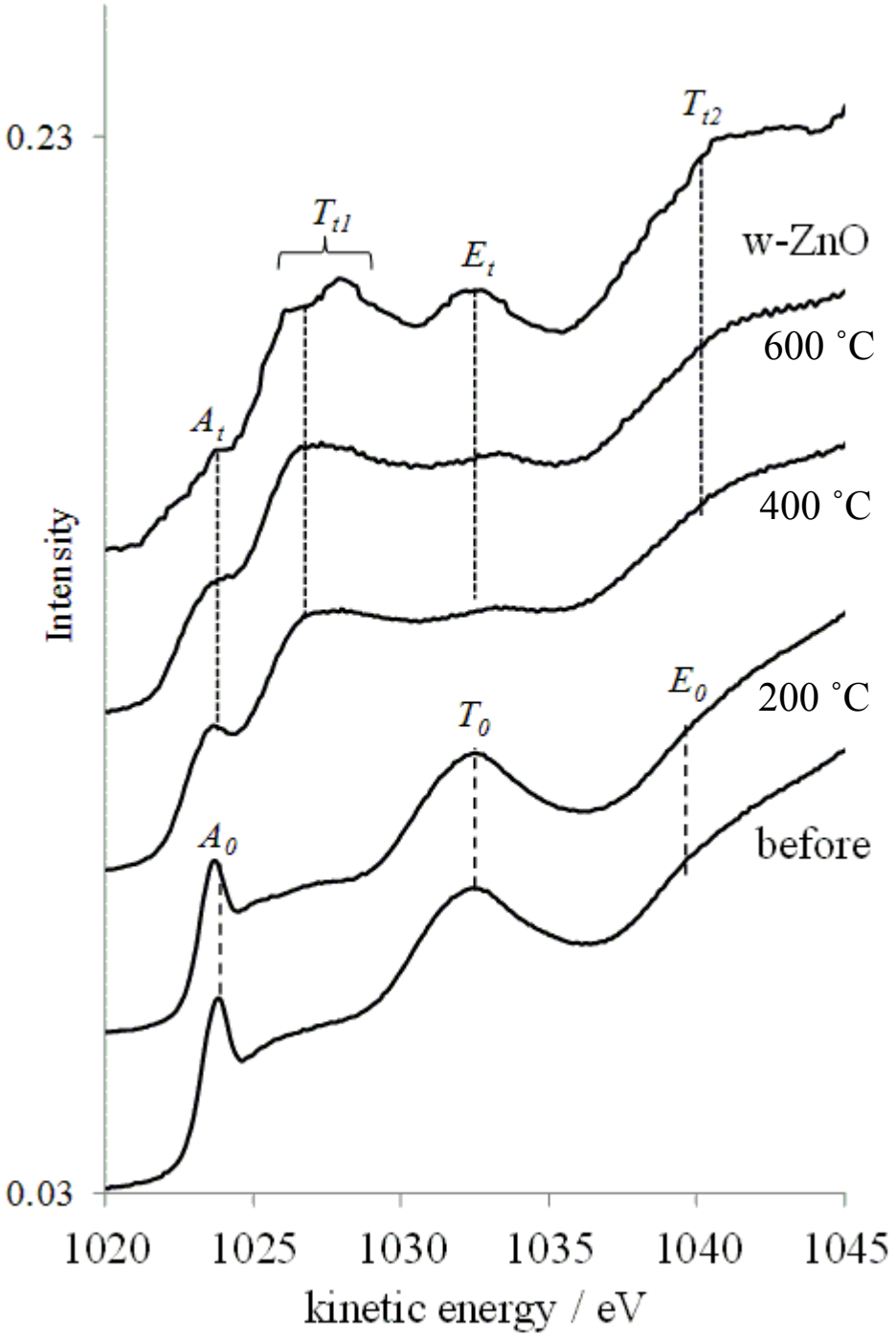

Figure 5-3. XANES Zn L-edge spectra of ZnAl-LDH before and after thermal treatment to 900 ˚C.

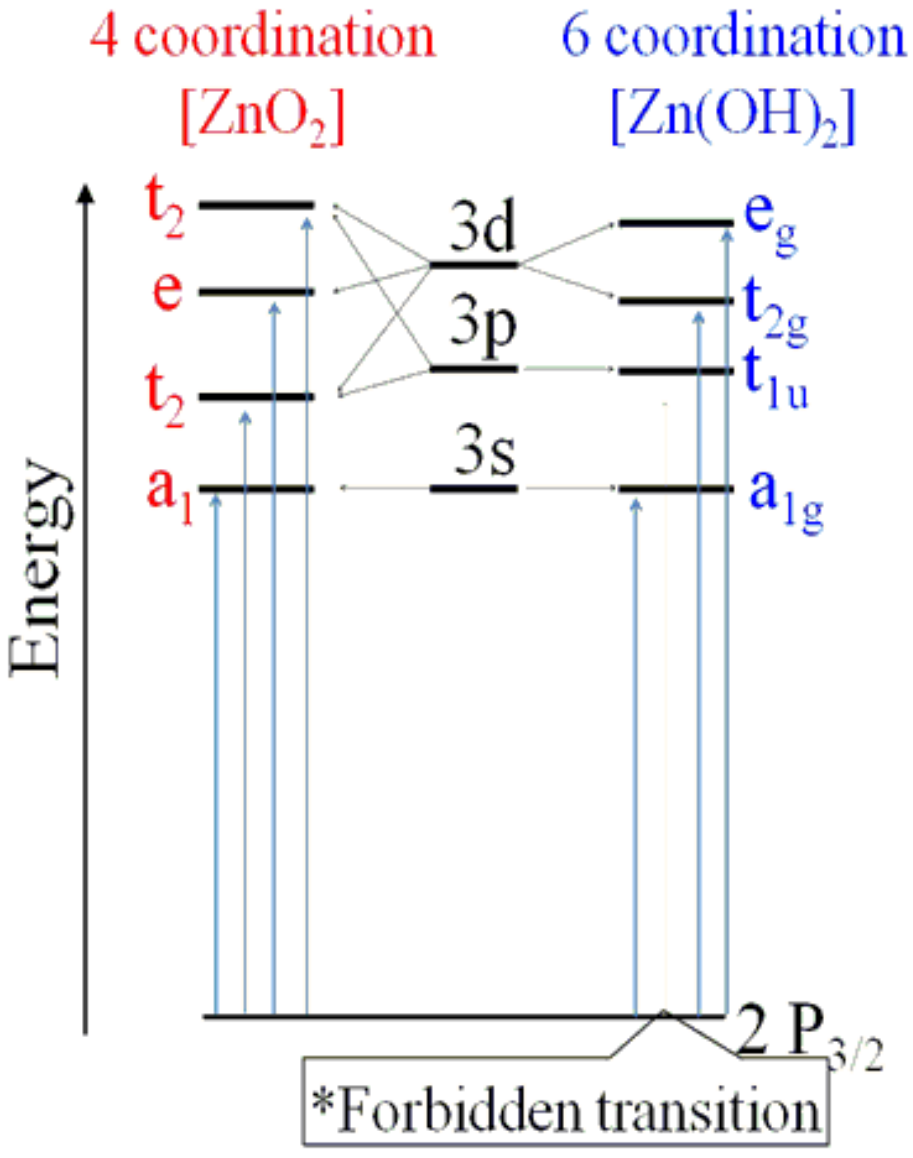

Figure5-4. Molecular orbital diagram of the corresponding primitive unit

The Al K-edge spectrum also showed the coordination change at 400 ˚C. Figure 5-5 shows the Al K-edge spectra of Zn/Al-LDH before and after thermal treatment. The spectrum of Zn/Al-LDH before thermal treatment (bottom) showed an intense peak A, shoulder (=B) around 1570 eV and broad peak(C) around 1590 eV. This spectrum was similar to the characteristic six fold coordination of A, such as Kaolinite ($Al_2Si_2O_5(OH)_4$) and Gibbsite (α-$Al(OH)_3$). The shoulder A was assigned as a dipole-forbidden $1s \rightarrow a_1$ (3p-like) transition. Peak B was assigned as electron transition from Al 1s electrons to the antibonding t_2 (3p-like) state. The broad peak C was attributed to multiple scattering (MS) from the more distant shell atoms.[63] At 400 ˚C, both features were shifted to lower energy by around 2.0 eV. The spectrum at 400 ˚C was similar to tetrahedral Al^{3+} of calcined Mg/Al-LDH.[64] It also has been reported that the Al 1s – 3p transition peak shifted around 2-3 eV to lower energy with the change to four-fold coordination.[63b] This confirms that Al^{3+} in the hydroxide phase was also changed to a metal oxide phase at 400 ˚C (fourfold coordination number) from the LDH phase (six coordination number).

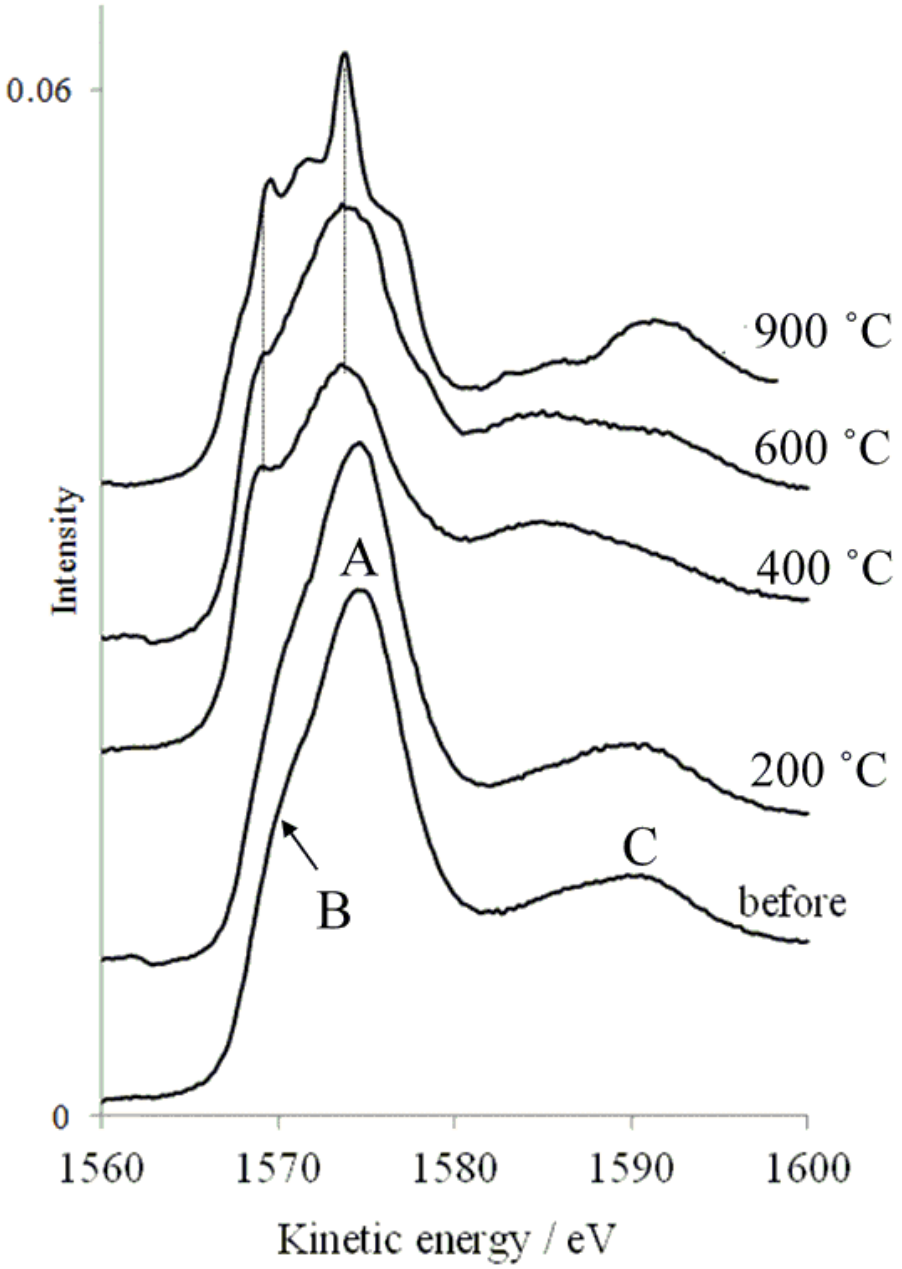

Figure 5-5. XANES Al K-edge spectra of ZnAl-LDH before and after thermal treatment to 900 ˚C.

A second specific insight was determined from the Zn L-edge during thermal treatment. Comparing the Zn L-edge spectra between the sample treated at 400 ˚C and the w-ZnO, it can be seen that the A_t peak at 400 ˚C was more intense than the corresponding peak of w-ZnO. This characteristic feature was also observed in the Zn L-edge spectra of Al doped ZnO.[65] In w-ZnO, the A_t peak was barely observed because the unoccupied Zn4s overlapped with the occupied O2p by hybridization between Zn4s and O2p.[66] This overlapping screened the electron transition of Zn2p(filled)→Zn4s(empty).

On the other hand, the intense A_t peak in the 400 ˚C sample implies that the electron transition Zn2p(filled)→Zn4s(empty) was enhanced compared with w-ZnO due to the Zn4s orbital becoming more empty compared with w-ZnO. This could be explained due to localization of the overlapped electron density around the O^{2-} through the hybridization between Zn4s and O2p by formation of Zn^{2+}-O^{2-}-Al^{3+} bonding. Since Al^{3+} having a net excess positive charge is replaced with Zn^{2+}, the excess positive charge attracted the overlapping electron density to the O^{2-} side of the Zn^{2+} and O^{2-} bond.

The O 2p orbital is hybridized with the Zn and the features observed in the O K-edge spectra were related to those seen in the Zn L-edge spectra following thermal treatment. The K-edge spectra of the LDH after heating at 200 ˚C, 400 ˚C and 600 ˚C, together with w-ZnO as a reference, are shown in Figure 5-6. The w-ZnO reference spectrum was assigned to the transition of O 1s electrons to the empty hybridized orbitals of O 2p and Zn 4 sp.[67] According to the literature,[68] features (a), (b), (c) are assigned to O 2p hybridization

with Zn 4s. Features (c), (d) are assigned to O 2p hybridization with Zn 4p and (f) is assigned to the O 2p- Zn 4d mixed states. Furthermore Møller et. al reported that the feature (a) is a hybridized Zn4s-O2pσ orbital which corresponds to σ-type interaction between Zn and O planes in the w-ZnO crystal. Thus, the peaks (a), (b) and (c) were associated with hybridization between Zn 4s and O2p. However, the O K-edge spectrum at 400 ˚C did not show the (a) (b) and (c) peaks. This can be also explained by the overlapping electron localized around O^{2-} and thus electron transitions from O1s to O 2p were screened because of the decreasing unoccupied character of the O2p.

The O K-edge spectrum of Al doped ZnO also showed similar results where the features (a), (b), (c) decrease due to a reduction in the number of unoccupied O 2p-derived states.[65] These peaks are clearly observed following thermal treatment at 600 ˚C because of the transformation to w-ZnO from the amorphous phase. Therefore both the Zn L-edge and the O K-edge spectra are consistent with the formation of the amorphous Zn and Al mixed oxide (ZAO) phase at a thermal treatment temperature of 400 ˚C and then the ZAO decomposed to pure ZnO at 600 ˚C.

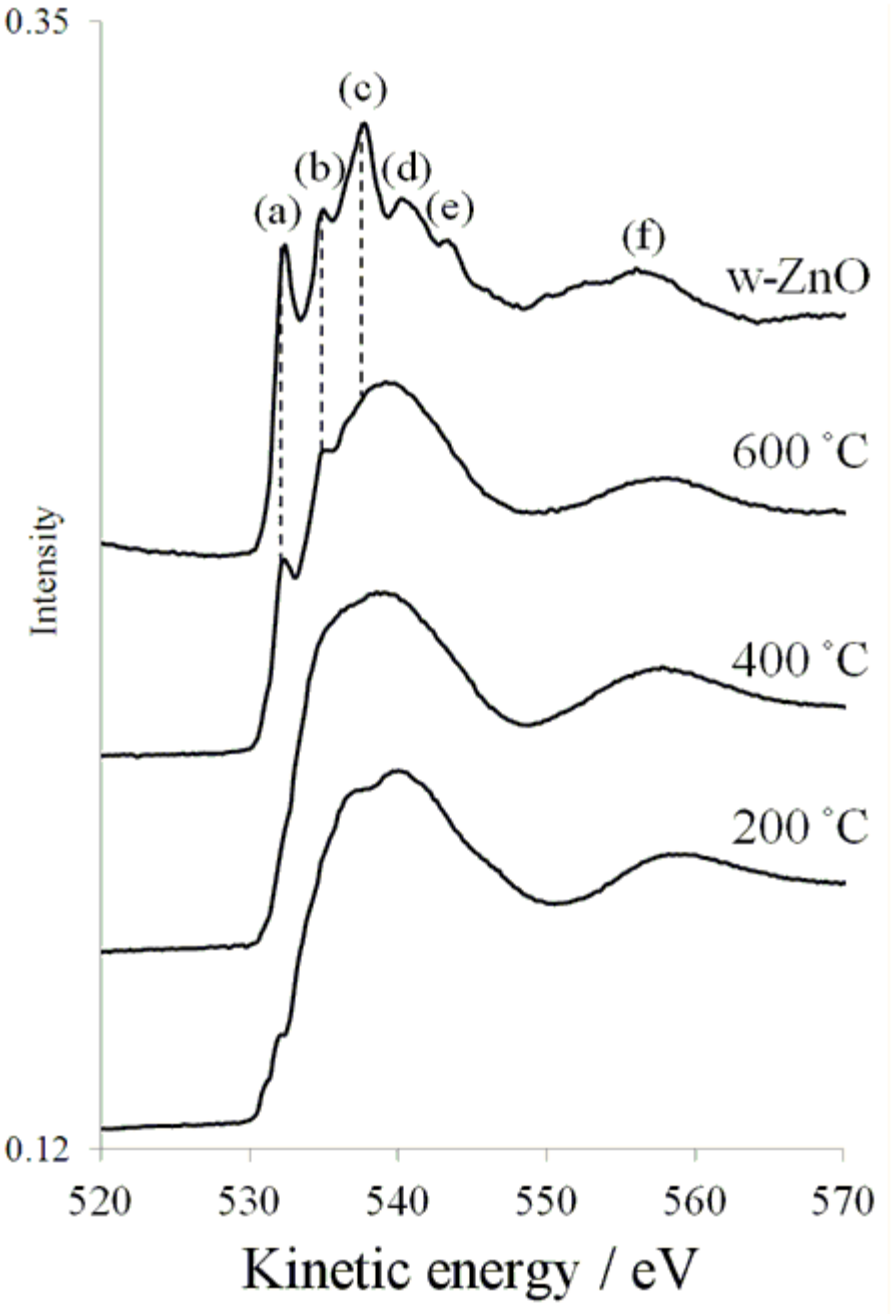

Figure 5-6. XANES O K-edge spectra of ZnAl-LDH before and after thermal treatment up to 900 ˚C.

5-4 Optical properties of calcined Zn/Al-LDH

The band gap energy of the calcined Zn/Al-LDH was examined by UV-VIS DR spectra since previous XANES result showed that the Zn/Al-LDH was changed to the ZAO phase around 400 ˚C. The UV-VIS DR spectra were converted by the Kubelka-Munk equation(equation II-III in Chapter 2-5) and shown in Figure 5-7.

Figure 5-8 shows theUV-vis DR spectra of calcined Zn/Al-LDH up to 900 ˚C along with the w-ZnO. The spectrum at 200 ˚C did not show an absorption edge in the spectral range examined due to the LDH hydroxyl layer remaining until 200 ˚C. However, the calcined Zn/Al-LDH above 300 ˚C started absorbing UV light.

It has been reported that the electronic transition of calcined Zn/Al-LDH at 400 ˚C is a direct process from the oxygen 2p state to the metal ns or np (n=4 for Zn and n=3 for Al).[69] The UV-vis DR spectra were converted to obtain the energy gap (E_g) based on the Kubelka-Munk model according to the following equationV-I)

$$(F(R_\infty)\ h\nu\ )^2=A(h\nu- E_g)\ldots(V\text{-}I)$$

where hν is the photon energy and A is a proportionality constant. $F(R_\infty)$ was obtained from the Kubelka-Munk equation and plotted as $(F(R_\infty)h\nu)^2$ against hν, from which the energy gap (E_g) of the samples can be easily observed (Figure 5-8). Figure 5-9 shows the calculated band gap energy (E_g) of the samples.

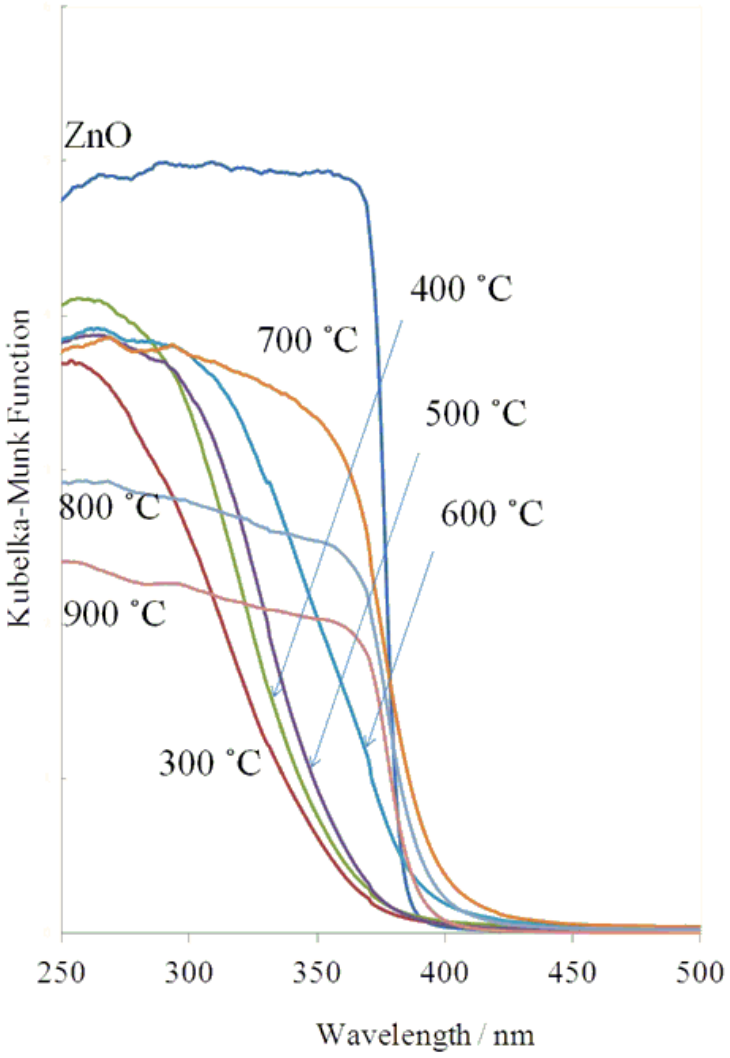

Figure 5-7. UV-VIS DR spectra of ZnAl-LDH before and after thermal treatment up to 900 ˚C

The E_g at 300 ˚C was 3.76 eV which is much higher than the typical ZnO band gap energy(3.3 eV).[70] This is thought to be due to the expansion caused by Al doping into ZnO.[65] The E_g did not change much at 400 ˚C, however it decreased beyond 500 ˚C. The E_g decreased to 3.24 eV at 700 ˚C and was essentially constant beyond that.

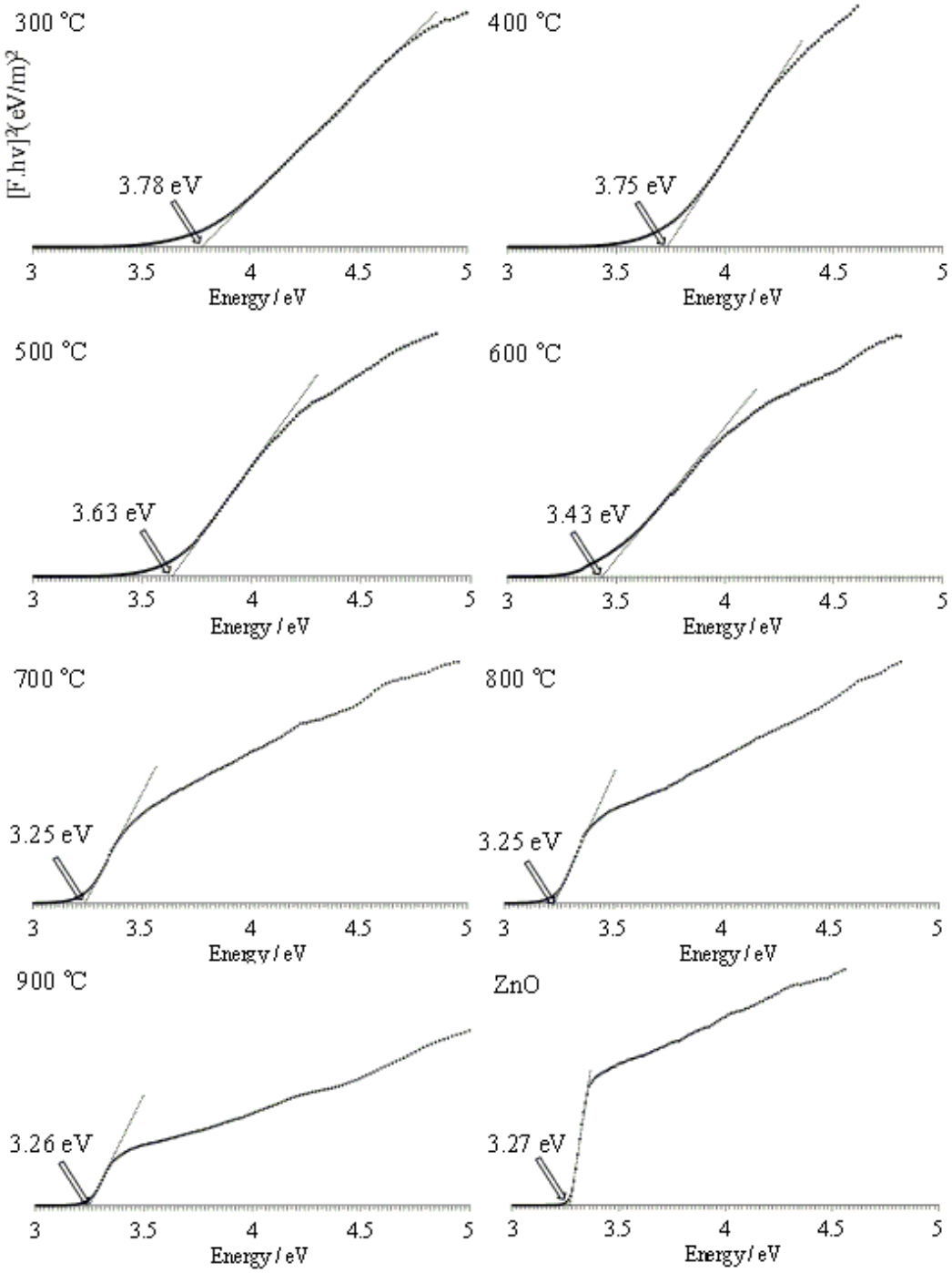

Figure 5-8. Kubelka-Munk model curves of Zn/Al-LDH after thermal treatment up to 900 ˚C

The E_g value of 3.26 eV at 900 ˚C is similar to that of the w-ZnO (3.3eV). A schematic illustration of the thermal structural transition of Zn/Al-LDH is shown in Figure 5-10. The bang gap experiments indicated that the Zn/Al-LDH phase maintained until 200 ˚C. The Zn/Al-LDH(six coordination number) transformed to ZAO(four coordination number) between 300 and 400 ˚C. The ZAO gradually decomposed to w-ZnO from 500 ˚C. The Al^{3+} species above 500 ˚C is not clear. However, since spinel($ZnAl_2O_4$) was observed around 900 ˚C, the Al^{3+} is probably still bonded with a small number of Zn^{2+} and crystallized as spinel at 900 ˚C.

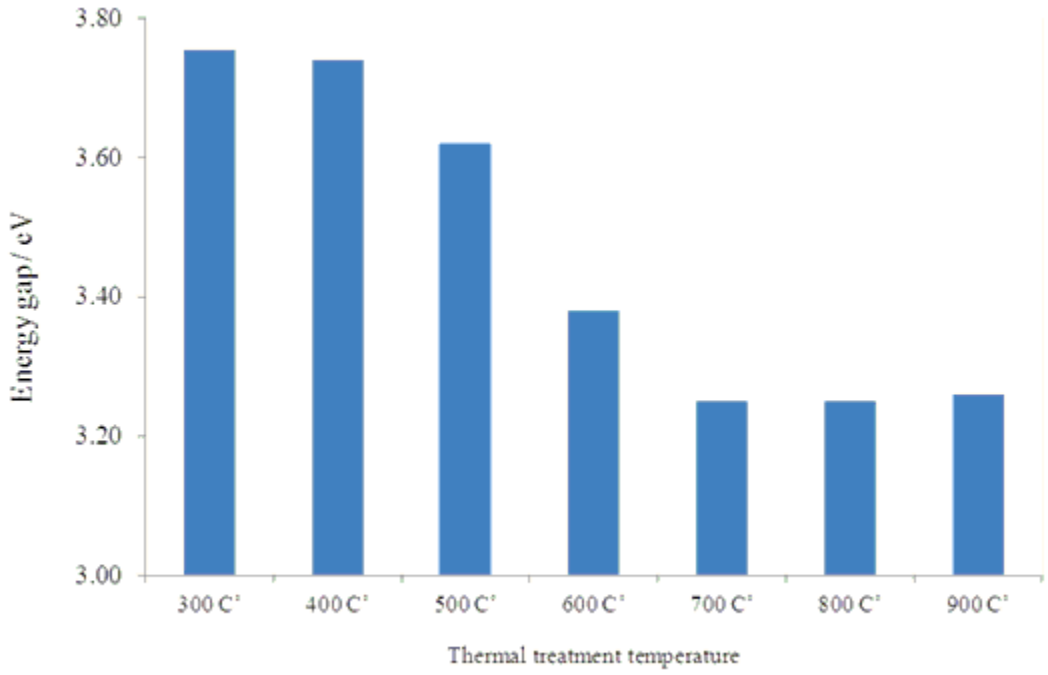

Figure 5-9. Band gap energy of calcined ZnAl-LDH up to 900 ˚C.

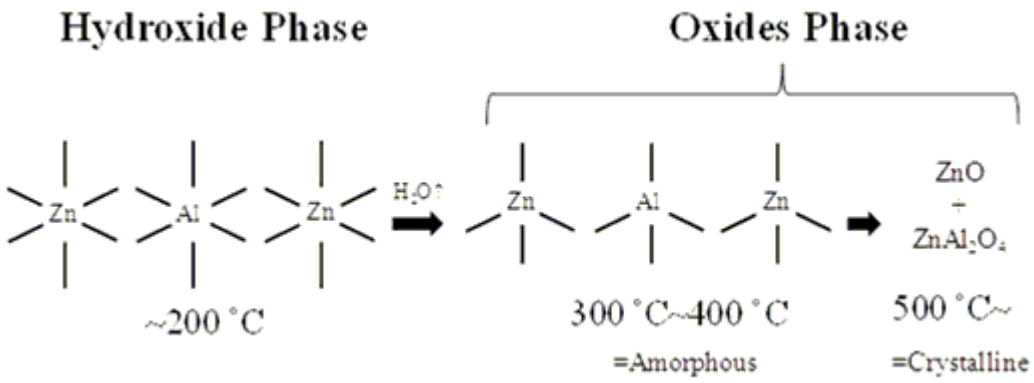

Figure 5-10. Representative of thermal transformation from hydroxide phase to oxide phase by thermal treatment.

5-5 Summary

This research directly observed the formation of an amorphous Zinc/Aluminium mixed oxide derived from a Zn/Al- layered double hydroxides through thermal transition. Below 200 ˚C, the Zn^{2+} and Al^{3+} in Zn/Al-LDH maintain six-fold coordination, which is typical of LDH material, even though the crystal structure of LDH became disordered at 200 ˚C.

The coordination number was changed to four-fold coordination due to the formation of a metal oxide phase by dehydration of the hydroxide layer of Zn/Al-LDH(Figure 4-10). In addition to the information regarding changes to the coordination number, the Zn L-edge and O K-edge XANES spectra provided characteristic features of the formation of chemical

bonding between Zn-O-Al due to the formation of the amorphous Zinc/Aluminium mixed oxide (ZAO). The optical property measurements showed that the ZAO exists over only a short temperature range between 300 ˚C and 400 ˚C. The ZAO gradually decomposed to crystalline ZnO after 400 ˚C.

This research is believed to be the first to apply Zn L-edge, along with O K-edge XANES spectra to analyze and clarify the thermal behaviour of Zn/Al-LDH. It was concluded that Zn L-edge measurement is a powerful tool to identify the nature of the amorphous phase derived from LDH materials. Since the Zn/Al-LDH template approach has potential as an alternative method for the fabrication of a wide variety of mixed metal oxides, and calcined Zn based LDH materials have been found to be potentially useful as a new type photo catalyst, this spectroscopic method should be useful for analysis of those catalysts.

Chapter 6:

Fabrication and characterization of zinc/aluminum mixed oxide films on metal substrate via formation of Zn/Al-layered double hydroxides

6-1 Study of LDH fabrication on metal substrates

Zn/Al-LDH material has been known as a precursor for mixed metal oxide catalysts of because of the structure where two different types of cation (M^{II+} and M^{III+}) are uniformly dispersed and form the layered hydroxides.[22] In the previous chapter it was shown that Zn/Al-LDH powder was transformed in to an amorphous Zn/Al mixed metal oxide (ZAO) phase on thermal treatment at 300 ˚C. The ZAO was stable until around 400 ˚C and then started to decompose in to ZnO and spinel ($ZnAl_2O_4$). The activity of this ZAO is thus likely based on what is effectively a heavily doped ZnO. ZnO has been widely used as a semiconductor material because of its attractive physical properties such as a wide, direct band gap (3.3 eV) and a large exciton binding energy of 60 meV at room temperature.[71] Based on these properties, ZnO has been chosen as a suitable material for the fabrication of photonic devices, conversion of solar light, light emitting diodes (LEDs), piezoelectric, transparent and spin electronics devices etc.[72] The band gap energy of ZAO is about 0.3~1.0eV higher than the band gap of zinc oxide (ZnO) due to the incorporation of the Al^{3+} into ZnO,[65] which makes the material useful for UV sensors, and transparent conducting film.[73]

A number of recent studies have reported the fabrication of LDH materials on metal substrates.[57a, 74] There are essentially two approaches to the fabrication of LDH on metal substrates. One approach is the “co-precipitation method”, which utilises an alkaline solution such as ammonia or sodium hydrate to adjust the pH of the solution. Metal substrates are placed in the solution which contains metal ions and the pH of the solution is

increased by adding a range of alkaline reagents. Cations in the solution start reacting on the surface of the metal with increasing pH. Mg/Fe-LDH and Mg/Al-LDH have been fabricated on magnesium metal substrates by this co-precipitation method.[74d] Cheng et. al. fabricated Zn/Al-LDH and Ni/Al-LDH on alumina/aluminum metal substrate by the co-precipitation method and then the substrate went through hydrothermal treatment to induce crystallization.[75] Another approach is "direct hydrothermal crystallization" using urea. Metal substrates are immersed in to a solution containing metal ions and urea. The resulting solution is transferred to an autoclave vessel, and heated.[74c] The urea decomposes to CO_2 and NH_3 by hydrothermal treatment around 90 ˚C.[76] The pH of the solution increases gradually and the cations in solution react with the metal atoms on the substrate surfaces. Li et. al. reported that crystalline Mg/Al-LDH was fabricated on Magnesium substrate by the hydrothermal method at 100 ˚C for 24 hours.[74c] Zn/Al LDH has also been fabricated on both zinc and aluminum substrate by hydrothermal treatment.[74a, 77]

The mechanism for growth of LDH on metal substrates has been proposed in several reports. For instance, in the case Zn/Al-LDH on Aluminium substrate under hydrothermal treatment with HMTA (Hexamethylenetetramine), the formation of the LDH is described by the following reaction sequence.[77] HMTA, which is as alkaline source, produces ammonia and formaldehyde via hydrolysis.[78]

$2Al(substrate) + 2OH^- + 6H_2O \rightarrow 2Al(OH)_4^- + 3H_2$ ……..…..…….....(6-1)

$Al(OH)_4^- \leftrightarrow Al(OH)_3 + OH^-$ ……..…….....(6-2)

$Zn^{2+} + 4OH^- \rightarrow Zn(OH)_4^{2-}$. …….....(6-3)

$Zn^{2+} + 4NH_3 \rightarrow Zn(NH_3)_4^{2+}$ …….....(6-4)

$Zn(OH)_2 + NH_3 \rightarrow Zn(NH_3)_4^{2+} + 2OH^-$…….……..... …….(6-5)

$Al(OH)_3/Al(OH)_4^- + Zn(OH)_4^{2-}/Zn(NH)_4^{2+} + OH^- + NO_3^- + H_2O \rightarrow$ Zn/Al-LDH ….....(6-6)

Under alkaline conditions, the Al metal can dissolve at the interface to form $Al(OH)_3$ or $Al(OH)_4^-$ species (at pH 7–8) as described by reactions 6-1 and 6-2. At mild alkaline pH when involving ammonia, Zn^{2+} ions can get converted to a number of water soluble species such as $Zn(OH)_2$ (partially soluble), $Zn(OH)_4^-$ or $Zn(NH_3)_4^{2+}$ (Reactions 6-3~6-5). The reaction between $Al(OH)_4^-$ with any of these Zn species, gives rise to the Zn/Al-LDH phase by reaction 6-6. The formation of Zn/Al-LDH with urea under reflux conditions has also been reported using the same reactions.[29]

The calcined product of such a coating producing $ZnO/ZnAl_2O_4$ has been employed as an anode material for Li-ion batteries. However, although there are numerous reports on the fabrication of LDH, there is no work reporting photocurrent detection from such calcined Zn/Al-LDH. Fabricating mixed metal oxides via Zn/Al-LDH on metal substrates has the potential for a new type of photonic material, converting solar light and potentially useful in LEDs. In this chapter, the synthesis of ZAO for photocatalysis on zinc substrates via the formation of Zn/Al LDH has been investigated. The chapter is separated in to two sections. The first focuses on the fabrication of Zn/Al-LDH on zinc metal substrates by direct hydrothermal crystallization. The “direct hydrothermal crystallization” method is employed since the “co-precipitation method” needs hydrothermal treatment for crystallization after

fabrication of the LDH on the substrate, whereas the “direct hydrothermal crystallization” method can fabricate LDH on substrates in a one step process. The hydrothermal reaction conditions were investigated by varying the hydrothermal temperature and reaction time. The second part of the chapter describes the transformation of Zn/Al-LDH into a mixed metal oxide (ZAO) by thermal treatment, and an investigation of the photocatalytic properties of the ZAO by electrochemical analysis. The structure and nature of the ZAO films was characterized by XRD and SEM.

6-2 Zn/Al-LDH fabrication on Zinc substrate by hydrothermal treatment

6-2-1 Role of hydrothermal temperature and reaction time

The hydrothermal temperature was varied between 60 and 105 ˚C with a fixed reaction time of 8 hours. The hydrothermal temperature of sample names are reflected in the sample descriptions, for example, 60HT, 75HT, 90HT instead of 60 ˚C, 75 ˚C and 90 ˚C to avoid confusing hydrothermal temperature (HT) and subsequent thermal treatment (˚C). The hydrothermal reaction time was also varied from 4 to 12h at a hydrothermal temperature of 75 ˚C in order to assess the effects of time on the growing LDH layer. The thickness of LDH layer was estimated from cross section measurement from the SEM images.

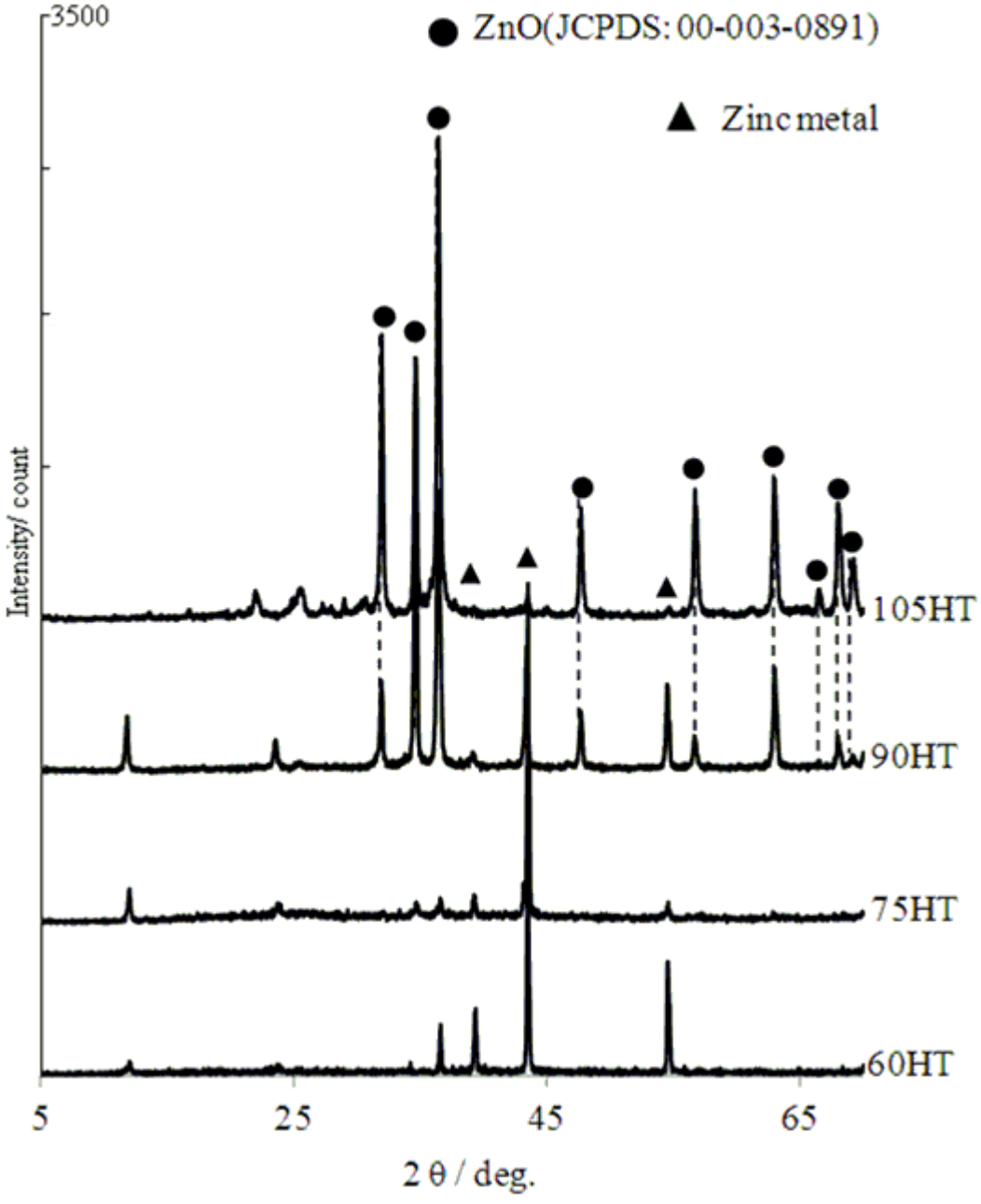

Figure 6-1 XRD patterns of Zinc metal substrate depending on hydrothermal temperature

Figure 6-1 shows XRD patterns of Zn/Al-LDH at different hydrothermal temperatures from 60 to 105 ˚C. For the sample at 60 ˚C the main diffraction peaks come from the Zn substrate with small diffraction peaks at 2θ values of around 11˚ and 22˚ which can be assigned as typical *00l* diffraction lines of Zn/Al-LDH.[29] The intensity of these peaks increased for the 75HT sample, and the calculated basal spacing of 0.79 nm is the same as the basal spacing of carbonate intercalated Zn/Al-LDH.[49] The relative intensity of these Zn/Al-LDH diffraction peaks increased further for the 90HT sample, but at this temperature peaks assigned as zinc oxide(JCPDS: 00-003-0891) were also observed. When the hydrothermal temperature was increased to 105 ˚C, the zinc oxide phase was dominant and the peaks assigned to LDH diffraction had almost disappeared. Table 6-1 shows the pH of the solution following the hydrothermal treatment at each temperature, which increased with increasing hydrothermal temperature due to the decomposition of urea which occurs around 90 ˚C.[76] The lack of LDH for the 60HT is therefore attributed to the low pH since the temperature is below the urea decomposition temperature. Although the 75 ˚C is still below the urea decomposition temperature, LDH was observed in the XRD patterns and the pH was seen to increase and it is thought that the urea decomposition may be enhanced by hydrothermal treatment. The pH had slightly increased above 90HT. It has been reported that the Zn/Al-LDH structure is stable until a pH 11.[79] But in this work ZnO was first observed at hydrothermal temperature of 90 ˚C and was dominant at 105 ˚C where the pH was still below 8. Therefore, the formation of crystalline zinc oxide was thought to be not due to the increased pH of the solution. It appears as though high hydrothermal temperature (above 90 ˚C) enhanced the formation of the zinc oxide instead of the LDH structure. It has

been reported that ZnO nanowires could be synthesized on silicon substrates at a hydrothermal treatment of 90 ˚C .[80]

Figure6-2 shows SEM images of 60HT, 75HT and 105HT, and the observations from these images are in good agreement with the data from XRD. LDH materials are known to possess a plate like structure with high aspect ratio.[29, 81] The XRD pattern for 60HT showed that LDH crystallization did not occur to any great extent at this temperature, and no obvious evidence of this typical LDH appearance was observed in the SEM image for 60HT. Typical LDH plate like structures were observed on the Zinc substrate for the 75HT and appear to grow vertically on the substrate. All of the LDH material had disappeared at 105HT and instead of the platelike structures, the surface was seen to be composed of rod like particles which is the reported morphology for zinc oxide.[82]

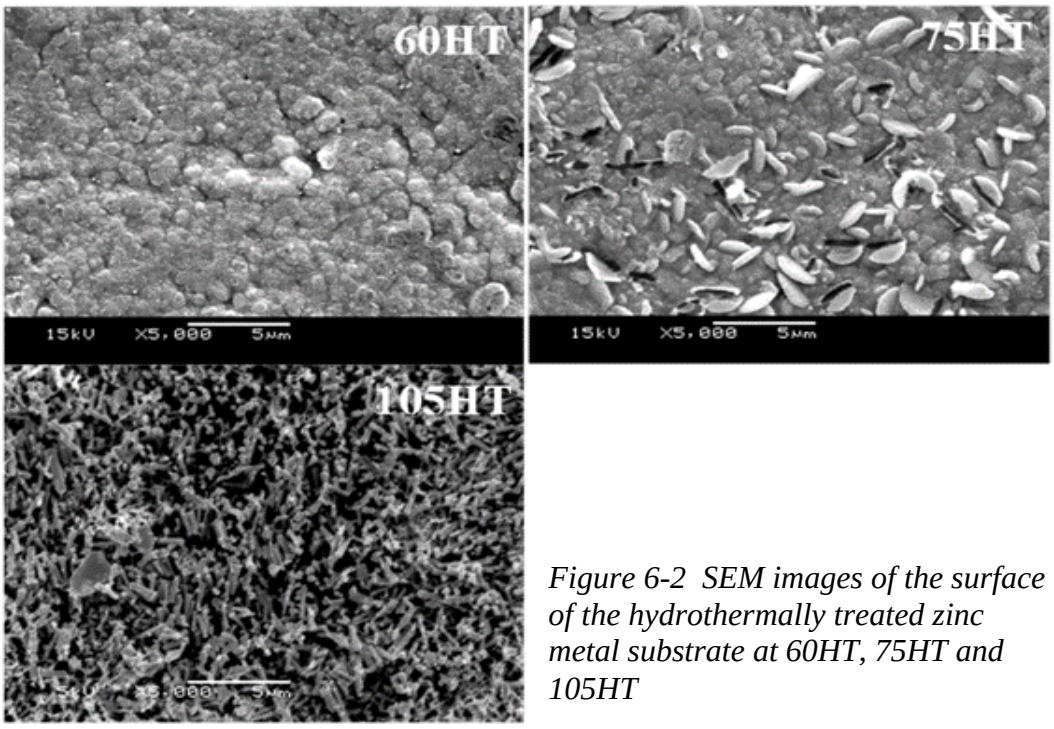

Figure 6-2 SEM images of the surface of the hydrothermally treated zinc metal substrate at 60HT, 75HT and 105HT

The hydrothermal reaction time was changed from 4h to 12h in order to assess how the growth of the LDH layer depends on reaction time. The LDH layer was investigated by SEM. Figure 6-3 shows SEM images of the Zn substrate following hydrothermal treatment at various times from 4 to 12 hours at a fixed temperature of 75 ˚C. After 4 hours, a thin film with thickness of less than 1 µm was formed on the surface of the zinc substrate. The thickness of the film increased to around 2µm after 8 hours but did not change significantly after longer periods. The pH after a 4 hour reaction time was 4.90 and increased to 6.80 after 8 hours. At 12 hours there was almost no change with a final pH of 6.85. It is concluded from these images that the growth of the LDH layer on the zinc substrate had stopped after 8 hours due to depletion of the urea resulting in the termination of reaction (6) due to a lack of an alkaline source.

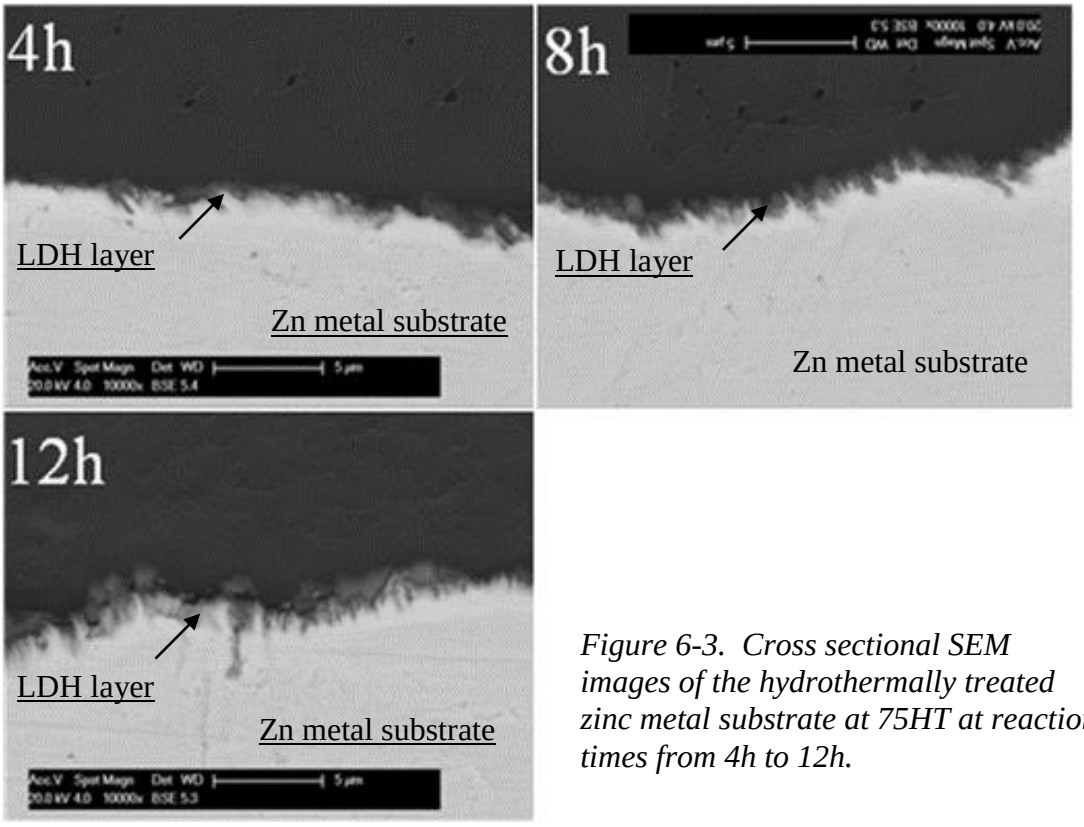

Figure 6-3. Cross sectional SEM images of the hydrothermally treated zinc metal substrate at 75HT at reaction times from 4h to 12h.

Table 6-1 pH of resulting solution after thermal treatment from 60HT to 105HT

	60HT	75HT	90HT	105HT
pH	5.8	6.8	7.0	7.7

6-2-2 Surface analysis of Zn/Al-LDH on Zn substrate by XPS

The surface composition of the Zn/Al-LDH layer on the zinc substrate was characterized by XPS. XPS analysis of the Zn/Al-LDH film from the 75HT sample was carried out by investigation of the Zn 2p, O ls and Al2p core level spectra as shown in Figure 6-4. The Zn2p core level spectrum can be distinguished as 2p3/2 and 2p1/2 peaks with binding energies of 1022.5eV and 1046eV, respectively, which are closer to the reported binding energies of Zn^{2+}2p (1022.4eV: 2p3/2 and 1046eV: 2p1/2.[83]) than to that of the 2p 3/2 of metallic Zn (1021.8eV). This suggests that as expected the surface of the Zn metal was converted to Zn^{2+} species under the hydrothermal conditions at 75 ˚C. The O1s peak at 75HT was around 531.8 eV. The O1s of zinc hydroxide is reported at 531.9eV whilst that of ZnO is reported at 530.2~530.5eV.[84] The Al2p for 75HT was at a binding energy of 74.0eV which again is close to the 74.2±0.6 eV reported for Al^{3+} in Zn/Al-LDH[85]. Thus, the XPS data also confirmed that Zn/Al-LDH material was formed on the surface of the Zn substrate. The atomic ratio of Zn/Al, calculated from the integrated area of the Zn2s and Al2s peaks was 1.3:1(=Zn:Al) as the atomic ratio.

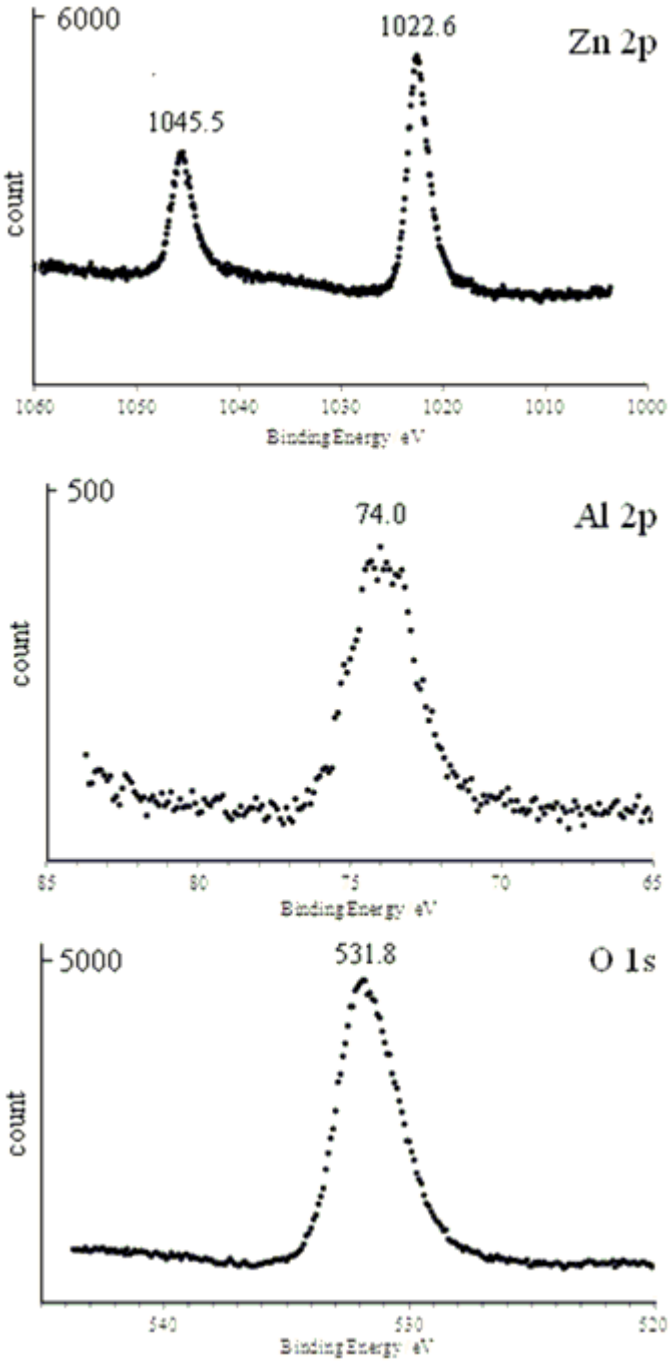

Figure 6-4 XPS spectra of hydrothermal treated zinc substrate at 75HT, Zn2p, Al2p andO1s

Based on this atomic ratio of Zn/Al from the XPS result and the general formula of the LDH material, which is $Zn_{1-x}Al_x(OH)_2A_{x/n} \cdot mH_2O$, the composition of the LDH for the 75HT sample can be estimated as $Zn_{0.57}Al_{0.43}(OH)_2(CO_3)_{0.21}\ xH_2O$.

6-2-3 Mechanism of Zn/Al-LDH formation on Zn substrates by hydrothermal treatment

Following the hydrothermal reaction, there was a small amount of sediment observed on the bottom of the reaction vessel. Figure 6-5 shows the XRD pattern of the sediment, and the peaks and lattice parameters can be ascribed to Zn/Al-LDH with carbonate intercalation.[29]

The Zn metal substrate was the only source of Zn, and the formation of Zn/Al-LDH precipitation indicates that some of the Zn was dissolved in to solution from the Zn metal substrate under the hydrothermal conditions and then the Zn^{2+} ions formed the LDH material with Al^{3+} on the Zn substrate. The mechanism of Zn/Al-LDH formation on Zn substrate is proposed as following the reaction sequence described below:

$2Zn + 6OH^- \rightarrow 2Zn(OH)^+ + 2H_2O + O_2$ ..…..……..(6-7)

$Al^{3+} + 4OH^- \rightarrow Al(OH)_4^-$ ..…..……..... .....(6-8)

$2Zn(OH)^+ + Al(OH)_4^- + 0.5CO_3^{2-} \rightarrow Zn_2Al(OH)_6(CO_3^{2-})_{0.5}H_2O$...(6-9)

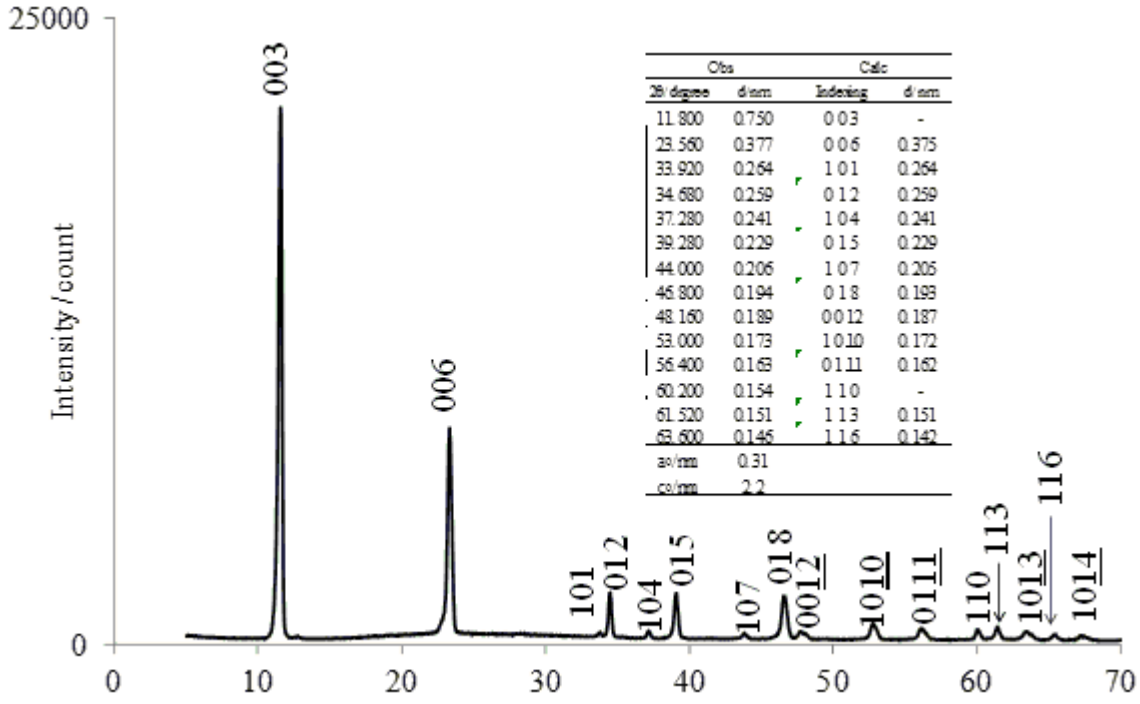

Figure 6-5 XRD pattern of precipitation on bottom of reaction vessel at 75HT

Urea produces ammonia and carbonate via hydrolysis.[76] In alkaline conditions, Zn metal can dissolve at the interface to form $Zn(OH)^+$ species (pH 6-11) in reaction (5-7).[86] Al^{3+} ions can get converted to $Al(OH)_4^-$ in reaction (5-8). The reaction between $Zn(OH)^+$ and $Al(OH)_4^-$ with carbonate and H_2O on the zinc substrate gives rise to Zn/Al-LDH by reaction (5-9).

6-3 Thermal transformation to amorphous phase Zinc/Aluminium mixed metal oxide (ZAO) and investigation of photocatalytic properties of the amorphous phase

In the previous section, the hydrothermal conditions for Zn/Al-LDH formation were investigated and the optimum conditions in terms of producing a single phase Zn/Al-LDH with the maximum thickness were shown to be at a hydrothermal temperature of 75 ˚C and reaction time of 8h (sample name:75HT). The pH following reaction was 6.8. This section describes a photoactivity study of the ZAO formed from the Zn/Al-LDH by thermal treatment. The first part of this section describes the conversion of the optimum Zn/Al-LDH (75HT-8 hours) to the amorphous phase by subsequent thermal treatment at temperatures from 100-300 ˚C, and investigation of its photcatalytic properties as a function of thermal treatment temperature. The second part describes the effect of the initial Zn/Al-LDH hydrothermal treatment conditions, in terms of time and temperature, on the photocatalytic properties of the amorphous phase produced by subsequent heat treatment at 200 ˚C.

6-3-1 Thermal transformation of Zn/Al-LDH to amorphous phase

The Zn/Al-LDH fabrication conditions were based on the previous results of section 6-2 and chosen to be 75 ˚C and a reaction time of 8h (75HT sample). The fabricated Zn/Al-LDH on zinc substrate was thermally treated in a furnace in air at temperatures of 100, 200 and 300 ˚C since the melting point of zinc metal is 416 ˚C. The samples were held for 2 hours and then cooled down to room temperature under normal cooling. Changes to the crystalline phase structure as a result of heat treatment were investigated by XRD using the

same conditions as described in section 6-2. Figure 6-6 shows XRD patterns of the Zn/Al-LDH before and after thermal treatment. The Zn substrate was seen in all cases due to the low thickness of the coatings. The Zn/Al-LDH pattern was observed until 100 ˚C, however, diffraction from the LDH was not observed at temperatures of 200 ˚C and above. This has been reported as the typical thermal behavior of LDH materials.[48b, 48d] The crystalline LDH material was converted to an amorphous phase between 200 ˚C and 300 ˚C due to dehydration of the metal hydroxides layers of the LDH.

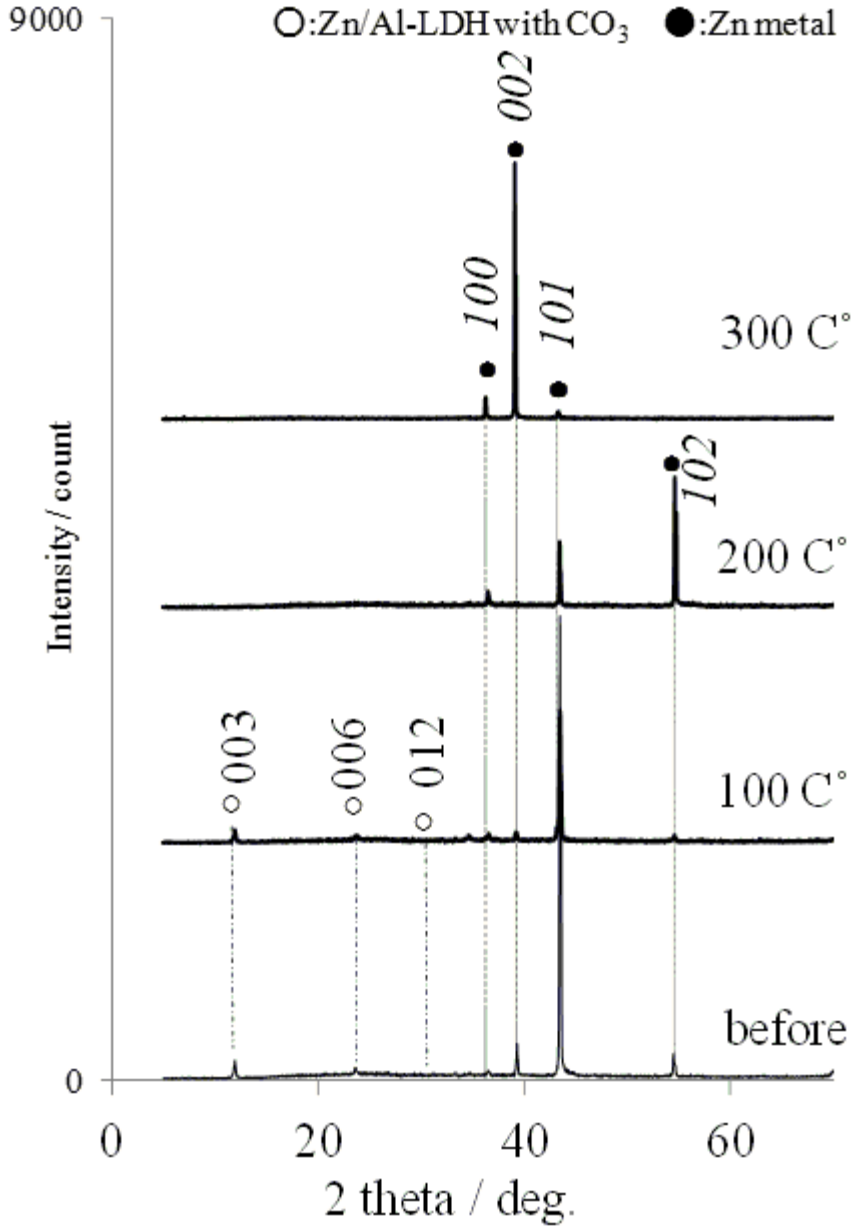

Figure 6-6. XRD pattern of hydrothermally treated Zinc metal substrates at 75HT before and after thermal treatment up to 300 ˚C.

In the previous chapter describing the thermal behaviour of powdered Zn/Al-LDH, the amorphous phase was identified as a Zn and Al mixed oxide (ZAO). Furthermore, since the ZnO species is not volatile between 200 ˚C and 300 ˚C,[87] the loss of diffraction from the crystalline Zn/Al-LDH on the Zn substrate at temperatures of 200 ˚C and above may is likely indicative of the formation of the Zn and Al mixed oxides as an amorphous phase and can be described by the reaction (6-10);

$Zn_{0.57}Al_{0.43}(OH)_2(CO_3)_{0.21}\ xH_2O \rightarrow [\ Zn_{0.57}Al_{0.43}O][\ 0.21CO_3^{2-}] + (2+x)H_2O$.....(6-10)

The photocatalytic properties of the amorphous phase samples produced by heat treatment were studied as a function of thermal treatment temperatures using a three electrode potentiostat (working electrode, counter electrode and reference electrode) in methanol.[88] Figure 8 shows a schematic of the system.

The working electrode was the produced sample of zinc substrate whilst the counter electrode was platinum, and the reference electrode was composed of silver metal wire and a silver chloride electrolyte. In this experiment the working electrode acts as the anode since the amorphous phase can be assumed as based on ZnO which is known as an n type semiconductor.[89] Methanol was used to scavenge the holes from the mixed oxide.[32] High pressure mercury, which has a maximum peak at 365 nm was used as light source for the photocatalysis experiment. Figure 6-8 shows photocurrent curves from the Zn/Al-LDH before and after thermal treatment. The photocurrent was measured from anodic electrode. No photocurrent was detected for either the initial sample of the one treated at 100 ˚C, consistent with the XRD pattern which showed the Zn/Al-LDH diffraction pattern until 100

˚C. This indicates the photocatalytic oxide was not formed at 100 ˚C. On the other hand, a significant photocurrent was detected for samples treated at both 200˚C and 300 ˚C. These results indicate that the amorphous phases at 200 ˚C and 300 ˚C possess photoactivity under 365 nm UV light. As the chemical reaction (10) showed, the Zn/Al-LDH was transformed into an amorphous Zn/Al mixed oxide(ZAO) phase at 200 ˚C and 300 ˚C. Thus, the amorphous phase of the 75HT sample at 200 ˚C and 300 ˚C (ZAO) can be confirmed as a photocatalytic material. ZnO is a known n type photocatalyst, which provide anodic current,[90] under 365nm light[60] thus the question which arises for these materials is whether they are behaving effectively as a heavily Al doped ZnO or a phase separated material, part of which is photoactive.

The result showed the photocurrent was also observed from anode electrode. The catalysis can be assigned as n type semiconductor. Since the XRD pattern showed amorphous phase on the substrate, the photoactiytic material might be heavily Al doped ZnO rather than pure ZnO because the pure ZnO has crystalline structure and XRD pattern shows strong X-ray reflection and Al doped ZnO has been reported as amorphous phase on XRD pattern.[91] However, the band gap energy of the sample has not been measured because the measurement require x-ray absorption and emission spectroscopies in synchrotron, which can be conducted in the Australian synchrotron. The current at 200 ˚C was slightly higher and more stable than that at 300 ˚C. However, the reason for this is not clear.

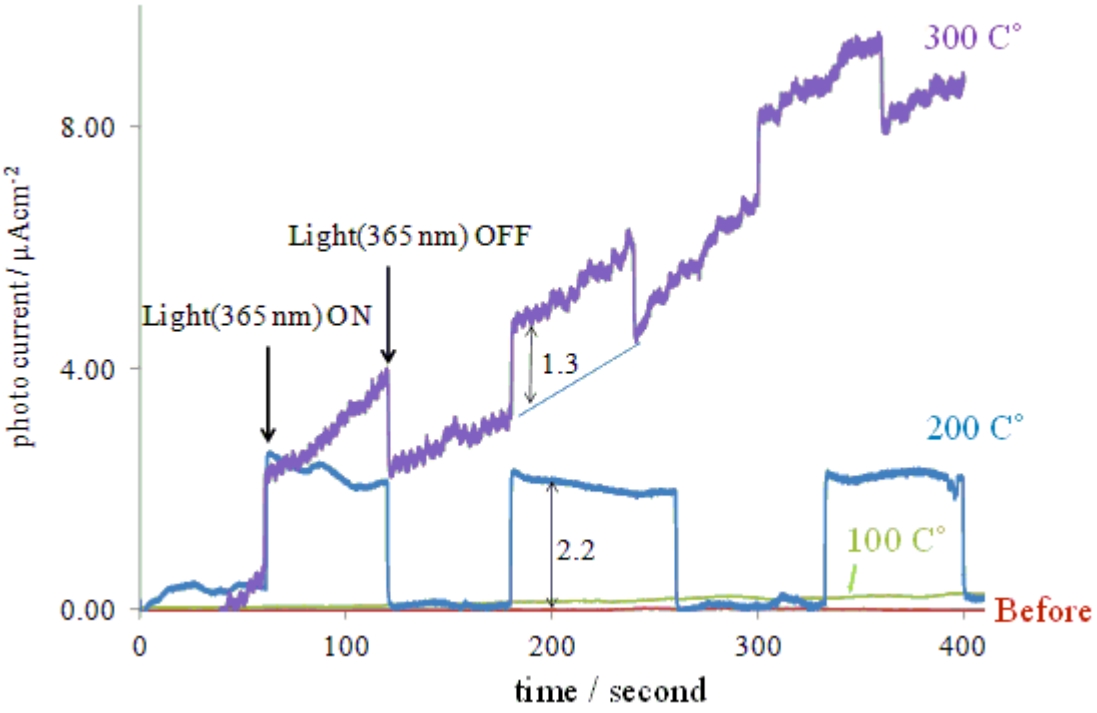

Figure 6-8. Photocurrent curve of hydrothermally treated ZnAl-LDH material (75HT) on a Zinc metal substrate before and after thermal treatment.

6-3-2 Photocurrent properties of ZAO depending on hydrothermal conditions

The previous section showed that the photocatalytic property was observed from calcined LDH sample after thermal treatment at 200 ˚C and 300 ˚C. This section describes the effects of the initial hydrothermal temperatures for the formation of the Zn/Al-LDH on the photocatalytic properties following a thermal treatment at 200 ˚C for 2h. The photocurrent of the samples was measured under 365 nm light as described previously. Figure 6-9 shows photocurrent curves when the hydrothermal temperature was changed from 60 ˚C to 105 ˚C. When the LDH was synthesized at a hydrothermal temperature 60 ˚C, the photocurrent was

small compared with other samples. The photocurrent increased when the hydrothermal temperature was increased to 75 ˚C. However, the photocurrent decreased with increasing hydrothermal temperature above 90 ˚C. Since the photocatalytic phase was converted from the Zn/Al-LDH, the small photocurrent at 60HT sample was simply due to lack of the Zn/Al-LDH formation. The photocurrent was increased for the 75HT sample because the LDH formation was enhanced at hydrothermal temperature at 75 ˚C. At this temperature, XRD diffraction from the 75HT sample (Figure 5-2) showed intense, single phase diffraction from the LDH. Figure 6-10 shows cross section SEM images of the samples.

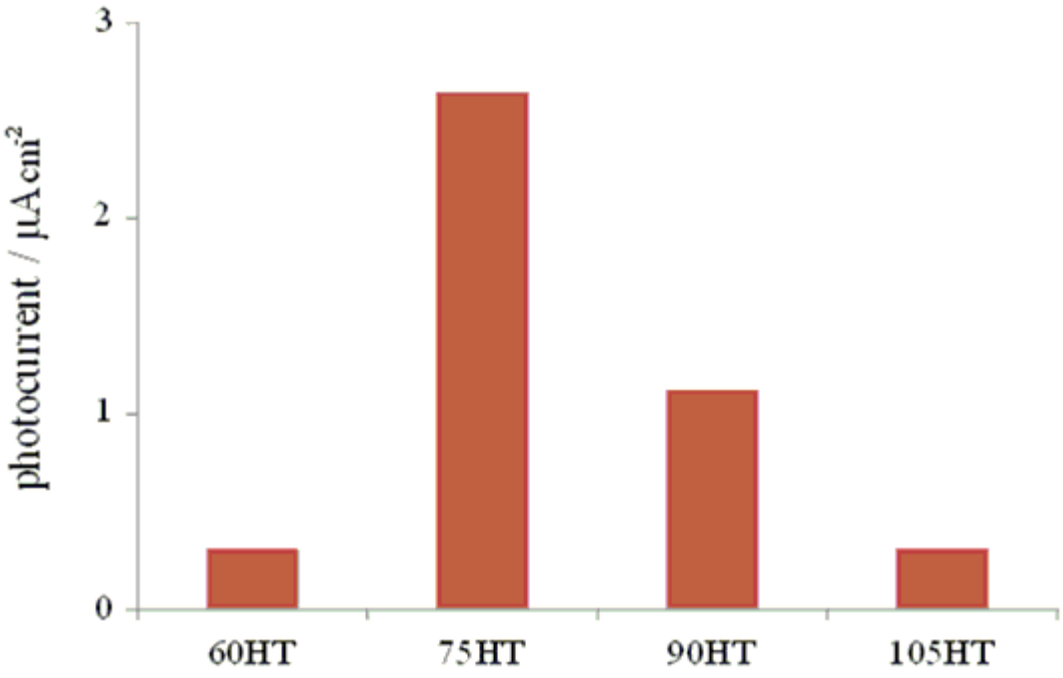

Figure 6-9. Photocurrent values of ZAO surfaces depending on hydrothermal treatment temperature from 75HT to 105HT.

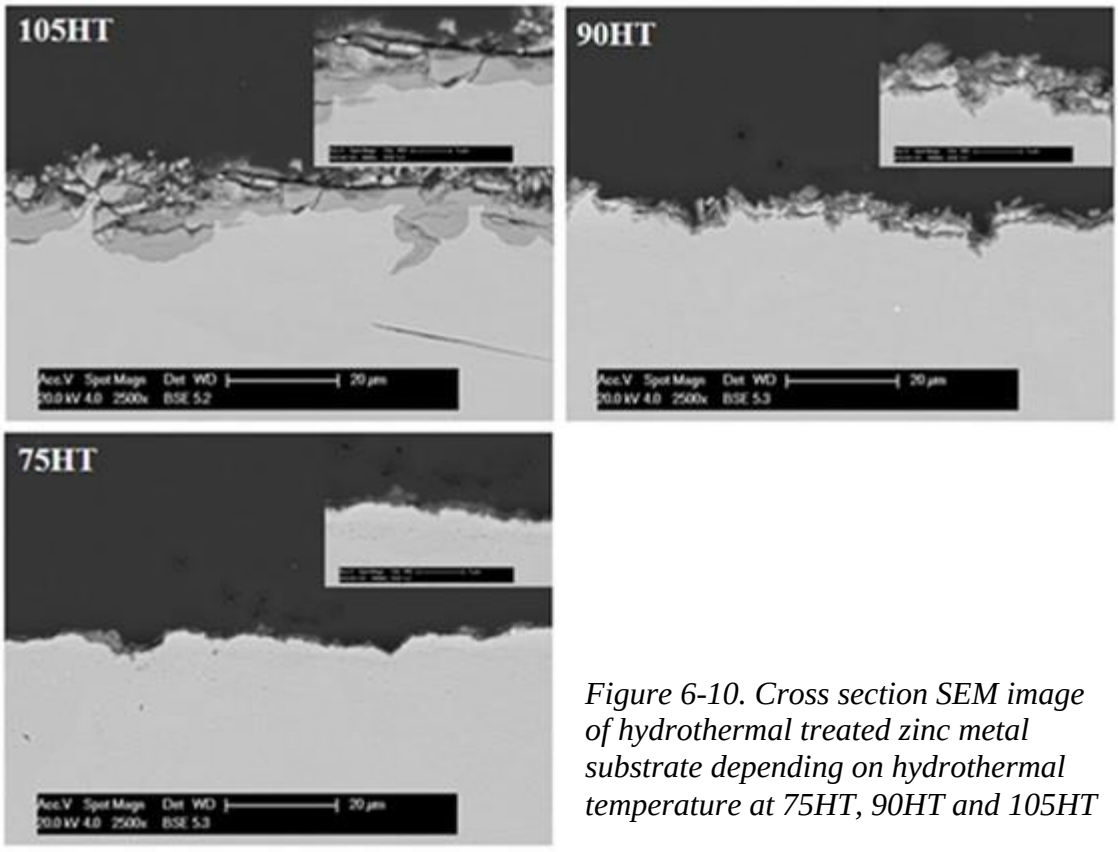

Figure 6-10. Cross section SEM image of hydrothermal treated zinc metal substrate depending on hydrothermal temperature at 75HT, 90HT and 105HT

The thickness of the layers at 75HT, 90HT and 105HT were around 2 μm, 3 μm and 3~8 μm, respectively. The layers on the substrate at 90HT and 105HT were found to contain a large number of cracks, and the reason for the decrease in photocurrent above 75HT is thought to be that the cracks interrupt the photon path to the substrate even if electrons were produced on the surface by photo reaction. Therefore, the strongest photocurrent observed from the phase prepared from the 75HT Zn/Al-LDH was due to the fact that only Zn/Al-LDH formed on the Zn substrate. For hydrothermal temperatures lower than 75 ˚C, the photocurrent was low because the Zn/Al-LDH could not be formed on the Zn substrate due to lower pH. For hydrothermal temperatures higher than 90 ˚C, the photocurrent

decreased due to the appearance of cracks in the photocatalytic phase and this interrupted the photocurrent path to the Zn substrate.

Figure 6-11 shows photocurrent data when the hydrothermal reaction time was changed from 4 hour to 18 hour at 75 ˚C. The photocurrent increased from 4 to 8 hours but was similar for longer times. The low photocurrent at 4 h is due to the thin nature and incomplete coverage of the film of amorphous mixed metal oxide phase formed via Zn/Al-LDH. The constant nature of the photocurrent at times beyond 8h meant that the growth of the photocatalytic phase had stopped after 8 h. This is related to the fact that the formation of the LDH layer had reached a maximum at 8 h as was shown in the XRD patterns and SEM images (Figure 6-3).

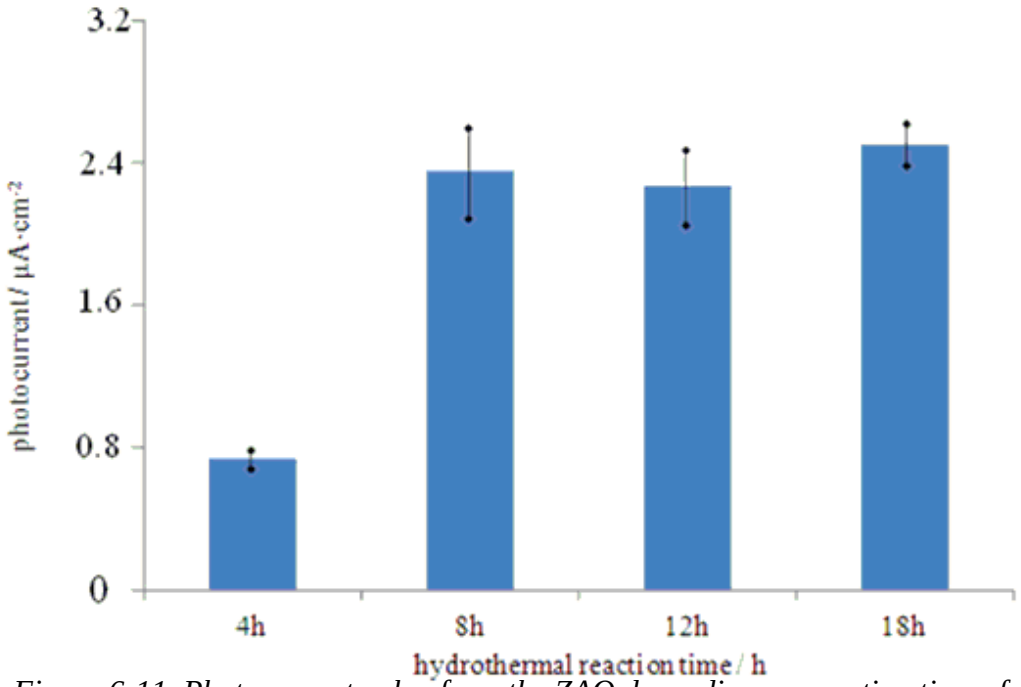

Figure 6-11. Photocurrent value from the ZAO depending on reaction time of the LDH synthesis from 4h to 18h at 75HT

6-4 Summary

The photocurrent from an amorphous LDH derived Zn/Al mixed metal oxide (ZAO) has been successfully observed under UV light (365nm). The Zn/Al mixed metal oxide was fabricated on a zinc metal substrate via the formation of Zn/Al-LDH through hydrothermal treatment. The hydrothermal temperature for fabrication of the Zn/Al-LDH on the zinc substrate and the thermal treatment for transformation of this Zn/Al-LDH to the photocatalytic phase were shown to be important factors for inducing photocurrents . At a hydrothermal temperature of 75 ˚C single phase LDH was formed on the zinc substrate, whereas at higher hydrothermal temperatures, the appearance of zinc oxide as an impurity phase was observed along with the Zn/Al-LDH phase. The formation of Zn/Al-LDH reached a maximum at a reaction time of 8 hour at a hydrothermal treatment 75 ˚C. The Zn/Al-LDH on Zinc substrate was transformed to the photocatalytic phase during subsequent heat treatment from 200 ˚C. Optimized conditions for achieving maximum photocurrent were determined to be a hydrothermal temperature of 75 ˚C, a reaction time of 8h and then transformation of the Zn/Al-LDH to the photocatalytic phase at 200 ˚C.

Chapter 7:
Conclusions and Outlook

The research reported in this thesis shows that following phosphate uptake, it is possible to remove interlayer phosphate completely from layered double hydroxides (LDH) by a two cycle anion exchange reaction with surfactant anions. Even a single anion exchange with surfactant results in more than 90 % phosphate removal from the LDH. This high phosphate desorption rate dramatically improves recyclability of the LDH materials as reusable adsorbents of phosphate. Compared with the conventional method which uses concentrated sodium carbonate solution or mixed solutions of sodium chloride and caustic soda, the re-adsorption properties are improved to almost 3 times higher loadings than the conventional methods.

The desorption ability of the surfactant is related to formation micelles at and above the critical micelle concentration (CMC). Micelle formation enhances removal of interlayer phosphate by anion exchange with surfactant anions. In particular, from a range of surfactants tested, dodecyl benzene sulfonate (DBS), which is one of the most common surfactants and is a low-cost material biodegradable material and indeed one of the main components of detergents for laundry and dish washing, is particularly effective. After a series of trials at varying concentrations, it was established that DBS achieves 95 % phosphate removal at 0.003 M. The 0.003 M is almost same level DBS concentration as waste water from laundry and washing processes.

Furthermore, the pH of the DBS solution is weakly alkaline (pH8~9). On the other hand, the conventional methods use highly alkaline solutions (more than pH11). In fact, the

desorption ratio using 1.0M of Na_2CO_3 solution (pH11.6), which is the most common conventional method of phosphate removal, removed 58.8 % of phosphate from LDH. In the recycling process, phosphate re-adsorption is 90 % when DBS is used as the eluting solution for the phosphate. This is due to the high desorption ratio of interlayer phosphate by anion exchanged with DBS anion. However, re-adsorption when the Na_2CO_3 solution is used is 23 %. This is because more than 40 % of interlayer phosphate remained in the interlayer region after the desorption process with Na_2CO_3 solution due to carbonate having strong affinity to LDH material.[92] The method described in the thesis using DBS is thus significantly superior to the conventional method in term of environmental-friendliness and efficiency.

The mechanism of efficient phosphate desorption associated with surfactant micelle formation is demonstrated in this research. Below the CMC, surfactant anion exists as monomer anion. Since the monomer surfactant has only one negative charge, interlayer phosphate is not readily exchanged with the monomer anions of the surfactant. As concentration approaches the CMC, monomer surfactants aggregate and form a micelle structure. The formation of surfactant micelles increases local negative charge density on the surface of the micelle by locally gathering sulfonate group of surfactant in the micelles. The increasing local negative charge provides a driving force for the intercalation of the micelle into the interlayer spacing and exchange with interlayer phosphate.

The outlook arising from this research using surfactant micelles for phosphate desorption, has potential in several other directions. As LDH material has been studied as an adsorbent of oxo-anion, such as chromate, molybdate, vanadate, arsenate, and selenate etc, this method can significantly improve the recyclability properties of the LDH materials for other oxo-anions. Phosphate is known to have the highest affinity other than other carbonate for LDHs material, which means these species are particularly difficult to remove from the LDH material. In fact, Kanezaki, et. al. reported after the present study of phosphate desorption with surfactant that 93 % removal of molybdate from LDH material has been achieved by anion exchange with DBS.[93] This method is a substantial step towards the practical use of the LDH material as recyclable adsorbents for problematic oxo-anions.

A further and novel application of LDHs is reported in the preparation of photoactive materials. A photoelectrode has been developed based on Zn/Al-LDH deposited on a zinc substrate. The photoelectrode shows 2.6μAcm^{-2} under UV light (365 nm). The photocatalytic material, which has 1~2 μm thickness, is fabricated through Zn/Al-LDH formation and subsequent treatment. The Zn/Al-LDH is turned into a photocatalyst material which is composed of amorphous Zn/Al mixed metal oxides, by thermal treatment between 200 ˚C and 300 ˚C.

This optimal thermal treatment temperature was decided from the results of the treatment of Zn/Al-LDH powders. The study of thermal behaviour of the Zn/Al-LDH powder

observes the formation of the amorphous Zn/Al mixed metal oxides directly by X-ray Absorption Near Edge Structure (XANES). The band gap energy of the Zn/Al mixed metal oxides has about 3.7 eV which is wider band gap than the pure ZnO (3.3 eV). This is due to formation of mixed oxide with Al^{3+} because the band gap energy of ZnO is expanded by doping Al^{3+} into pure ZnO. The XANES shows the amorphous Zn/Al mixed metal was decomposed by thermal treatment after 400 ˚C. Thus, the XANES measurement is useful method to detect formation of the amorphous Zn/Al mixed oxide and probe its chemistry.

The Zn/Al-LDH film is initially fabricated on the zinc substrate by hydrothermal treatment. The hydrothermal treatment is optimized at a hydrothermal temperature of 75 ˚C and hydrothermal reaction time of 8h. These hydrothermal conditions allowed the formation of a single phase of the Zn/Al-LDH without impurity materials. Otherwise an impurity phase of the zinc oxide appears, along with the Zn/Al-LDH phase, at higher temperatures and causes cracks in the material. The Zn/Al-LDH on the substrate is turned to photocatalytic material by thermal treatment between 200 ˚C and 300 ˚C. The photocatalytic material showed $0.3\mu Acm^{-2}$ ~ $2.6\mu Acm^{-2}$ of photocurrent under 365 nm UV light depending on hydrothermal condition. Furthermore, the photocurrent is observed from the sample is anodic current and this is same as pure-ZnO which is typical n type semiconductor. The photocatalytic material can be assigned as n type semiconductor. However, characterization of the photocatalytic material has not been conducted, such as efficiency and band gap measurement. This characterization will be conducted as future work.

Despite many studies reporting the hydrothermal treatment of LDH and the thermal treatment of other precursors for formation of a photocatalytic phase, this is the first report of a photocurrent from a phase formed via treatment of Zn/Al-LDH. This study shows the fabrication of the photocatalytic material on the metal substrate through a pathway which is easier than conventional methods such as using complex sputtering systems or chemical vapor deposition (CVD). Furthermore, since the LDH synthesis has been used as the precursor for the mixed metal oxide, this method it should provide a simple path to stoichiometric control of other amorphous mixed phases such as Zn/Al combined with other elements such as Cr^{3+}, Fe^{3+} and Mn^{3+}. This calcined LDH material deposited on metal substrates has significant potential for new types of photonic devices, solar light conversion and LEDs.

References

1. Kostura, B.; Kovanda, F.; Valaskova, M.; Lesko, J., Rehydration of calcined Mg-Al hydrotalcite in acidified chloride-containing aqueous solution. *Collection of Czechoslovak Chemical Communications* **2007,** *72* (9), 1284-1294.
2. Li, F.; Duan, X., Applications of layered double hydroxides. Evans, D. G.; Duan, X., Eds. 2005; Vol. 119, pp 193-223.
3. (a) Dutta, P. K.; Puri, M., Anion exchange in lithium aluminate hydroxides. *The Journal of Physical Chemistry* **1989,** *93* (1), 376-381; (b) Miyata, S., Anion-exchange properties of hydrotalcite-like compounds. *Clays & Clay Minerals* **1983,** *31* (4), 305-311.
4. Goh, K.-H.; Lim, T.-T.; Dong, Z., Application of layered double hydroxides for removal of oxyanions: A review. *Water Research* **2008,** *42* (6-7), 1343-1368.
5. Liu, Y. T.; Wang, M. K.; Chen, T. Y.; Chiang, P. N.; Huang, P. M.; Lee, J. F., Arsenale sorption on lithium/aluminum layered double hydroxide intercalated by chloride and on gibbsite: Sorption isotherms, envelopes, and spectroscopic studies. *Environmental Science and Technology* **2006,** *40* (24), 7784-7789.
6. Yang, L.; Shahrivari, Z.; Liu, P. K. T.; Sahimi, M.; Tsotsis, T. T., Removal of Trace Levels of Arsenic and Selenium from Aqueous Solutions by Calcined and Uncalcined Layered Double Hydroxides (LDH). *Industrial & Engineering Chemistry Research* **2005,** *44* (17), 6804-6815.
7. (a) Terry, P. A., Characterization of Cr ion exchange with hydrotalcite. *Chemosphere* **2004,** *57* (7), 541-546; (b) Manju, G. N.; Gigi, M. C.; Anirudhan, T. S., Hydrotalcite as adsorbent for the removal of chromium (VI) from aqueous media: Equilibrium studies. *Indian Journal of Chemical Technology* **1999,** *6* (3), 134-141.
8. Lazaridis, N. K.; Pandi, T. A.; Matis, K. A., Chromium(VI) Removal from Aqueous Solutions by Mg-Al-CO_3 Hydrotalcite: Sorption-Desorption Kinetic and Equilibrium Studies. *Industrial and Engineering Chemistry Research* **2004,** *43* (9), 2209-2215.
9. Das, J.; Patra, B. S.; Baliarsingh, N.; Parida, K. M., Adsorption of phosphate by layered double hydroxides in aqueous solutions. *Applied Clay Science* **2006,** *32* (3-4), 252-260.

10. Chitrakar, R.; Tezuka, S.; Sonoda, A.; Sakane, K.; Ooi, K.; Hirotsu, T., Adsorption of phosphate from seawater on calcined MgMn-layered double hydroxides. *Journal of Colloid and Interface Science* **2005,** *290* (1), 45-51.
11. Seida, Y.; Nakano, Y., Removal of phosphate by layered double hydroxides containing iron. *Water Research* **2002,** *36* (5), 1306-1312.
12. You, Y. W.; Zhao, H. T.; Vance, G. F., Removal of arsenite from aqueous solutions by anionic clays. *Environmental Technology* **2001,** *22* (12), 1447-1457.
13. Kiso, Y.; Jung, Y. J.; Yamada, T.; Nagai, M.; Min, K. S., Removal properties of arsenic compounds with synthetic hydrotalcite compounds. 2005; Vol. 5, pp 75-81.
14. (a) Goswamee, R. L.; Sengupta, P.; Bhattacharyya, K. G.; Dutta, D. K., Adsorption of Cr(VI) in layered double hydroxides. *Applied Clay Science* **1998,** *13* (1), 21-34; (b) Das, J.; Das, D.; Dash, G. P.; Das, D. P.; Parida, K., Studies on Mg/Fe hydrotalcite-like - Compound (HTlc): Removal of chromium (VI) from aqueous solution. *International Journal of Environmental Studies* **2004,** *61* (5), 605-616.
15. Goh, K.-H.; Lim, T.-T.; Banas, A.; Dong, Z., Sorption characteristics and mechanisms of oxyanions and oxyhalides having different molecular properties on Mg/Al layered double hydroxide nanoparticles. *Journal of Hazardous Materials* **2010,** *179* (1-3), 818-827.
16. Woods, N. C.; Sock, S. M.; Daigger, G. T., Phosphorus recovery technology modeling and feasibility evaluation for municipal wastewater treatment plants. *Environmental Technology* **1999,** *20* (7), 663-679.
17. (a) Stanisław, R. *PHOSPHORUS REMOVAL FROM WASTEWATER*; **Royal Institute of Technology**: 1997; (b) Metcalf; Eddy; Tchobanoglous, G., *Wastewater engineering: treatment disposal reuse*. McGraw-Hill: 1979.
18. Nomura, R.; Mori, T.; Kanezaki, E.; Yabutani, T., Removal of phosphate in water to layered double hydroxide. *International Journal of Modern Physics B* **2003,** *17* (8-9 I), 1458-1463.

19. Shin, H. S.; Kim, M. J.; Nam, S. Y.; Moon, H. C., Phosphorus removal by hydrotalcite-like compounds (HTLcs). *Phosphorus, Sulfur, and Silicon and the Related Elements* **1996,** *34*, 161-168.

20. Shimamura, A.; Kanezaki, E.; Jones, M. I.; Metson, J. B., Direct observation of grafting interlayer phosphate in Mg/Al layered double hydroxides. *Journal of Solid State Chemistry* **2012,** *186*, 116-123.

21. Kuzawa, K.; Jung, Y.-J.; Kiso, Y.; Yamada, T.; Nagai, M.; Lee, T.-G., Phosphate removal and recovery with a synthetic hydrotalcite as an adsorbent. *Chemosphere* **2006,** *62* (1), 45-52.

22. Sideris, P. J.; Nielsen, U. G.; Gan, Z.; Grey, C. P., Mg/Al ordering in layered double hydroxides revealed by multinuclear NMR spectroscopy. *Science* **2008,** *321* (5885), 113-117.

23. Zhang, F.; Xiang, X.; Li, F.; Duan, X., Layered Double Hydroxides as Catalytic Materials: Recent Development. *Catal Surv Asia* **2008,** *12* (4), 253-265.

24. (a) Xia, S. J.; Liu, F. X.; Ni, Z. M.; Xue, J. L.; Qian, P. P., Layered double hydroxides as efficient photocatalysts for visible-light degradation of Rhodamine B. *Journal of Colloid and Interface Science* **2013,** *405*, 195-200; (b) Alanis, C.; Natividad, R.; Barrera-Diaz, C.; Martínez-Miranda, V.; Prince, J.; Valente, J. S., Photocatalytically enhanced Cr(VI) removal by mixed oxides derived from MeAl (Me: Mg and/or Zn) layered double hydroxides. *Applied Catalysis B: Environmental* **2013,** *140-141*, 546-551; (c) Rezvani, Z.; Sarkarat, M.; Khataee, A. R.; Nejati, K., Mixed metal oxide nanocomposites derived from layered double hydroxides as photocatalysts for C.I. Basic Blue 3 degradation under UV light. *Crystal Research and Technology* **2012,** *47* (11), 1172-1184; (d) Ahmed, A. A. A.; Talib, Z. A.; Hussein, M. Z. b.; Zakaria, A., Improvement of the crystallinity and photocatalytic property of zinc oxide as calcination product of Zn–Al layered double hydroxide. *Journal of Alloys and Compounds* **2012,** *539* (0), 154-160; (e) Carriazo, D.; Del Arco, M.; García-López, E.; Marc, G.; Martín, C.; Palmisano, L.; Rives, V., Zn,Al hydrotalcites calcined at different temperatures:

Preparation, characterization and photocatalytic activity in gas-solid regime. *Journal of Molecular Catalysis A: Chemical* **2011,** *342-343*, 83-90.

25. Liu, J.; Song, J.; Xiao, H.; Zhang, L.; Qin, Y.; Liu, D.; Hou, W.; Du, N., Synthesis and thermal properties of ZnAl layered double hydroxide by urea hydrolysis. *Powder Technology* **2014,** *253*, 41-45.

26. Cross, J., *Anionic surfactants: chemical analysis*. M. Dekker: 1977.

27. Kurashina, M.; Amatsu, T.; Ochi, T.; Ohigashi, N.; Kanezaki, E., ELUTION BEHAVIOR OF PHOSPHATE CONTAINED IN Mg/Fe AND Zn/Fe LAYERED DOUBLE HYDROXIDES. *International Journal of Modern Physics: Conference Series* **2012,** *06* (01), 156-161.

28. Iyi, N.; Matsumoto, T.; Kaneko, Y.; Kitamura, K., Deintercalation of Carbonate Ions from a Hydrotalcite-Like Compound: Enhanced Decarbonation Using Acid-Salt Mixed Solution. *Chemistry of Materials* **2004,** *16* (15), 2926-2932.

29. Liu, Z.; Ma, R.; Ebina, Y.; Iyi, N.; Takada, K.; Sasaki, T., General Synthesis and Delamination of Highly Crystalline Transition-Metal-Bearing Layered Double Hydroxides. *Langmuir* **2007,** *23* (2), 861-867.

30. Cullity, B. D.; Stock, S. R., *Elements of X-ray Diffraction*. Prentice Hall: 2001.

31. (a) Meyn, M.; Beneke, K.; Lagaly, G., Anion-exchange reactions of layered double hydroxides. *Inorganic Chemistry* **1990,** *29* (26), 5201-5207; (b) Miyata, S.; Okada, A., Synthesis of hydrotalcite-like compounds and their physico-chemical properties-The systems Mg^{2+}-Al^{3+}-SO4^{2-} and Mg^{2+}-Al^{3+}-CrO_4^{2-}. *Clays and Clay Minerals* **1977,** *25* (1), 14-18; (c) Rajamathi, J. T.; Ravishankar, N.; Rajamathi, M., Delamination-restacking behaviour of surfactant intercalated layered hydroxy double salts, $M_3Zn_2(OH)_8(surf)_2 \cdot 2H_2O$ [M = Ni, Co and surf = dodecyl sulphate (DS), dodecyl benzene sulphonate (DBS)]. *Solid State Sciences* **2005,** *7* (2), 195-199; (d) Ulibarri, M. A.; Pavlovic, I.; Barriga, C.; Hermosín, M. C.; Cornejo, J., Adsorption of anionic species on hydrotalcite-like compounds: Effect of interlayer anion and crystallinity. *Applied Clay Science* **2001,** *18* (1-2), 17-27; (e) Crepaldi, E. L.; Pavan, P. C.; Valim, J. B., Anion

exchange in layered double hydroxides by surfactant salt formation. *Journal of Materials Chemistry* **2000,** *10* (6), 1337-1343.

32. Miyoshi, H.; Katayama, S.; Kurashina, M.; Kanezaki, E., Novel accumulation of photo-induced $MV^{+\bullet}$ embedded in a TiO_2 shell and discharge of electrons to a Pt electrode. *Chemical Communications* **2010,** *46* (21), 3797-3799.

33. (a) Zou, P.; Fu, J.; Cao, Z., Chronosequence of paddy soils and phosphorus sorption-desorption properties. *Journal of Soils and Sediments* **2011,** *11* (2), 249-259; (b) Saad, R.; Hamoudi, S.; Belkacemi, K., Adsorption of phosphate and nitrate anions on ammonium-functionnalized mesoporous silicas. *Journal of Porous Materials* **2008,** *15* (3), 315-323; (c) Rodrigues, L. A.; Da Silva, M. L. C. P., Adsorption kinetic, thermodynamic and desorption studies of phosphate onto hydrous niobium oxide prepared by reverse microemulsion method. *Adsorption* **2010,** *16* (3), 173-181; (d) He, H.; Kang, H.; Ma, S.; Bai, Y.; Yang, X., High adsorption selectivity of ZnAl layered double hydroxides and the calcined materials toward phosphate. *Journal of Colloid and Interface Science* **2010,** *343* (1), 225-231; (e) Saha, B.; Griffin, L.; Blunden, H., Adsorptive separation of phosphate oxyanion from aqueous solution using an inorganic adsorbent. *Environmental Geochemistry and Health* **2010,** *32* (4), 341-347.

34. (a) Watanabe, Y.; Ikoma, T.; Yamada, H.; Stevens, G. W.; Moriyoshi, Y.; Tanaka, J.; Komatsu, Y., Formation of Hydroxyapatite Nanocrystals on the Surface of Ca–Al-Layered Double Hydroxide. *Journal of the American Ceramic Society* **2010,** *93* (4), 1195-1200; (b) Radha, A. V.; Vishnu Kamath, P.; Shivakumara, C., Mechanism of the anion exchange reactions of the layered double hydroxides (LDHs) of Ca and Mg with Al. *Solid State Sciences* **2005,** *7* (10), 1180-1187; (c) Xu, Y.; Dai, Y.; Zhou, J.; Xu, Z. P.; Qian, G.; Lu, G. Q. M., Removal efficiency of arsenate and phosphate from aqueous solution using layered double hydroxide materials: Intercalation vs. precipitation. *Journal of Materials Chemistry* **2010,** *20* (22), 4684-4691.

35. Radha, A. V.; Kamath, P. V.; Ravishankar, N.; Shivakumara, C., Suppression of the Reversible Thermal Behavior of the Layered Double Hydroxide (LDH) of Mg with Al: Stabilization of Nanoparticulate Oxides. *Langmuir* **2007,** *23* (14), 7700-7706.

36. Miyauchi, H.; Yamamoto, T.; Chitrakar, R.; Makita, Y.; Wang, Z.; Kawai, J.; Hirotsu, T., Phosphate Adsorption Site on Zirconium Ion Modified MgAl-layered Double Hydroxides. *Top Catal* **2009,** *52* (6-7), 714-723.

37. Triantafyllidis, K. S.; Peleka, E. N.; Komvokis, V. G.; Mavros, P. P., Iron-modified hydrotalcite-like materials as highly efficient phosphate sorbents. *Journal of Colloid and Interface Science* **2010,** *342* (2), 427-436.

38. (a) Badreddine, M.; Khaldi, M.; Legrouri, A.; Barroug, A.; Chaouch, M.; De Roy, A.; Besse, J. P., Chloride-hydrogenophosphate ion exchange into the zinc-aluminum-chloride layered double hydroxide. *Materials Chemistry and Physics* **1998,** *52* (3), 235-239; (b) Ookubo, A.; Kanezaki, E.; Ooi, K., ESR, XRD, and DRS studies of paramagnetic Ti^{3+} ions in a colloidal solid of titanium oxide prepared by the hydrolysis of $TiCl_3$. *Langmuir* **1990,** *6* (1), 206-209; (c) Khaldi, M.; Badreddine, M.; Legrouri, A.; Chaouch, M.; Barroug, A.; De Roy, A.; Besse, J. P., Preparation of a well-ordered layered nanocomposite from zinc-aluminum-chloride layered double hydroxide and hydrogenophosphate by ion exchange. *Materials Research Bulletin* **1998,** *33* (12), 1835-1843.

39. Shimamura, A.; Kurashina, M.; Kanezaki, E., Thermal behavior of phosphate intercalated Mg/al-layered double hydroxides. *International Journal of Modern Physics B* **2010,** *24* (15-16), 3226-3229.

40. Moyo, L.; Nhlapo, N.; Focke, W., A critical assessment of the methods for intercalating anionic surfactants in layered double hydroxides. *Journal of Materials Science* **2008,** *43* (18), 6144-6158.

41. (a) Trujillano, R.; Holgado, M. J.; Pigazo, F.; Rives, V., Preparation, physicochemical characterisation and magnetic properties of Cu–Al layered double hydroxides with CO_3^{2-} and anionic surfactants with different alkyl chains in the interlayer. *Physica B: Condensed Matter* **2006,** *373* (2), 267-273; (b) Kopka, H.; Beneke, K.; Lagaly, G., Anionic surfactants between double metal hydroxide layers. *Journal of Colloid and Interface Science* **1988,** *123* (2), 427-436.

42. Lv, L.; Sun, P.; Wang, Y.; Du, H.; Gu, T., Phosphate Removal and Recovery with Calcined Layered Double Hydroxides as an Adsorbent. *Phosphorus, Sulfur, and Silicon and the Related Elements* **2008,** *183* (2), 519 - 526.

43. Okamoto, K.; Iyi, N.; Sasaki, T., Factors affecting the crystal size of the MgAl-LDH (layered double hydroxide) prepared by using ammonia-releasing reagents. *Applied Clay Science* **2007,** *37* (1-2), 23-31.

44. Socrates, G., *Infrared and Raman characteristic group frequencies : tables and charts / George Socrates*. Chichester ; New York : Wiley, 2001.: 2001.

45. Kanezaki, E., Fourier transform infrared spectra of naphthalene disulfonates between layers of Mg and Al double hydroxide: Intercalation by means of coprecipitation and direct observation of coordination from the interlayer anion to the metal cation in the layer. *Journal of Inclusion Phenomena* **2000,** *36* (4), 447-453.

46. Corbridge, D. E. C.; Lowe, E. J., The infra-red spectra of some inorganic phosphorus compounds. *Journal of the Chemical Society (Resumed)* **1954**, 493-502.

47. Baril, J.; Max, J. J.; Chapados, C., Infrared spectroscopy of phosphoric acid. *Titrage infrarouge de l'acide phosphorique* **2000,** *78* (4), 490-507.

48. (a) Voyer, N.; Soisnard, A.; Palmer, S. J.; Martens, W. N.; Frost, R. L., Thermal decomposition of the layered double hydroxides of formula $Cu_6Al_2(OH)_{16}CO_3$ and $Zn_6Al_2(OH)_{16}CO_3$. *Journal of Thermal Analysis and Calorimetry* **2009,** *96* (2), 481-485; (b) Kooli, F.; Depege, C.; Ennaqadi, A.; De Roy, A.; Besse, J. P., Rehydration of Zn-Al layered double hydroxides. *Clays and Clay Minerals* **1997,** *45* (1), 92-98; (c) Britto, S.; Radha, A. V.; Ravishankar, N.; Kamath, P. V., Solution decomposition of the layered double hydroxide (LDH) of Zn with Al. *Solid State Sciences* **2007,** *9* (3-4), 279-286; (d) Ennadi, A.; Legrouri, A.; De Roy, A.; Besse, J. P., X-Ray Diffraction Pattern Simulation for Thermally Treated [Zn-Al-Cl] Layered Double Hydroxide. *Journal of Solid State Chemistry* **2000,** *152* (2), 568-572.

49. Lombardo, G. M.; Pappalardo, G. C.; Costantino, F.; Costantino, U.; Sisani, M., Thermal Effects on Mixed Metal (Zn/Al) Layered Double Hydroxides: Direct Modeling

of the X-Ray Powder Diffraction Line Shape Through Molecular Dynamics Simulations. *Chemistry of Materials* **2008,** *20* (17), 5585-5592.

50. Frost, R. L.; Martens, W. N.; Erickson, K. L., Thermal decomposition of the hydrotalcite: Thermogravimetric analysis and hot stage Raman spectroscopic study. *Journal of Thermal Analysis and Calorimetry* **2005,** *82* (3), 603-608.

51. Zhao, X.; Zhang, F.; Xu, S.; Evans, D. G.; Duan, X., From layered double hydroxides to ZnO-based mixed metal oxides by thermal decomposition: Transformation mechanism and UV-blocking properties of the product. *Chemistry of Materials* **2010,** *22* (13), 3933-3942.

52. Song, J.; Leng, M.; Fu, X.; Liu, J., Synthesis and characterization of nanosized zinc aluminate spinel from a novel Zn-Al layered double hydroxide precursor. *Journal of Alloys and Compounds* **2012,** *543*, 142-146.

53. Thomas, G. S.; Radha, A. V.; Kamath, P. V.; Kannan, S., Thermally Induced Polytype Transformations among the Layered Double Hydroxides (LDHs) of Mg and Zn with Al. *The Journal of Physical Chemistry B* **2006,** *110* (25), 12365-12371.

54. Schulze, D. G.; Bertsch, P. M., Synchrotron X-Ray Techniques in Soil, Plant, and Environmental Research. In *Advances in Agronomy*, Donald, L. S., Ed. Academic Press: 1995; Vol. Volume 55, pp 1-66.

55. Jens Kruse, P. L., Phosphorus $L_{2,3}$-edge XANES: overview of reference compounds. *Journal of Synchrotron Radiation* **2009,** *16* (2), 247-259.

56. Wang, H.-C.; Wei, Y.-L.; Yang, Y.-W.; Lee, J.-F., XAS study of Zn-doped Al_2O_3 after thermal treatment. *Journal of Electron Spectroscopy and Related Phenomena* **2005,** *144–147* (0), 817-819.

57. (a) Liu, J.; Huang, X.; Li, Y.; Sulieman, K. M.; He, X.; Sun, F., Facile and Large-Scale Production of ZnO/Zn−Al Layered Double Hydroxide Hierarchical Heterostructures. *The Journal of Physical Chemistry B* **2006,** *110* (43), 21865-21872; (b) Seftel, E. M.; Popovici, E.; Mertens, M.; Witte, K. D.; Tendeloo, G. V.; Cool, P.; Vansant, E. F., Zn-Al layered double hydroxides: Synthesis, characterization and

photocatalytic application. *Microporous and Mesoporous Materials* **2008,** *113* (1-3), 296-304.

58. Miyata, S., The syntheses of hydrotalcite-like compounds and their structures and physico-chemical properties-i: The systems Mg^{2+}-Al^{3+}-NO_3^-, Mg^{2+}-Al_{3+}-Cl^-, Mg^{2+}-Al^{3+}-ClO_4^-, Ni^{2+}-Al^{3+}-Cl^- and Zn^{2+}-A^{l3+}-Cl. *Clays and Clay Minerals* **1975,** *23* (5).

59. Mizoguchi, T.; Tanaka, I.; Yoshioka, S.; Kunisu, M.; Yamamoto, T.; Ching, W. Y., First-principles calculations of ELNES and XANES of selected wide-gap materials: Dependence on crystal structure and orientation. *Physical Review B - Condensed Matter and Materials Physics* **2004,** *70* (4), 045103-1-045103-10.

60. Bates, C. H.; White, W. B.; Roy, R., New high-pressure polymorph of zinc oxide. *Science* **1962,** *137*, 993.

61. Mizoguchi, T.; Yoshiya, M.; Li, J.; Oba, F.; Tanaka, I.; Adachi, H., Electron-energy-loss near edge structures of six-fold-coordinated Zn in MgO. *Ultramicroscopy* **2001,** *86* (3–4), 363-370.

62. Chiou, J. W.; Kumar, K. P. K.; Jan, J. C.; Tsai, H. M.; Bao, C. W.; Pong, W. F.; Chien, F. Z.; Tsai, M. H.; Hong, I. H.; Klauser, R.; Lee, J. F.; Wu, J. J.; Liu, S. C., Diameter dependence of the electronic structure of ZnO nanorods determined by x-ray absorption spectroscopy and scanning photoelectron microscopy. *Applied Physics Letters* **2004,** *85* (15), 3220-3222.

63. (a) Dien, L.; Bancroft, G. M.; Fleet, M. E.; Feng, X. H.; Pan, Y., Al K-edge XANES spectra of aluminosilicate minerals. *American Mineralogist* **1995,** *80* (5-6), 432-440; (b) Ildefonse, P.; Cabaret, D.; Sainctavit, P.; Calas, G.; Flank, A. M.; Lagarde, P., Aluminium X-ray absorption near edge structure in model compounds and earth's surface minerals. *Physics and Chemistry of Minerals* **1998,** *25* (2), 112-121.

64. (a) Van Bokhoven, J. A.; Roelofs, J. C. A. A.; De Jong, K. P.; Koningsberger, D. C., Unique structural properties of the Mg-Al hydrotalcite solid base catalyst: An in situ study using Mg and Al K-edge XAFS during calcination and rehydration. *Chemistry - A European Journal* **2001,** *7* (6), 1258-1265; (b) Roelofs, J. C. A. A.; Bokhoven, J. A. v.; Dillen, A. J. v.; Geus, J. W.; Jong, K. P. d., The Thermal Decomposition of Mg-Al

Hydrotalcites: Effects of Interlayer Anions and Characteristics of the Final Structure. *Chemistry - A European Journal* **2002,** *8* (24), 5571-5579.

65. Huang, W. H.; Sun, S. J.; Chiou, J. W.; Chou, H.; Chan, T. S.; Lin, H. J.; Kumar, K.; Guo, J. H., Electronic structure of Al-doped ZnO transparent conductive thin films studied by x-ray absorption and emission spectroscopies. *Journal of Applied Physics* **2011,** *110* (10), 103705.
66. Zuo, C.; Wen, J.; Zhong, C., First-principles study of the electronic structures and optical properties of C-F-Be doped wurtzite ZnO. *Journal of Semiconductors* **2012,** *33* (7).
67. Møller, P. J.; Komolov, S. A.; Lazneva, E. F., A total current spectroscopy study of metal oxide surfaces: I. Unoccupied electronic states of ZnO and MgO. *Journal of Physics Condensed Matter* **1999,** *11* (48), 9581-9588.
68. (a) Dong, C. L.; Persson, C.; Vayssieres, L.; Augustsson, A.; Schmitt, T.; Mattesini, M.; Ahuja, R.; Chang, C. L.; Guo, J. H., Electronic structure of nanostructured ZnO from x-ray absorption and emission spectroscopy and the local density approximation. *Physical Review B - Condensed Matter and Materials Physics* **2004,** *70* (19), 1-5; (b) Persson, C.; Dong, C. L.; Vayssieres, L.; Augustsson, A.; Schmitt, T.; Mattesini, M.; Ahuja, R.; Nordgren, J.; Chang, C. L.; Ferreira da Silva, A.; Guo, J. H., X-ray absorption and emission spectroscopy of ZnO nanoparticle and highly oriented ZnO microrod arrays. *Microelectronics Journal* **2006,** *37* (8), 686-689.
69. Ahmed, N.; Shibata, Y.; Taniguchi, T.; Izumi, Y., Photocatalytic conversion of carbon dioxide into methanol using zinc-copper-M(III) (M = aluminum, gallium) layered double hydroxides. *Journal of Catalysis* **2011,** *279* (1), 123-135.
70. Liu, Y. T.; Chen, T. Y.; Wang, M. K.; Huang, P. M.; Chiang, P. N.; Lee, J. F., Mechanistic study of arsenate adsorption on lithium/aluminum layered double hydroxide. *Applied Clay Science* **2010,** *48* (3), 485-491.
71. Shi, R.; Yang, P.; Dong, X.; Ma, Q.; Zhang, A., Growth of flower-like ZnO on ZnO nanorod arrays created on zinc substrate through low-temperature hydrothermal synthesis. *Applied Surface Science* **2013,** *264* (0), 162-170.

72. Panda, D.; Tseng, T.-Y., One-dimensional ZnO nanostructures: fabrication, optoelectronic properties, and device applications. *Journal of Materials Science* **2013,** *48* (20), 6849-6877.

73. (a) Fan, P.; Li, Y. Z.; Zheng, Z. H.; Lin, Q. Y.; Luo, J. T.; Liang, G. X.; Zhang, M. Q.; Chen, M. C., Thermoelectric properties optimization of Al-doped ZnO thin films prepared by reactive sputtering Zn-Al alloy target. *Applied Surface Science* **2013,** *284*, 145-149; (b) Pan, Z.; Luo, J.; Tian, X.; Wu, S.; Chen, C.; Deng, J.; Xiao, C.; Hu, G.; Wei, Z., Highly transparent and conductive Sn/F and Al co-doped ZnO thin films prepared by sol-gel method. *Journal of Alloys and Compounds* **2013,** *583*, 32-38; (c) Wang, C. Y.; Ma, S. Y.; Li, F. M.; Chen, Y.; Xu, X. L.; Wang, T.; Yang, F. C.; Zhao, Q.; Liu, J.; Zhang, X. L.; Li, X. B.; Yang, X. H.; Zhu, J., The effect of Mg and Al co-doping on the structural and photoelectric properties of ZnO thin film. *Materials Science in Semiconductor Processing* **2014,** *17*, 27-32.

74. (a) Liu, J.; Li, Y.; Huang, X.; Li, G.; Li, Z., Layered Double Hydroxide Nano- and Microstructures Grown Directly on Metal Substrates and Their Calcined Products for Application as Li-Ion Battery Electrodes. *Advanced Functional Materials* **2008,** *18* (9), 1448-1458; (b) Zhang, F.; Zhao, L.; Chen, H.; Xu, S.; Evans, D. G.; Duan, X., Corrosion Resistance of Superhydrophobic Layered Double Hydroxide Films on Aluminum. *Angewandte Chemie* **2008,** *120* (13), 2500-2503; (c) Li, S.; Shen, Y.; Liu, D.; Fan, L.; Zheng, X.; Yang, J., One-step fabrication of oriented Mg/Al-layered double hydroxide film on magnesium substrate with urea hydrolysis and its corrosion resistance. *Composite Interfaces* **2012,** *19* (8), 489-498; (d) Uan, J.-Y.; Lin, J.-K.; Tung, Y.-S., Direct growth of oriented Mg-Al layered double hydroxide film on Mg alloy in aqueous HCO3-/CO32- solution. *Journal of Materials Chemistry* **2010,** *20* (4), 761-766.

75. Chen, Q.; Shi, S.; Liu, X.; Jin, L.; Wei, M., Studies on the oxidation reaction of l-cysteine in a confined matrix of layered double hydroxides. *Chemical Engineering Journal* **2009,** *153* (1-3), 175-182.

76. Kieke, M. L.; Schoppelrei, J. W.; Brill, T. B., Spectroscopy of hydrothermal reactions. 1. The CO2-H2O system and kinetics of urea decomposition in an FTIR

spectroscopy flow reactor cell operable to 725 K and 335 bar. *Journal of Physical Chemistry* **1996,** *100* (18), 7455-7462.

77. Dutta, K.; Das, S.; Pramanik, A., Concomitant synthesis of highly crystalline Zn-Al layered double hydroxide and ZnO: Phase interconversion and enhanced photocatalytic activity. *Journal of Colloid and Interface Science* **2012,** *366* (1), 28-36.

78. Yan, X.; Li, Z.; Chen, R.; Gao, W., Template growth of ZnO nanorods and microrods with controllable densities. *Crystal Growth and Design* **2008,** *8* (7), 2406-2410.

79. Chang, Z.; Evans, D. G.; Duan, X.; Vial, C.; Ghanbaja, J.; Prevot, V.; de Roy, M.; Forano, C., Synthesis of [Zn–Al–CO_3] layered double hydroxides by a coprecipitation method under steady-state conditions. *Journal of Solid State Chemistry* **2005,** *178* (9), 2766-2777.

80. Greene, L. E.; Law, M.; Goldberger, J.; Kim, F.; Johnson, J. C.; Zhang, Y.; Saykally, R. J.; Yang, P., Low-temperature wafer-scale production of ZnO nanowire arrays. *Angewandte Chemie - International Edition* **2003,** *42* (26), 3031-3034.

81. Geng, F.; Matsushita, Y.; Ma, R.; Xin, H.; Tanaka, M.; Iyi, N.; Sasaki, T., Synthesis and Properties of Well-Crystallized Layered Rare-Earth Hydroxide Nitrates from Homogeneous Precipitation. *Inorganic Chemistry* **2009,** *48* (14), 6724-6730.

82. Guo, J. H.; Vayssieres, L.; Persson, C.; Ahuja, R.; Johansson, B.; Nordgren, J., Polarization-dependent soft-x-ray absorption of highly oriented ZnO microrod arrays. *Journal of Physics Condensed Matter* **2002,** *14* (28), 6969-6974.

83. Chen, M.; Wang, X.; Yu, Y. H.; Pei, Z. L.; Bai, X. D.; Sun, C.; Huang, R. F.; Wen, L. S., X-ray photoelectron spectroscopy and auger electron spectroscopy studies of Al-doped ZnO films. *Applied Surface Science* **2000,** *158* (1–2), 134-140.

84. Valtiner, M.; Borodin, S.; Grundmeier, G., Preparation and characterisation of hydroxide stabilised ZnO(0001)-Zn-OH surfaces. *Physical Chemistry Chemical Physics* **2007,** *9* (19), 2406-2412.

85. Kanezaki, E., Variable interlayer distance of intercalates of naphthalenedisulfonate isomers in hydrotalcite-like Zn and A1 layered double-hydroxides. *Journal of Inclusion Phenomena and Molecular Recognition in Chemistry* **1996,** *24* (4), 341-351.

86. RANDYA, R.; EITHG, M.; LORENG, H., Zinc Hydroxide: Solubility Product and Hydroxy-complex Stability Constants from 12.5-75 C. *Canadian Journal of Chemistry* **1975,** *53*, 3841-3845.

87. Nistor, S. V.; Nistor, L. C.; Stefan, M.; Ghica, D.; Aldica, G.; Barascu, J. N., Crystallization of Disordered Nanosized ZnO Formed by Thermal Decomposition of Nanocrystalline Hydrozincite. *Crystal Growth & Design* **2011,** *11* (11), 5030-5038.

88. MIYOSHI, H.; SAKAMOTO, K.; KURASHINA, M.; KANEZAKI, E., PHOTOINDUCED ELECTRON ACCUMULATION OF TITANIUM DIOXIDE NANOPARTICLES MODIFIED ELECTRODES. *International Journal of Modern Physics: Conference Series* **2012,** *06* (01), 61-66.

89. (a) Look, D. C.; Hemsky, J. W.; Sizelove, J. R., Residual native shallow donor in ZnO. *Physical Review Letters* **1999,** *82* (12), 2552-2555; (b) Seghier, D.; Gislason, H. P., Shallow and deep donors in n-type ZnO characterized by admittance spectroscopy. *Journal of Materials Science: Materials in Electronics* **2008,** *19* (8-9), 687-691; (c) Seghier, D.; Gislason, H. P., Characterization of donor states in ZnO. *Physica B: Condensed Matter* **2007,** *401-402*, 404-407.

90. Hofmann, D. M.; Hofstaetter, A.; Leiter, F.; Zhou, H.; Henecker, F.; Meyer, B. K.; Orlinskii, S. B.; Schmidt, J.; Baranov, P. G., Hydrogen: A Relevant Shallow Donor in Zinc Oxide. *Physical Review Letters* **2002,** *88* (4), 045504.

91. (a) Kalyanaraman, S.; Thangavel, R.; Vettumperumal, R., High mobility formation of p-type Al doped ZnO:N films annealed under NH3 ambient. *Journal of Physics and Chemistry of Solids* **2013,** *74* (3), 504-508; (b) T-Thienprasert, J.; Rujirawat, S.; Klysubun, W.; Duenow, J. N.; Coutts, T. J.; Zhang, S. B.; Look, D. C.; Limpijumnong, S., Compensation in Al-doped ZnO by Al-related acceptor complexes: Synchrotron X-ray absorption spectroscopy and theory. *Physical Review Letters* **2013,** *110* (5); (c) Park,

K. C.; Ma, D. Y.; Kim, K. H., The physical properties of Al-doped zinc oxide films prepared by RF magnetron sputtering. *Thin Solid Films* **1997,** *305* (1–2), 201-209.

92. (a) Iyi, N.; Tamura, K.; Yamada, H., One-pot synthesis of organophilic layered double hydroxides (LDHs) containing aliphatic carboxylates: Extended "homogeneous precipitation" method. *Journal of Colloid and Interface Science* **2009,** *340* (1), 67-73; (b) Iyi, N.; Sasaki, T., Decarbonation of MgAl-LDHs (layered double hydroxides) using acetate-buffer/NaCl mixed solution. *Journal of Colloid and Interface Science* **2008,** *322* (1), 237-245.

93. Muranishi, K.; Shimamura, A.; Kurashina, M.; Kanezaki, E., GRAFTING INTERLAYER MoO42- IN Mg/Al LAYERED DOUBLE HYDROXIDE BY THERMAL TREATMENT BELOW COLLAPSING THE LAYERED STRUCTURE. *International Journal of Modern Physics: Conference Series* **2012,** *06* (01), 127-132.